



5-2001

Computer simulation of a ceramic core injection molding process

Thanh Cong Nguyen

Follow this and additional works at: https://trace.tennessee.edu/utk_gradthes

Recommended Citation

Nguyen, Thanh Cong, "Computer simulation of a ceramic core injection molding process. " Master's Thesis, University of Tennessee, 2001.
https://trace.tennessee.edu/utk_gradthes/9698

This Thesis is brought to you for free and open access by the Graduate School at TRACE: Tennessee Research and Creative Exchange. It has been accepted for inclusion in Masters Theses by an authorized administrator of TRACE: Tennessee Research and Creative Exchange. For more information, please contact trace@utk.edu.

To the Graduate Council:

I am submitting herewith a thesis written by Thanh Cong Nguyen entitled "Computer simulation of a ceramic core injection molding process." I have examined the final electronic copy of this thesis for form and content and recommend that it be accepted in partial fulfillment of the requirements for the degree of Master of Science, with a major in Mechanical Engineering.

Rao W. Arimilli, Major Professor

We have read this thesis and recommend its acceptance:

Masood Parang, Belle Upadhyaya

Accepted for the Council:

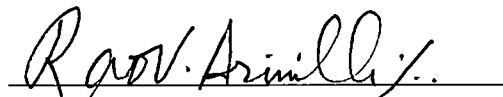
Carolyn R. Hodges

Vice Provost and Dean of the Graduate School

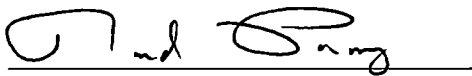
(Original signatures are on file with official student records.)

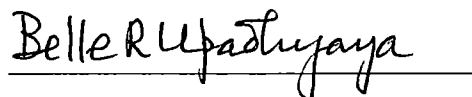
To the Graduate Council:

I am submitting herewith a thesis written by Thanh Cong Nguyen entitled "Computer Simulation of a Ceramic Core Injection Molding Process." I have examined the final copy of this thesis for form and content and recommend that it be accepted in partial fulfillment of the requirements for the degree of Master of Science, with a major in Mechanical Engineering.



Rao W. Arimilli, Major Professor

We have read this thesis
and recommend its acceptance:





Accepted for the Council:


Interim Vice Provost and
Dean of the Graduate School

Computer Simulation of a Ceramic Core Injection Molding Process

A Thesis

Presented for the

Master of Science

Degree

The University of Tennessee, Knoxville

Thanh Cong Nguyen

May 2001

DEDICATION

This thesis is dedicated to my lovely mother

Mrs. Trần Thị Ngó

all my family members,

my aunt

Mrs. Trương Thị Phước

and

her family members,

also

my best friend

Tôn Nữ Cẩm Bình

for their loves, invaluable supports, and encouragement throughout my study.

ACKNOWLEDGMENTS

Numerous people have provided great support and encouragement to me throughout my research. First and foremost, I would like to thank my committee chairman and adviser, Dr. Rao V. Arimilli, for his constant guidance throughout my research, for his advice and assistance in preparing this thesis, and most of all for his patience and support. Secondly, I would like to express my appreciation to my thesis committee members, Drs. Masood Parang and Belle Upadhyaya for their patience, suggestions, and for serving on my thesis committee.

I am very grateful to Howmet Research Corporation for their financial support which made this research possible. I, also, would like to thank Dr. John Johnson for his time and help in making available the injection molding machine and the operators for the conducting of the test, with minimal disruption to Howmet production schedule.

In addition, I would like to thank the following people for their assistance:
Dr. Ke Nguyen for his advice and support throughout my undergraduate years;
Mr. Winston Holmes, Director of the Engineering Computing Center at UTK for his help on using the Unix operating system; Mr. Matthew Lewis for providing the experimental results for the validation of the modeling study.

Finally, I would like to thank the Mechanical and Aerospace Engineering and Engineering Science Department for financially supporting me throughout my graduate study.

ABSTRACT

Complex ceramic cores, which form the internal cooling passages of investment-cast turbine blades and used in the aircraft-engine and industrial-gas-turbine industries, are made by ceramic injection molding. The high injection pressure, the high viscosity of the ceramic/wax mixture, and the high injection velocity during the injection molding process result in high rate of erosion, or wear, of the internal surfaces of die. The resurfacing of eroded surfaces of core dies is very costly. In addition to that, inappropriate injection parameters introduce defects, such as weld line and mis-fill, into the quality of the final products. It is desirable to increase the productivity of the ceramic injection molding process and also cut back maintenance costs by evaluating the process performance with computer modeling and simulation to identify means to reduce these problems.

In this study, a computer model and simulation of a three-dimensional transient ceramic/wax injection molding (CIM) process including filling and solidification, developed by the Advanced Casting Laboratory at the University of Tennessee for Howmet Research Corporation, was utilized and experimentally validated. The effect of variation of the interfacial heat transfer coefficients on the filling, solidification, and quality of the final products were carefully studied via the computer simulation of the ceramic injection molding process. Experiments were designed and conducted to measure the temperature of ceramic core material as a function of time for both filling and packing stages of the injection molding process. The experiments were conducted under production conditions at Howmet Casting Support in Morristown,

Tennessee. The results from the experiments were used to validate the realism and accuracy of the ProCAST simulation of the ceramic core injection molding process.

The results from the computer simulations indicated that the interfacial heat transfer coefficient modeled as a ramp function described in this work best represented the experimentally observed thermal characteristics of the filling and solidification process. The flow pattern from this computer simulation yielded a very desirable filling pattern that would avoid the introduction of weld line into the quality of the final product. Also, the computer model predicted the regions of high shear rate and the associated heating where excessive wear of the die was observed.

In summary, the model developed was shown to predict successfully the thermal characteristics of the core filling process. The results of this research contributes to the formation of a database of process variables that can be used for control of the injection molding process and for predicting the final geometry as a result of the process.

TABLE OF CONTENTS

CHAPTER	PAGE
1. INTRODUCTION	1
2. BACKGROUND	5
3. REVIEW OF LITERATURE ON THE INJECTION MOLDING PROCESS AND ITS MODELING	8
4. PROBLEM STATEMENT	37
5. MODEL DEVELOPMENT FOR COMPUTER SIMULATIONS	39
5.1 INTRODUCTION	39
5.2 SOLID MODEL DEVELOPMENT OF SOLIDWORKS	40
5.3 MESH GENERATION WITH MESHCAST	43
5.3.1 Surface Mesh of Core	43
5.3.2 Solid Mesh of Core	45
5.4 THERMAL-FLUID MODEL DEVELOPMENT	48
5.4.1 Setting All Necessary Parameters for Computer Simulation	48
5.4.2 Error Checking with DataCAST	58
5.4.3 Performing Simulation Analysis with ProCAST	58
5.5 POST PROCESSING OF RESULTS	59
5.5.1 Visualization of Casting Process with ViewCAST	60

5.5.2	Extraction of Time-Temperature Data from the Computer Simulation	60
5.6	EXPERIMENT OBJECTIVE AND CRITERIA	64
6.	RESULTS AND DISCUSSIONS	66
6.1	COMPARISON OF EXPERIMENTAL AND SIMULATION RESULTS	66
6.1.1	Constant Heat Transfer coefficient (Cases V-1, V-2, and V-3)	69
6.1.2	Step Function Model (Case V-4)	83
6.1.3	Ramp Function Model (Case V-5)	84
6.1.4	Results of Computer Simulation Case P-1	86
6.1.5	Results of Computer Simulation Case P-2	92
6.2	SUMMARY OF RESULTS	98
7.	CONCLUSIONS AND RECOMMENDATIONS FOR FUTURE RESEARCH	100
7.1	CONCLUSIONS	100
7.2	RECOMMENDATIONS FOR FUTURE WORK	101
	LIST OF REFERENCES	102
	APPENDICES	106
	APPENDIX A. TEMPERATURE CONTOUR PLOTS OF CASE V-5	107

APPENDIX B.	PRESSURE CONTOUR PLOTS OF CASE V-5	116
APPENDIX C.	TEMPERATURE CONTOUR PLOTS OF CASE P-2	123
APPENDIX D.	PRESSURE CONTOUR PLOTS OF CASE P-2	134
VITA		139

LIST OF TABLES

TABLE	PAGE
1. Comparison of Calculated Axis Temperatures for a Long Cylinder by Finite Difference and Analytical Methods	26
2. Material Properties Used in both Experiment and Simulation.....	30
3. Simulation Conditions Applied in Figure 20	33
4. Simulation Conditions Applied in Figure 21	34
5. Initial and Some Boundary Conditions Common for All Computer Simulations	50
6. Summary of Vent Boundary Conditions Common.....	50
7. Inlet Velocity Boundary Conditions Used in Computer Simulation Cases V-1 through V-5.....	50
8. Injection Pressure Boundary Conditions Used in Computer Simulation Cases P-1 and P-2.....	50

LIST OF FIGURES

FIGURE	PAGE
1. A typical dewaxed ceramic shell	2
2. Typical turbine blades	7
3. Flow chart of the ceramic injection molding process	10
4. Schematic of a screw-type machine	12
5. Relationships between relative viscosity and ceramic volume fraction.....	13
6. An example of a solid model of a stationary part in the auxiliary power unit of an aircraft engine	16
7. A finite-element mesh of the structural casting	17
8. A finite-element mesh of a ceramic mold	18
9. Mold filling sequence at 5.23 second after pouring	20
10. Mold filling sequence at 6.13 second after pouring	21
11. Effective stress of the casting part	23
12. Side-gated cylindrical moldings	25
13. Element of the cylinder used for temperature calculations	26
14. Surface temperature of 20-mm cylinders for a mold temperature of 20°C for various values of heat transfer coefficient. Experimental points are superimposed	27
15. Surface temperature of 40-mm cylinders for a mold temperature of 20°C for various values of heat transfer coefficient. Experimental points are superimposed	27
16. Surface temperature of 20-mm cylinders for a mold temperature of 80°C for various values of heat transfer coefficient. Experimental points are superimposed.....	28

17.	Surface temperature of 40-mm cylinders for a mold temperature of 80°C for various values of heat transfer coefficient. Experimental points are superimposed	28
18.	Silhouette of the actual part geometry used for the test and the approximate part geometry used in computer simulation	30
19.	Effective specific heat of the feedstock as a function of temperature	31
20.	Silhouette of the numerical simulation results for two different injection pressures showing formation of short shots	33
21.	Silhouette of the numerical simulation solutions for two different injection melt temperatures showing that short shot defects are eliminated with increasing injection melt temperature	34
22.	A flowchart of the computer modeling process	41
23.	3-D solid model of the ceramic core built in SolidWorks®	42
24.	Overall view of the surface mesh of the ceramic core	46
25.	Surface mesh of the trailing edge of the core	47
26.	Time step change function of the film coefficient h	51
27.	Time ramp change function of the film coefficient h	52
28.	Injection inlet pressure used for computer simulation case P-1	52
29.	Injection inlet pressure used for computer simulation case P-2	53
30.	Inlet temperature applied to all nodes of the injection surface	54
31.	Inlet velocity applied to all interior nodes of the injection surface	55
32.	Heat transfer coefficient assigned to all surfaces of nodes except injection surface.....	56
33.	No-slip velocity assigned to all surfaces of nodes except injection surface.....	56
34.	Vent boundary conditions assigned to nodes along the trailing edge at nine locations with properties listed in Table 6 ...	57

35.	Example of a ProSTAT Report	59
36.	An example of ViewCAST of the temperature contour plot of the injection molding process of the ceramic core	61
37.	Selected locations on the ceramic core model that best represent locations of thermocouples on die cavity	62
38.	Die cavity and thermocouples locations	63
39.	Average time-temperature of experimental channel 3, 7, 9, and 11 in dimensional form with the started-time shifted. Note the overlap of measured temperatures for channels 9 and 11.....	68
40.	Locations of nodes selected on mesh of the solid core model	68
41.	Filling pattern of computer simulation case V-1 at time of 0.0 ms	70
42.	Filling pattern of computer simulation case V-1 at time of 14.6 ms	70
43.	Filling pattern of computer simulation case V-1 at time of 30 ms	71
44.	Filling pattern of computer simulation case V-1 at time of 47.8 ms	71
45.	Filling pattern of computer simulation case V-1 at time of 59.8 ms	72
46.	Filling pattern of computer simulation case V-1 at time of 65.7 ms	72
47.	Filling pattern of computer simulation case V-1 at time of 70.8 ms	73
48.	Filling pattern of computer simulation case V-1 at time of 73.0 ms	73
49.	Filling pattern of computer simulation case V-1 at time of 74.7 ms	74
50.	Filling pattern of computer simulation case V-1 at time of 76.5 ms	74
51.	Filling pattern of computer simulation case V-1 at time of 78.4 ms	75
52.	Filling pattern of computer simulation case V-1 at time of 80.6 ms	75
53.	Filling pattern of computer simulation case V-1 at time of 81.5 ms	76
54.	Filling pattern of computer simulation case V-1 at time of 1.3 sec	76
55.	Filling pattern of computer simulation case V-1 at time of 10 sec	77

56.	Filling pattern of computer simulation case V-1 at time of 49 sec	77
57.	Comparison of case V-1 ($h = 1400 \text{ W/m}^2 \text{ K}$) model predictions with experimental measurements of temperature distributions at four locations. Note the overlap of measured temperatures for channels 9 and 11.....	79
58.	Comparison of case V-2 ($h = 1800 \text{ W/m}^2 \text{ K}$) model predictions with experimental measurements of temperature distributions at four locations. Note the overlap of measured temperatures for channels 9 and 11.....	80
59.	Comparison of case V-3 ($h = 2200 \text{ W/m}^2 \text{ K}$) model predictions with experimental measurements of temperature distributions at four locations. Note the overlap of measured temperatures for channels 9 and 11.....	81
60.	Comparison of predicted temperature distributions for channel 3 of case V-2 ($h = 1800 \text{ W/m}^2 \text{ K}$) with predictions by Robbins ¹⁷ and measurements by Ly ²²	82
61.	Comparison of case V-4 (step function) model predictions with experimental measurements of temperature distributions at four locations. Note the overlap of measured temperatures for channels 9 and 11.....	85
62.	Comparison of case V-5 (ramp function) model predictions with experimental measurements of temperature distributions at four locations. Note the overlap of measured temperatures for channels 9 and 11.....	87
63.	Dimensionless temperature distributions of channel 3 of both model simulation and experiment of case V-5 (ramp function).....	88
64.	Dimensionless temperature distributions of channel 7 of both model simulation and experiment of case V-5 (ramp function).....	89
65.	Dimensionless temperature distributions of channel 9 of both model simulation and experiment of case V-5 (ramp function).....	90
66.	Dimensionless temperature distributions of channel 11 of both model simulation and experiment of case V-5 (ramp function).....	91
67.	Filling pattern of computer simulation case P-2 at time of 163.3 ms	93

68.	Comparison of experimental and predicted temperatures as a function of time for channel 3 of computer simulation cases P-1 and P-2 (Node 10554)	94
69.	Comparison of experimental and predicted temperatures as a function of time for channel 7 of computer simulation cases P-1 and P-2 (Node 29541)	95
70.	Comparison of experimental and predicted temperatures as a function of time for channel 9 of computer simulation cases P-1 and P-2 (Node 25798)	96
71.	Comparison of experimental and predicted temperatures as a function of time for channel 11 of computer simulation cases P-1 and P-2 (Node 49704)	97

LIST OF SYMBOLS AND ABBREVIATIONS

ACSMDL	Advanced Casting Simulation and Mold Design Laboratory
CIM	Ceramic Injection Molding
HRC	Howmet Research Corporation
UTK	University of Tennessee, Knoxville
FEA	Finite Element Analysis
DARPA	Defense Advanced Research Projects Agency
GUI	Graphical User Interface
CAD	Computer-Aid Design
IGES	International Graphics Exchange Standard
STEP	Standard for Exchange of Product
h	Convection Heat Transfer Coefficient, W/m^2K
T	Temperature
θ	Dimensionless Temperature

CHAPTER 1

INTRODUCTION

State-of-the-art turbine blades that are used in gas turbine engines are made from super alloy via the investment casting process. The investment casting process has been used throughout the world since 2000 BC. In its early days it was successfully applied to the production of art castings but it is reasonable to assume that the process was also utilized by skilled craftsmen to produce tools, armaments and domestic utensils. The earliest method of investment casting was the Lost Wax Process. During the late 19th century the Lost Wax Process was adapted by dentists to produce accurate castings for fillings, crowns, bridges, etc., to individual requirements, often in gold. The continued development of the process during this period laid the foundations of the engineering process as it is known today.

As the investment casting industry becomes increasingly global and competition continues to rise, foundries must meet the challenge and produce near-net-shape or net-shape components at high quality. At the heart of this challenge will be the foundry's ability to improve its metalcasting techniques and technology to attain these high-quality standards. A typical investment casting process involves the following operations. Wax tooling is made from product definitions provided by the part designers. The tooling may include gating information contributed by the casting house. Injection molding process is used to form the wax patterns of the desired casting. These wax patterns are assembled with other features of the gating such as the pour cup, downfeed, ring gates, and runners. The resulting wax assembly is dipped into ceramic slurry and sprinkled with ceramic

powder repetitively to form a shell that envelops the wax assembly. After the shell is air-dried for complete stabilization, the wax is then removed in an autoclave and/or burnout furnace. This produces a ceramic mold, the cavity of which takes on the shape of the original wax assembly. The mold is preheated, and the liquid metal is cast into it in the conventional process. Once the metal has solidified, the ceramic mold is then broken and the part is cut away from the gating system to complete the whole casting process.

Figure 1 shows an example of a dewaxed ceramic shell.

In the past, the casting process was unpredictable because the designers, engineers, and researchers did not have the ability to visualize the details of the filling process and to analyze the results of the process. Trial and error methods were used to determine the actual casting process. These trial and error methods require several prototypes to be built and are very expensive.



Figure 1. A typical dewaxed ceramic shell ¹.

Modern casting industries have employed and taken advantage of the thermal-fluid Finite Element Analysis (FEA) software programs in their everyday casting process. The thermal-fluid FEA software is a valuable tool in industrial and educational institutions. It offers integrated finite element modeling, thermal analysis, and display of results, enabling designers to implement the design for reliability of the products. The software delivers thermal solutions early in the design phase to ensure reliable, cost-effective, and timely delivery of products. Most of the thermal-fluid FEA software comes with very-easy-to-use Graphical User Interface (GUI) to guide the users through the process for setting-up, running, and analyzing simulation results. It also allows the users to view the results of the simulated process on the computer. It provides users the ability to visualize the effects of the geometric design changes and of the influences of process parameters. Most of the thermal-fluid FEA software packages use finite element modeling approach to perform heat transfer analysis on mechanical and electrical components. The benefits of the thermal-fluid FEA software are that they complement high-level analysis tools and allow users to test design concepts early in their designing phase. The software tools have a wide range of features for model creation, verification, and editing that shorten design cycles and reduce requirements for costly prototypes. ProCAST, a professional casting process simulation software, is one such thermal-fluid FEA software package. ProCAST models industrial casting processes and provides tools for the analysis of a wide variety of fully-coupled thermal, fluid, stress, and microstructure prediction. This advance suite of software modules uses the FEA method and comprehensive solvers to simulate the physics of the casting process and enable the designers to see the effects of design improvements using computer simulation prior to

the actual development of tooling for the casting processes. Complex geometries, including the casting, dies, molds, risers, gates, and chills, can be created and evaluated as a complete system or they could be isolated, depending upon individual project needs ².

CHAPTER 2

BACKGROUND

In the past decade, significant progress has been made, in fabricating turbine blades and vanes, to control the weak points (or low strength area) that develop between individual crystals as molten metal solidifies.

New casting techniques minimize weak areas in blades and vanes. Directional solidification casting, in which the grains all run along the same axis for greater strength, and single crystal casting, which results in an airfoil that is essentially single grain, are two casting techniques that offer superior mechanical properties. Rather than machining airfoils from a solid piece of nickel-based alloy, which is an expensive process, they are formed as close to the finished dimensions as possible by a process called investment casting. Modern day castings of turbine blades, which may include complex internal air cooling passages, should require a minimum of finishing to reduce cost³.

Howmet Casting Support in Morristown, Tennessee, a division of Howmet Corporation, and the Advanced Casting Simulation and Mold Design Laboratory (ACSMDL) at the University of Tennessee, Knoxville (UTK) have collaborated on research involving 3-D computer simulations of the ceramic injection modeling processes.

Howmet Casting Support is a major supplier of complex ceramic cores, which form the internal cooling passages of investment-cast turbine blades, used in the aircraft-engine and industrial-gas-turbine industries. This plant specializes in the high-volume production of complex ceramic cores used in the casting of reactive and non-reactive

single crystal and directionally solidified castings. These cores meet the most exacting design specifications and customer requirements for reducing weight and improving internal cooling performance of turbine blades ⁴.

Turbine blades are located in the very high temperature region of a gas turbine engine just down stream of the combustion zone. The hotter the turbine engine can run, the more efficient it becomes. The ceramic cores are used to create internal air passages within turbine blades to allow the blades to be cooled so that engine can operate at higher temperatures without damaging the metal blade. Air passes through the intricate internal passages to cool the turbine blade by convection. Ceramic cores are used in an investment casting process for creating turbine blades. Prior to the investment casting process of turbine blades, an injection molding process is used to form the green ceramic cores. The fired core is placed in die and a wax pattern is injected around it. A ceramic shell is built around the pattern, and molten metal is cast into it in a conventional way. Once the turbine blades have been cast, chemicals are used to leach out or remove the ceramic cores to create these air passages in the turbine blades ⁴. Typical turbine blades are shown in Figure 2.

At Howmet Casting Support cores are made from the injection of molten ceramic slurry into a steel die cavity. The material used in the filling process is a proprietary mixture of ceramic slurry and wax that exhibits non-Newtonian behavior. The advantages of the use of ceramic materials are the following:

- extreme hardness and high resistance to wear
- high resistance to heat (may be used at temperature as high as 1800 °C)
- high insulation against heat and cold



(Courtesy of Howmet Corporation)

Figure 2. Typical turbine blades ⁴.

These material properties make ceramics a top choice for meeting the demands of the investment casting processes.

CHAPTER 3

REVIEW OF LITERATURE ON THE INJECTION MOLDING PROCESS AND ITS MODELING

The injection molding process was developed in the 1870's for celluloid and has been expanded to become the backbone of the plastics industry. Injection molding was first used as a ceramic-fabrication process in early 1930's and became a production process for the manufacture of spark-plug insulators in 1937. Since then various other ceramic products have been produced by injection molding including ceramic cores, thread guides, electronic parts, welding nozzles, dental braces and brackets, etc. Ceramic injection molding is a high-volume production process, which has the capability of producing complex-shaped articles to net shape. The major disadvantages are the binder-removal process and high-tooling cost. In late 1960's, the development of high-strength structural ceramics, along with the development of the ceramic gas turbine engine prompted a renewed interest in ceramic injection molding⁵. Around 1970's, the Defense Advanced Research Projects Agency (DARPA) of the U.S. Department of Defense, initiated a program that successfully demonstrated the use of ceramics in demanding high-temperature structural applications⁶. Components for advanced heat engines are being extensively investigated. Of the ceramic materials, dense silicon nitride and dense silicon carbide are considered the favorite candidates. Lately, toughened zirconia has been considered favorably for some specific applications⁶. Shapes for most ceramic component parts are extremely complex. Furthermore, the components must meet strict dimensional tolerances and maintain very high reliability in use. It is necessary to

produce these components in large numbers at a competitive cost. The complexity of the components and the need for large quantities dictated the consideration of injection molding as a technologically and economically feasible fabrication technique. Current efforts are focused on fabricating the following components:

- Turbine Rotors and Stators: To operate at turbine inlet temperature of 1200 to 1400°C and withstand prevailing thermal and mechanical stresses during startup, steady state, and shutdown conditions.
- Combustion Prechamber Inserts: To replace high-nickel alloy in diesel engine combustor components. Also to reduce ignition delay on cold start up and to reduce idling and light-load noises.
- Turbocharging Rotors: To increase the power and efficiency of internal combustion engines by recovering a portion of the waste energy in exhaust gases.

The injection-molding process involves the injection of molten plastics (or molten plastics/ ceramic mixtures) into a cold die cavity in which they solidify to form a fabricated component. This type of molding is termed thermoplastic. White and Dee⁵ describe injection molding as a “non-isothermal fluid mechanical process involving solidifying liquids with complex rheological properties.” Injection molding of ceramics encompasses many basic phenomena, including physical characteristics and surface chemistry of the powders, dispersion, wettability and surface tension forces between the binder and powder. In actual shape forming, the flow of highly viscous mixture is dictated by the rheology of powder and organic mixture, and by the pressure and

temperature during molding, and process history. Once the shape is formed the binder must be removed prior to the densification process.

Ceramic injection molding consists (Figure 3) of the following steps ⁶:

- Tailoring the ceramic powder
- Developing some organic binder formulations
- Producing a homogeneous ceramic and organic binder mix
- Forming parts by injection molding
- Processing the parts to remove the organic binder and densifying the parts.

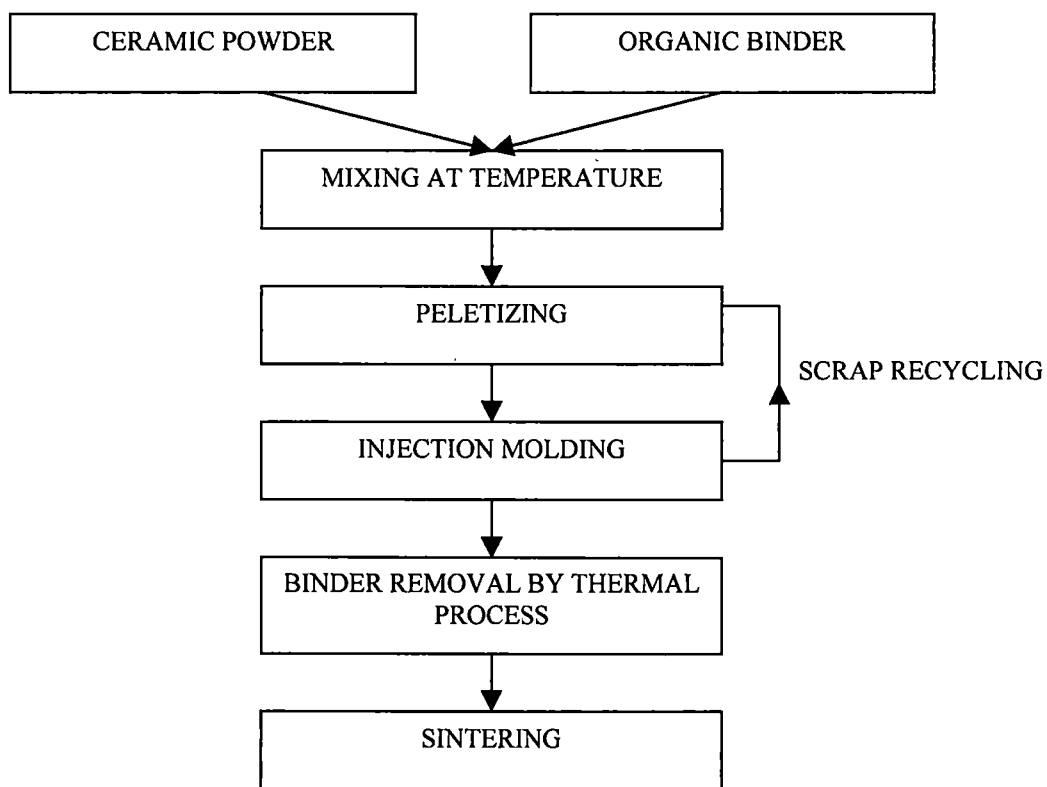


Figure 3. Flow chart of the ceramic injection molding process ⁶.

In the injection molding process the molten ceramic mixture is injected into a die cavity where it cools. Many types and sizes of molding machines are available. Screw-type machines are commonly used for both ceramic and plastic injection molding. In a screw-type injection molding machine, a major portion of heat comes from the frictional forces between screw, material, and cylinder. Figure 4 shows the schematic of a screw-type machine.

Selection of a specific machine type is influenced by the requirements of the molded product and by the degree of versatility desired. Regardless of the type, the following features in an injection-molding machine are of absolute necessity.

- Injection cylinder should have three individually controlled heater zones. (Nozzle temperature should be separately controlled.)
- Injection and post injection or packing pressures should be variable up to at least 14 MPa, and be controlled by individual timers.
- Variable speed ram should be controlled either by a flow control valve or by timed hydraulic pump.
- Feed adjustment should be precise.

With powder injection molding process the filling process is dependent on viscosity of the powder-binder mixture. Successful filling of the mold requires specific rheological characteristics of the mixture, which depend upon the powder/binder volume fraction as well as the size and shape to the powder particles. For most ceramic powders,

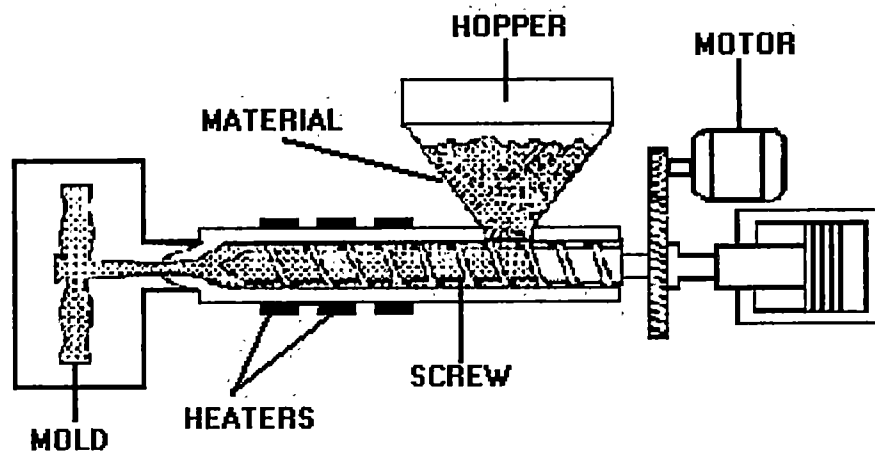


Figure 4. Schematic of a screw-type machine ⁵.

the maximum ceramic volume percentage that can be incorporated in the ceramic mixture is close to the percentage relative density achieved by dry pressing the same powder. The exact value depends critically on particle size distribution and shape. There is presently no way of predicting the maximum volume fraction from these properties and it is doubtful if such a method could ever achieve the needed accuracy of ± 0.5 percent of volume ⁷. Figure 5 shows a simple semi-empirical equation, which fits the relative viscosity-volume fraction behavior for most powders. Figure 5a shows the dependence of viscosity on V_m (maximum volume loading) representing the loading at which particles touch and viscosity approaches infinity.

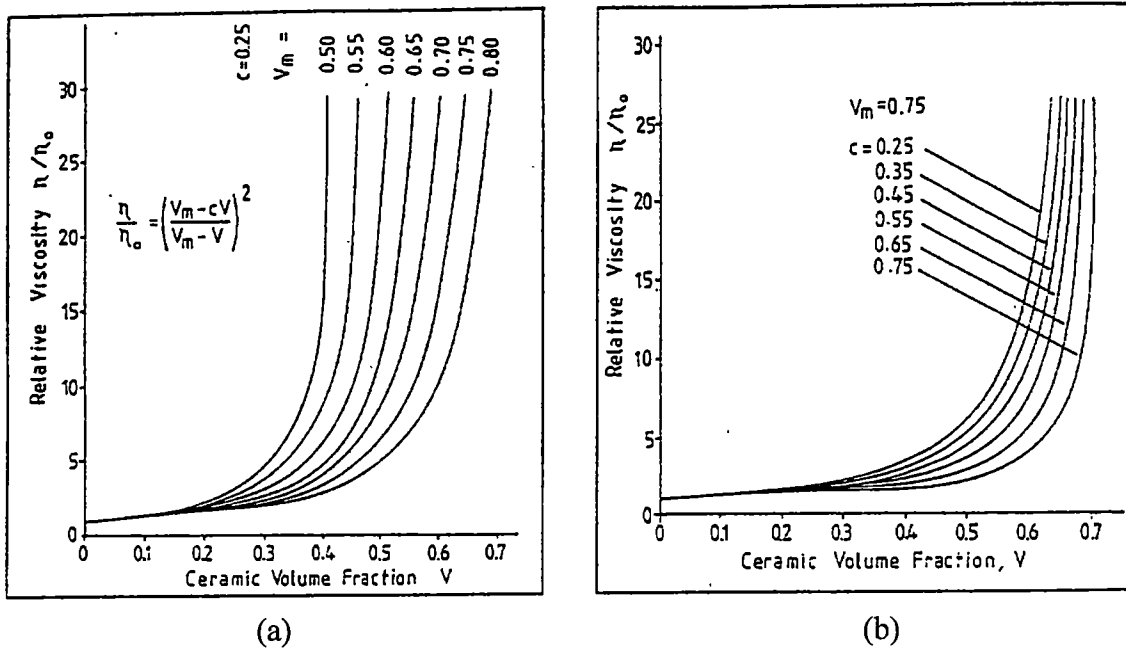


Figure 5. Relationships between relative viscosity and ceramic volume fraction: (a) for different maximum volume fractions V_m and $c = 0.25$ and (b) for different value of c .

Figure 5b shows how c is a constant that is defined in Figure 5(a) and represents the shape of the curve. The sensitivity of the viscosity to volume fraction as V_m is approached is the reason for the need for great accuracy in volume fraction. The term in the denominator ($V_m - V$) is the volume fraction of the mixture over and above that needed to fill interstitial space when particles are in contact⁷.

Overpacking factor must be also taken into consideration in the injection molding process. For a given geometry, it may be possible that one section fills before the other sections are filled due to the flow balance, friction, shearing, and / or cooling effects. In such a case, the material will continue to pack the area that was filled earlier while the

rest of the cavity is filled. The pressure in one area will increase producing pressure gradients in the overpacked region that are close to zero. The elements in this region are called overpacked elements. Overpacking some elements as compared to the others create a nonuniform density in the part. This nonuniform density causes warpage in the part due to differential shrinkage during the cooling phase.

Computer simulations of the injection molding and investment casting processes have been used for over a decade. They have been used extensively to design, troubleshoot, and enhance the injection molding process in the plastics industry. Computer simulations can be used to help provide information on mold filling characteristics such as pressure, velocity, temperature, total pressure drop, air trap locations, weld line integrity, maximum injection pressure, clamp force, effect of gate geometry and location, and shrinkage and warpage trends.

The investment casting process can be modeled and simulated by use of an integrated Computer-Aid Design (CAD)/Finite Element Analysis (FEA) approach. Tu, Roran, Hines, and Aimone⁸ described the modeling and simulation of the investment casting process as a seven step process: electronic data transfer, gating library, automatic mesh generation, automatic mold generation, finite-element preprocessing, coupled thermal, fluid flow, and stress analysis, and finite-element post-processing. Since more original equipment manufacturers are replacing the blueprints with CAD models, the FEA should take full advantage of the CAD data files to reduce model construction time and become an integral part of the product-design cycle. That is, a finite-element mesh should be generated from the CAD model directly. This will not only reduce the redundancy of building the geometric model, but it will also improve the geometric

accuracy utilized in the analysis. However, generating a mesh from a CAD model is not easy; a common standard on data format must be developed between original equipment manufacturers and the supplier. If different software packages are already well established in each company, a robust translation protocol should be adopted. The two most common protocols that have been used are international graphics exchange standard (IGES) and the standard for exchange of product model data (STEP). The STEP includes not only enhanced geometric information but also non-geometric information such as assembly, materials, and tolerances. An example of a solid model of a stationary part in the auxiliary power unit of an aircraft engine created in Unigraphics is shown in Figure 6.

FEA requires the construction of a congruent finite-element mesh (i.e, every element corner must join to the corners of its neighbor, never to an edge between two nodes). This poses a strenuous prerequisite on its application to complex three-dimensional geometry. Traditionally, a geometry is divided into simple shaped regions (hyperpatches in Patran or mesh volume in Ideas) that would be further subdivided into elements. The difficulty lies in the definition of congruent regions. It would typically take several weeks to prepare hyperpatches for meshing. There are several commercial software packages for automatic mesh generation from CAD model. When these packages are applied to a complicated geometry, their robustness becomes an issue. Each has strengths and weakness, and none consistently succeeds.

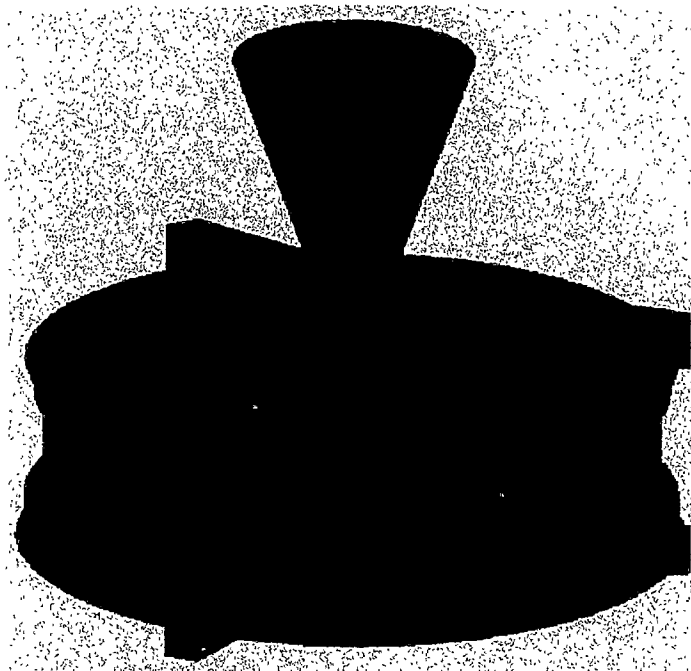


Figure 6. An example of a solid model of a stationary part in the auxiliary power unit of an aircraft engine ⁸.

Tu, Roran, Hines, and Aimone ⁸ evaluated a numbers of automatic meshing software packages to produce meshes on Unigraphics solid models, such as MeshCAST of UES, Finite Octree of Rensselaer Polytechnic Institute, and P3 of the MacNeal-Schwendler Corporation. MeshCAST uses a combination of Delaunay and the advancing-front method, which requires the generation of a surface mesh before meshing the enclosed region with tetrahedral. Finite Octree uses the octree method to generate linear- or higher-order tetrahedra given a parasolids file. P3 uses a paving/plastering method to generate linear or higher-order tetrahedral and has direct Unigraphics access. It also requires the generation of surface mesh either explicitly or implicitly before meshing the region with tetrahedral. Figure 7 shows a finite-element mesh of the structural casting generated by MeshCAST.

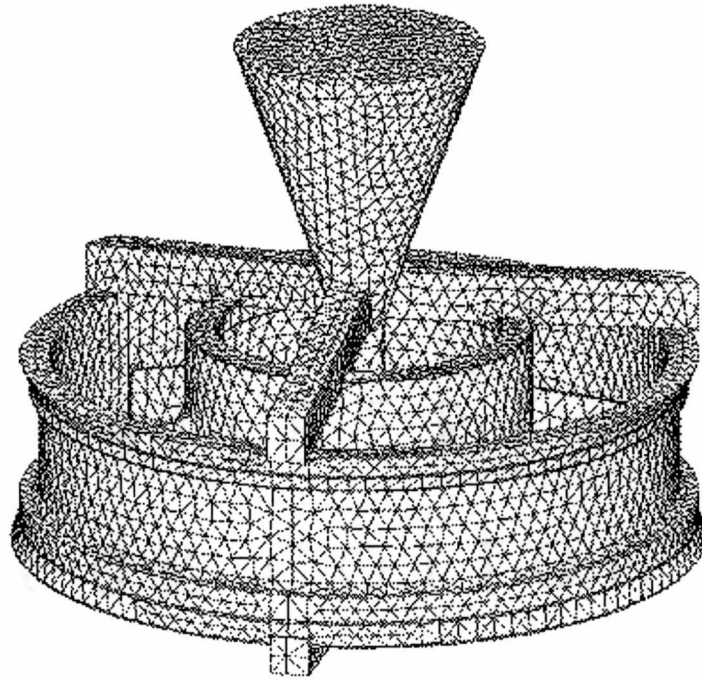


Figure 7. A finite-element mesh of the structural casting ⁸.

In most cases, it is very helpful for thermal analysis simulation to include the mold of the cast part to study the affects of the mold's physical geometry and initial conditions on the cast parts. The ceramic mold is a shell that surrounds the casting geometry. However, creating the mold is not easy. There are several possible approaches for creating a finite-element mesh of the mold. One is to create a solid of the shell by offsetting surfaces of the CAD solid and then mesh this shell solid using an automesher. The second approach is to create the finite-element mesh of the mold from the surface of the finite-element mesh of the metal, thus eliminating the extra effort of creating a CAD geometry of the shell. There are several FEA software packages available with the feature of automatic mold generation, such as MeshCAST, Patran, and Hypermesh. Figure 8 shows a finite-element mesh of a ceramic mold.

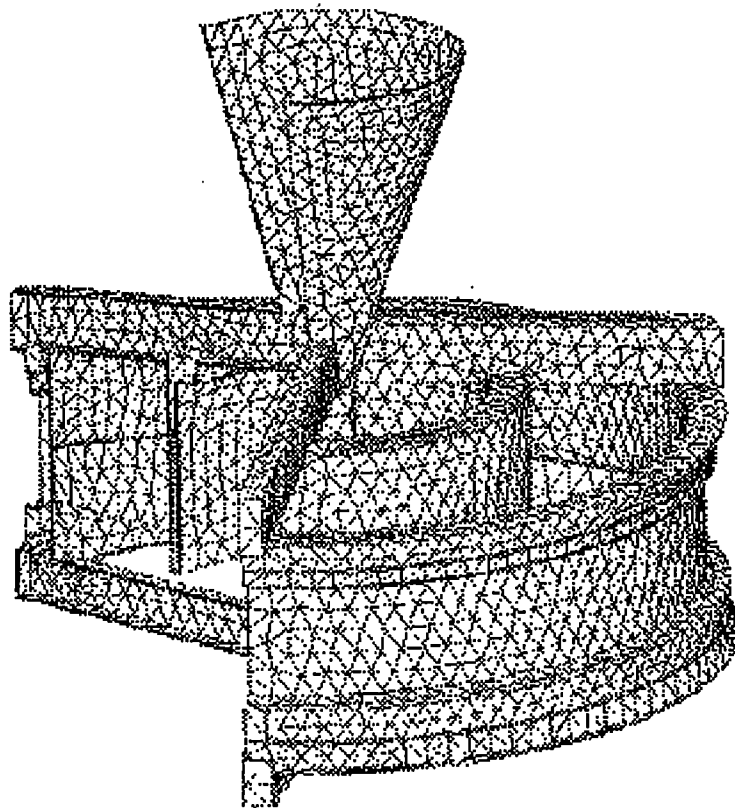


Figure 8. A finite-element mesh of a ceramic mold ⁸.

In the preprocessing step, all initial and boundary conditions are assigned to the model such as initial mold temperature, inlet velocity, and heat transfer coefficients. During the preheat cycle, the ceramic mold reaches an equilibrium temperature. This temperature becomes the initial condition for the mold in the model. Next, the ceramic mold is transported from the preheat furnace to the casting furnace. At this stage, radiative, conductive, and convective heat exchange start to occur with the environment. Since each location on the mold surface sees a different view of its environment, each will have a different rate of heat loss. The initial mold temperature and heat loss to the environment prior to casting dictate the thermal profiles that exist at the time of pour.

Molten metal is then poured into the non-uniform temperature mold. It has been found that the pouring profile has a significant impact on the filling sequence and casting defects. The cross-sectional areas of the pouring stream, the angle of pour, and the speed of pour all impact the final product. This information serves as inlet velocity boundary condition. During and after mold filling, solidification starts to take place. The energy content of the metal continually decreases by heat conduction with the cooler mold and by radiation from the mold surface and exposed metal in the pour cup. Depending on part geometry, solid metal starts to pull away from the mold or press against the mold. This changes the heat transfer mechanism across the metal-mold interface. Therefore, heat transfer coefficients between the metal and the mold are not constant and must be calculated from either first principles or an empirical approach. In the later stage of solidification, the majority of metal in the product component is solidified, while some portions of the gates are still in liquid or mushy states. This solid/liquid interaction creates a significant technical challenge for a stress analysis of the casting. This becomes the boundary condition for the stress calculation of metal.

After the preprocessing, the finite-element model was solved using the software ProCAST, which is tailored to casting simulation. Tu, Roran, Hines, and Aimone⁸ used the IN718 metal in their study.

The results can be displayed in the post-processing step. Users can visualize the filling pattern of the molten metal in the mold, the temperature distribution and the effective stress distribution on the casting part. Figures 9 and 10 present the mold filling sequences from the fluid-flow simulation at different time.

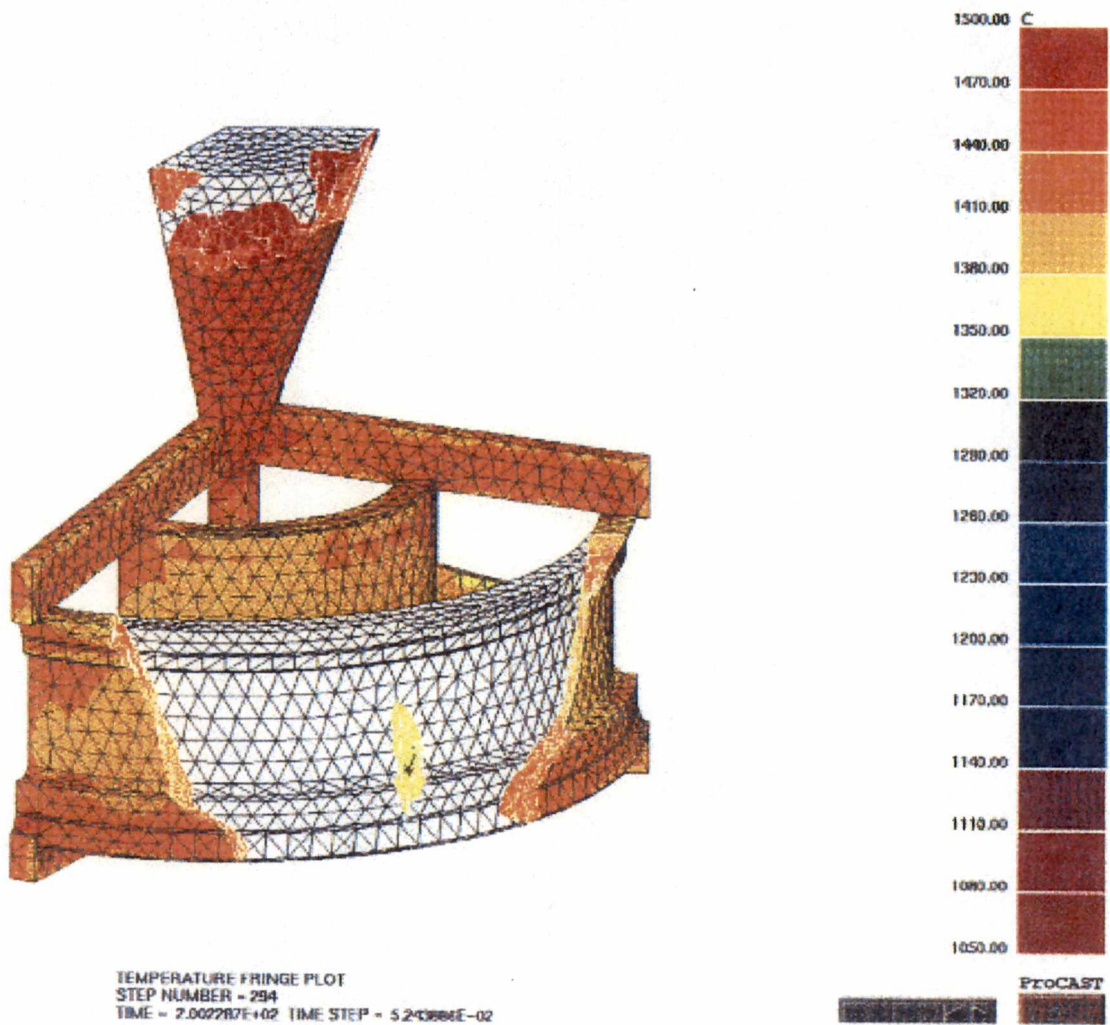


Figure 9. Mold filling sequence at 5.23 second after pouring ⁸.

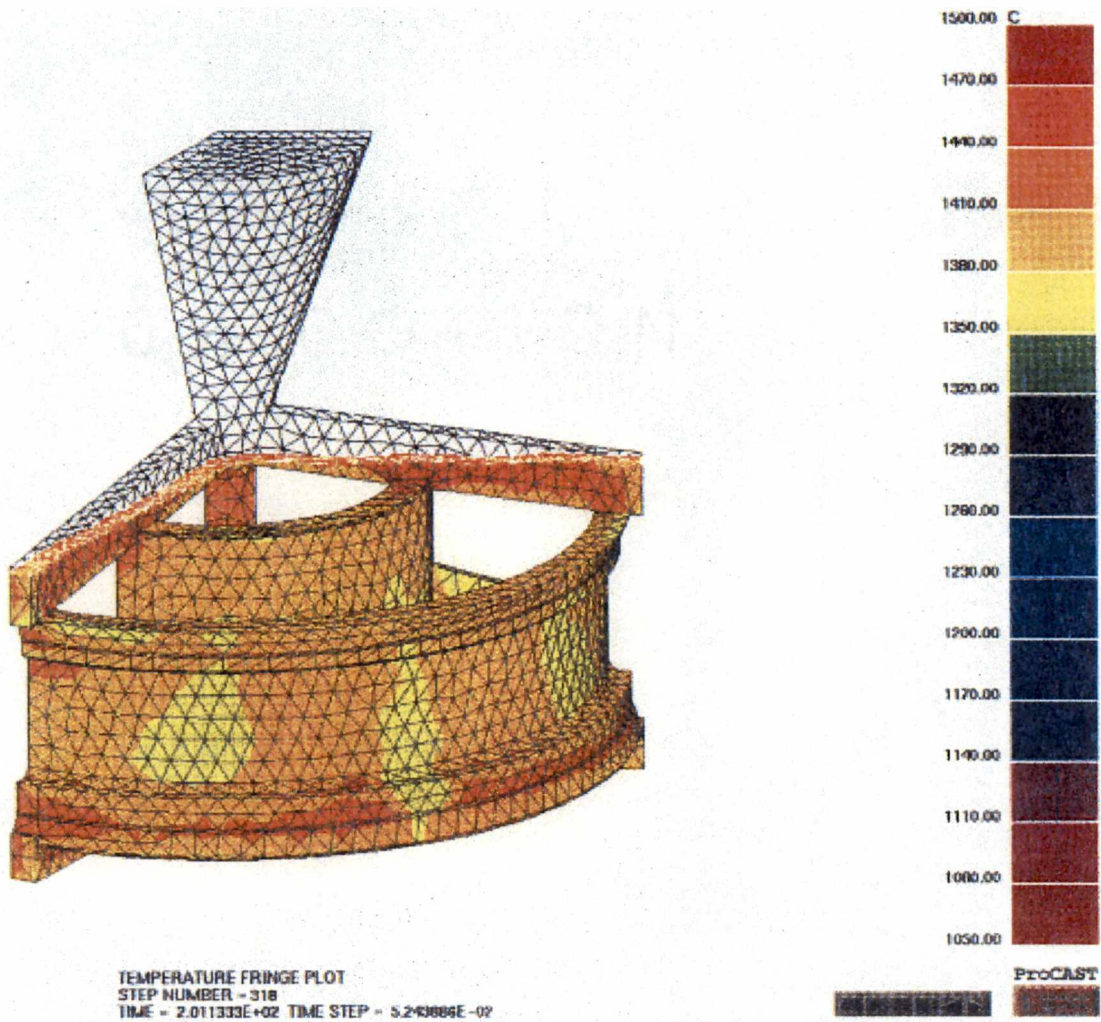


Figure 10. Mold filling sequence at 6.13 second after pouring⁸.

Figure 11 shows the predicted effective stress distribution on the casting part. It can be seen that the outer-shroud metal between the leading-edge ring gate and trailing-edge ring gate is subjected to a high tensile stress because its contraction due to cool down is being prevented by the locking mechanism provided by the ceramic mold surrounding the ring gates, as if it is going through tensile testing⁸. Users can also extract temperatures, pressures, and stressed data from the computer simulation for further analysis.

There are several papers⁹⁻¹³ that cover the subject of computer modeling of ceramic injection molding through the studies of temperature distribution during the solidification, measurement of thermal properties, shrinkage voids, selection of powders, measurement of residual stresses, and the effect of pressure on products.

Zhang and Evans⁹ carried out an extensive research to estimate the surface temperature of the molded body and hence deduce the surface heat transfer coefficient as a function of time during the solidification stage. The surface temperature distribution in a short cylinder was calculated by both finite element method in explicit form and analytical method and validated. In the experiment of Zhang and Evans⁹, the injection molding suspension consisted of 56 vol% alumina in an organic vehicle consisting of atactic polypropylene, isotactic polypropylene, and stearic acid in the weight ratio of 4:4:1. Injection molding was carried out on a Negri Bossi NB90 machine adapted for ceramics use. The ceramic mixture's temperatures were 190°C -210°C feed to die. The mold temperature was 20°C or 80°C and controlled by Conair Churchill 3/100 water circulating unit. The cavities consisted of side gated cylinders of 20-mm and

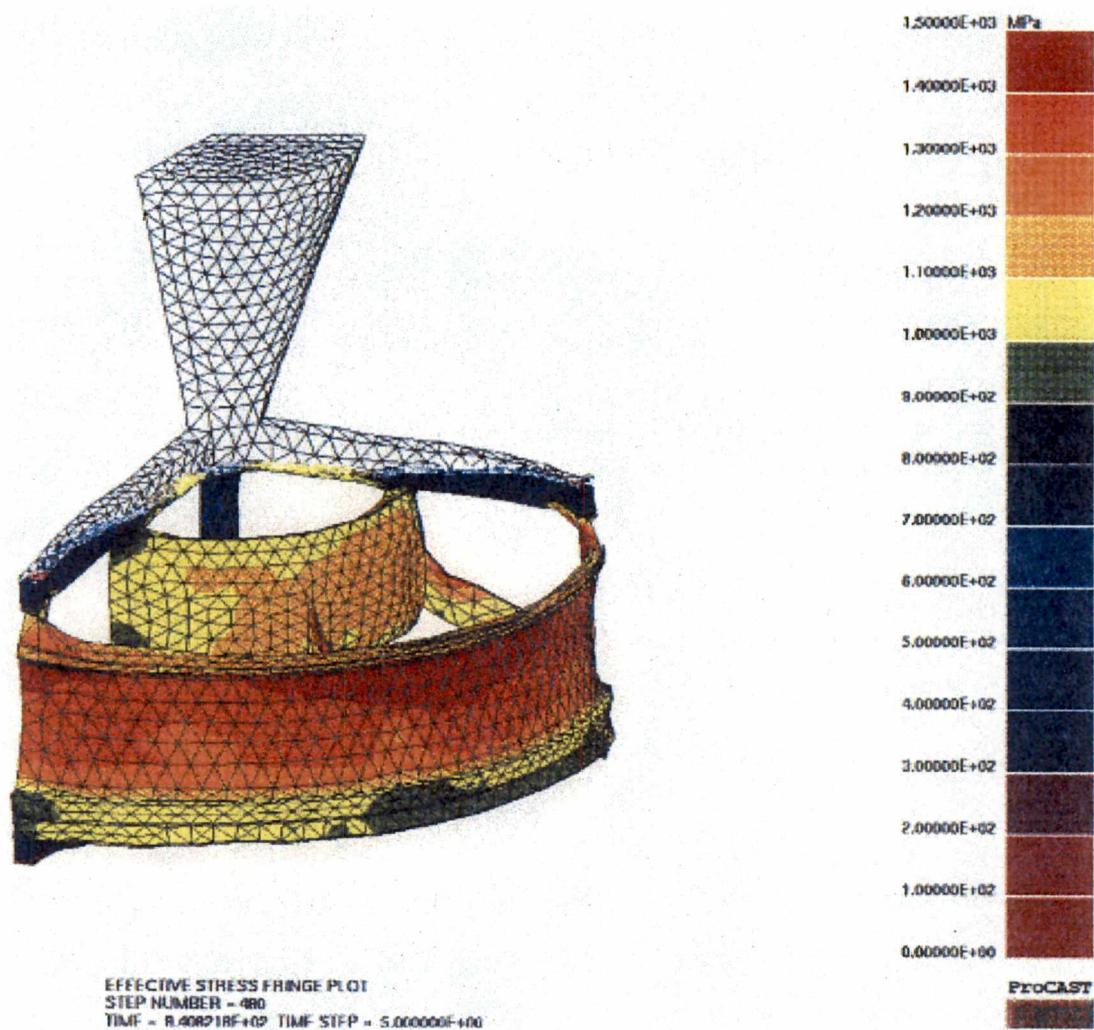


Figure 11. Effective stress of the casting part ⁸.

40-mm diameter, each 60 mm in length with a 1° taper (Figure 12). The injection speed was $4 \times 10^{-5} \text{ m}^3 \cdot \text{s}^{-1}$. An injection pressure of 140 MPa was used with a pressure trip to constant hold pressure, which was varied in the experiments. A 36 standard wire gauge thermocouple was used to measure the surface temperature of cylindrical moldings during cooling. The thermocouple was inserted between the mold halves before closing the clamp. When the melt was injected, the thermocouple embedded itself in the surface of the molding. When the molding underwent shrinkage away from the cavity wall, the thermocouple remained attached to the molding.

The temperature distributions in the short cylinders were calculated using a finite difference method in the explicit form by reference to the element in Figure 13. The analytical solution was also obtained and used to validate the finite difference method. The temperature at the center of the cylindrical molding was calculated as a function of time by the two methods, and the results are compared in Table 1. The error is generally less than 2°C ⁹. The temperature at the surface of the cylinders on the half-length position was calculated from the numerical method, for mold temperatures of 20°C and 80°C and for the 20-mm and 40-mm diameter cylinders and for a range of surface heat transfer coefficients from 500 to $4000 \text{ W} \cdot \text{m}^{-2} \cdot \text{K}^{-1}$. For the corresponding experimental conditions, the measured surface temperatures of the moldings at the center of the curved surface were recorded and are compared with the calculated values in Figures 14, 15, 16, and 17. The results suggest that at the higher mold temperature (Figs. 16-17), a heat transfer coefficient of $2000 \text{ W} \cdot \text{m}^{-2} \cdot \text{K}^{-1}$ corresponds well with the measured surface temperature⁹.

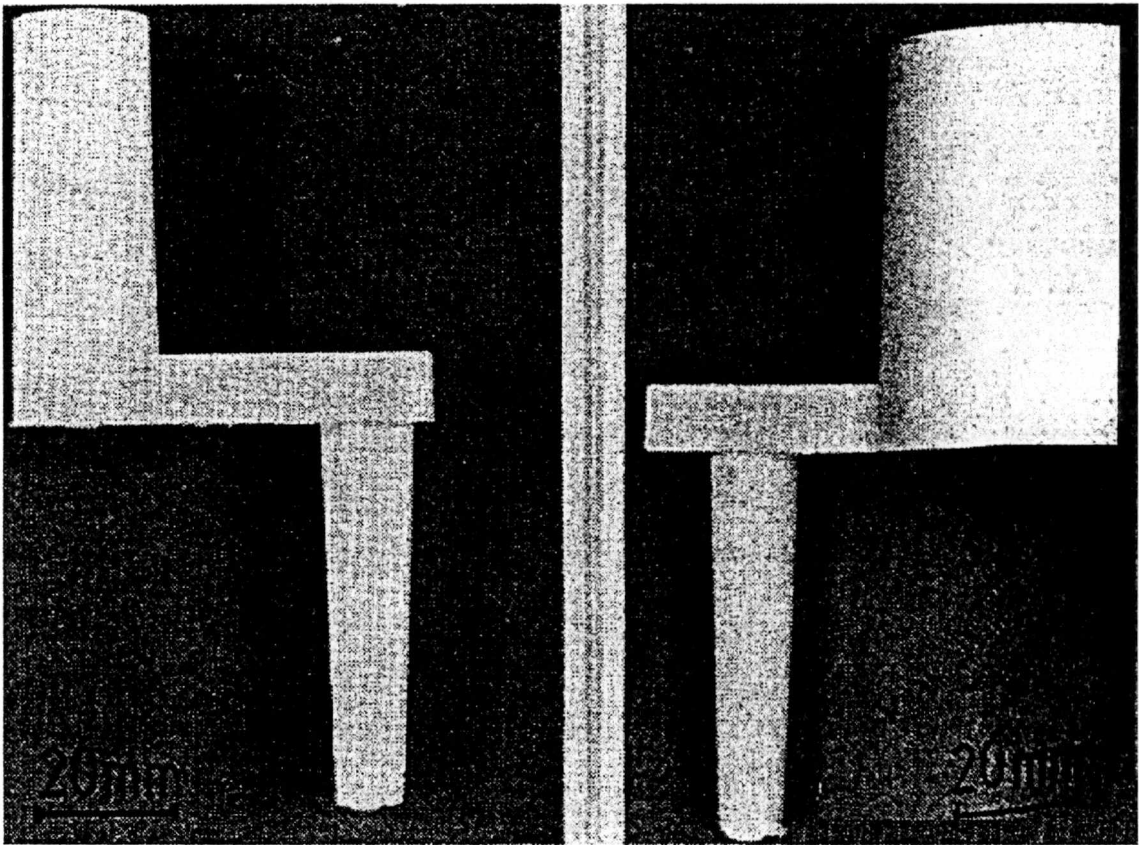


Figure 12. Side-gated cylindrical moldings⁹.

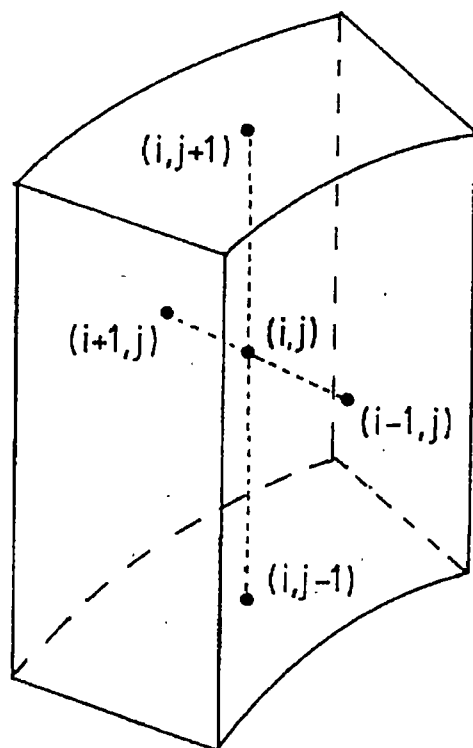


Figure 13. Element of the cylinder used for temperature calculations ⁹.

Table 1. Comparison of Calculated Axis Temperatures for a Long Cylinder by Finite Difference and Analytical Methods ⁹.

Time (s)	Axis Temperature (°C)	
	Numerical Method	Analytical Method
10	208.3	209.0
20	192.0	191.4
30	164.4	162.3
40	136.6	134.2
50	112.8	110.7
60	93.4	91.7
70	78.0	76.6
80	65.8	64.6
90	56.0	55.2
100	48.4	47.7

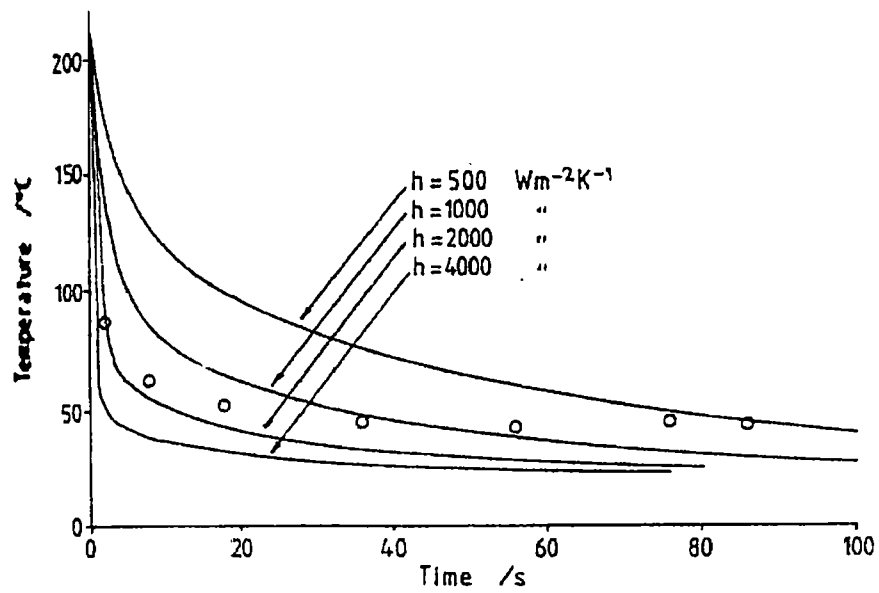


Figure 14. Surface temperature of 20-mm cylinders for a mold temperature of 20°C for various values of heat transfer coefficient. Experimental points are superimposed ⁹.

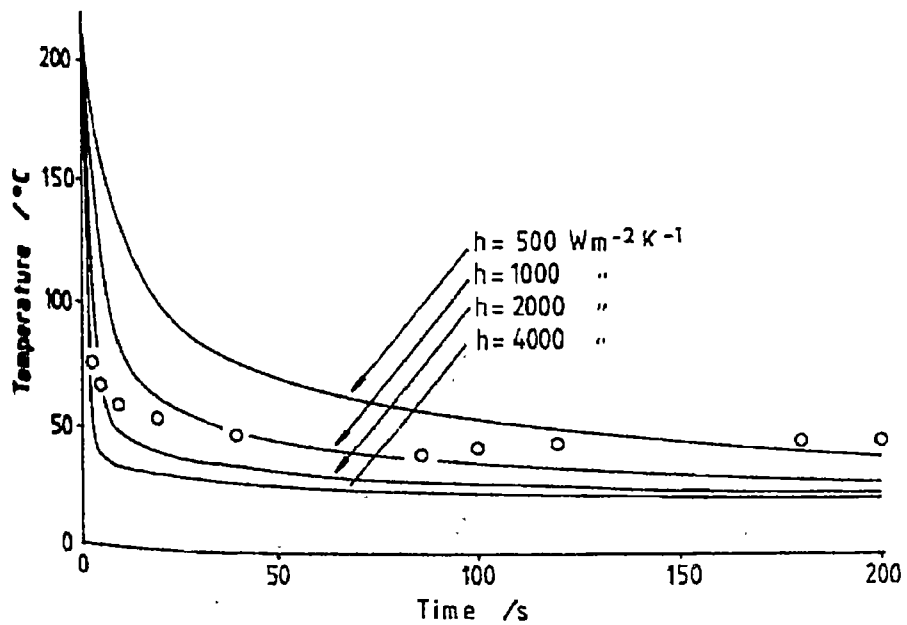


Figure 15. Surface temperature of 40-mm cylinders for a mold temperature of 20°C for various values of heat transfer coefficient. Experimental points are superimposed ⁹.

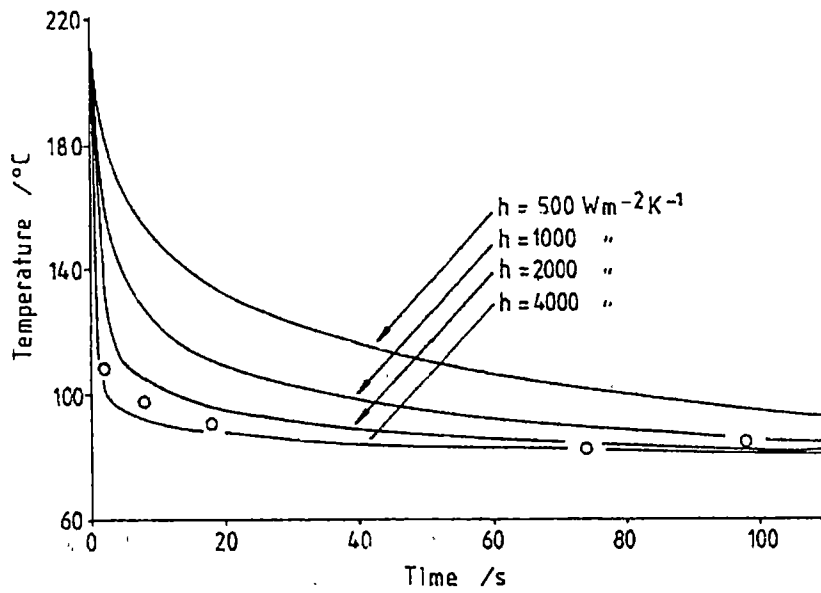


Figure 16. Surface temperature of 20-mm cylinders for a mold temperature of 80°C for various values of heat transfer coefficient. Experimental points are superimposed⁹.

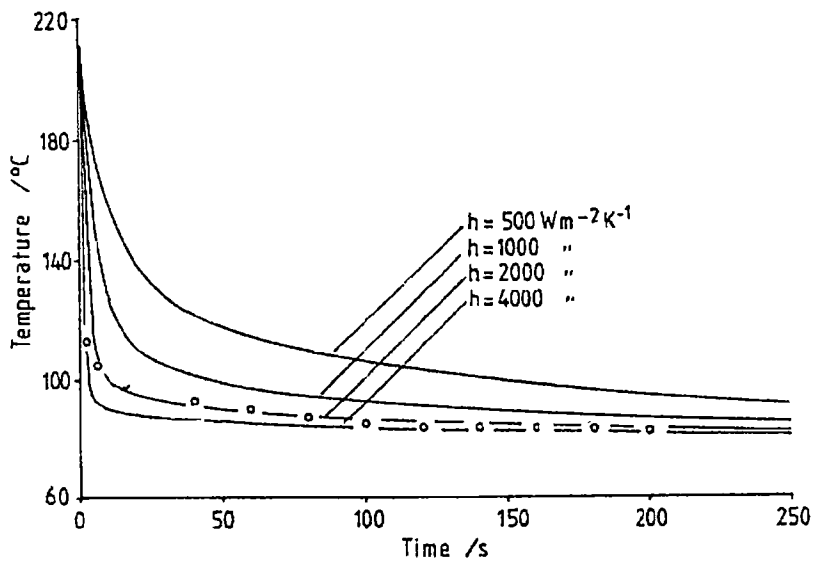


Figure 17. Surface temperature of 40-mm cylinders for a mold temperature of 80°C for various values of heat transfer coefficient. Experimental points are superimposed⁹.

Wang, Carr, and McCabe ¹⁴ demonstrated that injection pressure, in the powder injection molding process, plays a dominant role in determining the quality of the products. Insufficient injection pressure can cause defects in the injection-molded parts, such as short shots, voids, and density variations, which are unacceptable in the powder injection molding industry. Parts for which the mold does not fill completely are called short shots. They conducted a study of computer simulation of the powder injection molding process to develop a simulation technique to help design engineers understand the physical process, eliminate defects, reduce costs, and improve the quality of the parts. The results from the simulation are validated by comparing with those from the experiments. The actual part geometry used for the test and the approximate part geometry used in their computer simulation study are shown in Figures 18(a) and (b). The total length of the shank is 4.6 cm and the largest diameter of the flange is 3.8 cm. The part is filled from the fin section. For simplicity of computational, the detailed features of the gears on the flange have been approximated by a simple shape as seen in Figure 18(b). The material properties are listed in Table 2. The effective specific heat of the feedstock as a function of temperature is shown in Figure 19 ¹⁴.

Experiments have been conducted to test the predictive capability of the simulation code in modeling the short shot formation. A number of simulation runs have been made to determine the influence of various parameters, so that some design guidelines for eliminating short shot formation may be given. For a given melt and die temperature, higher injection pressure will increase the flow rate, and hence reduce the filling time. As a result, flow "hesitation" will be short and the possibility of forming short shots is reduced. This trend is clearly demonstrated by the simulation conditions

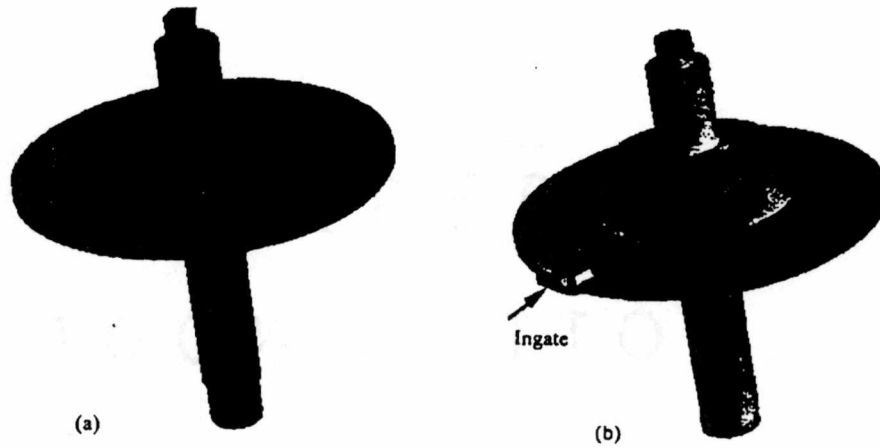


Figure 18. Silhouette of the actual and approximate part geometries used in computer simulation. (a) Actual part geometry (b) Approximate part geometry ¹⁴.

Table 2. Material Properties Used in both Experiment and Simulation ¹⁴.

Material Property	Feedstock	Die
Range of Melting Temperature, °C	40 - 140	
Density, kg.m ⁻³	5000	7800
Specific Heat, kg ⁻¹ °C ⁻¹	(Shown by Figure 19)	460
Thermal Conductivity, J sec ⁻¹ m ⁻¹ °C ⁻¹	1.7	33

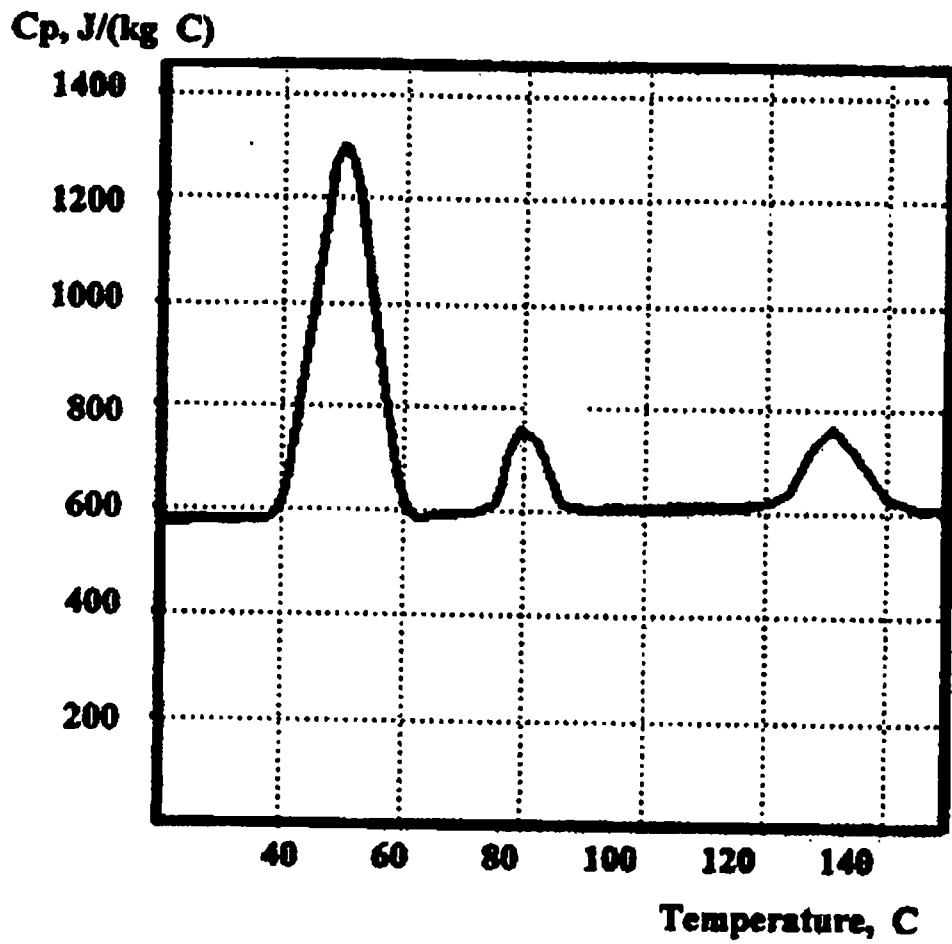


Figure 19. Effective specific heat of the feedstock as a function of temperature ¹⁴.

shown in Table 3 and the simulation results shown in Figure 20¹⁴. Figure 20(a) shows that with an injection pressure of 3 MPa, the larger portion of the fin section is not filled. When the injection pressure is increased as shown in Figure 20(b), the short shot problem is reduced.

Injection and die temperatures are also significant factors to the short shot formation. For a given injection pressure and die temperature, higher melt temperature results in a longer freezing time, and reduce the short shot formation. This improvement can be seen in Figure 21 with the simulation conditions shown in Table 4.

The results of the simulation program are in close agreement with a demonstration part molded to illustrate short shot formation. The simulation program predicts that short shot formation may be minimized by increasing injection pressure or melt temperature to reduce “hesitancy” and eliminate pre-mature freezing.

According to Zhang and Evans⁹, “The injection molding of large ceramic sections by conventional methods involves unsteady-state cooling, and the progress of solidification is accompanied by the decay of pressure in the molten core. An array of defects may therefore be generated during solidification. In some cases these defects may not become apparent until the organic binder has been removed and the body sintered”.

Zhang, Edirisinghe, and Evans¹⁵ described twenty two types of defects found in injection molded technical ceramics produced with thermoplastic binders and explained the reasons for the formation of the defects. These defects include:

- Undispersed agglomerates
- Undispersed polymer

Table 3. Simulation Conditions Applied in Figure 20 ¹⁴.

Melt Temperature	130°C
Die Temperature	25°C
Injection Pressure	
Figure 20(a)	3.0 MPa
Figure 20(b)	5.0 MPa

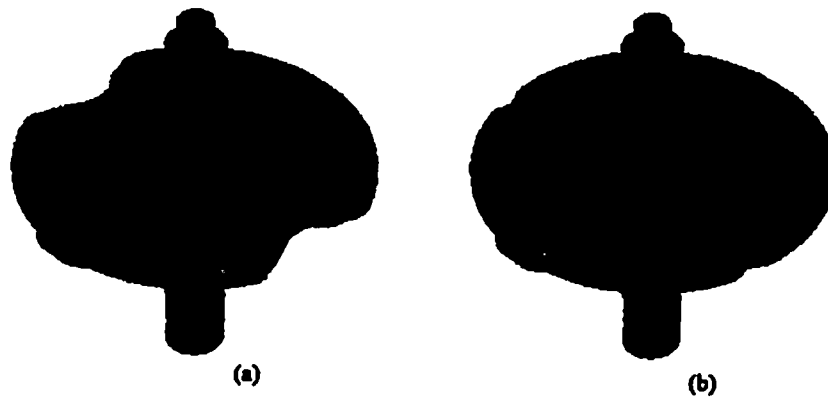


Figure 20. Silhouette of the numerical simulation results for two different injection pressures showing formation of short shots. (a) Injection pressure = 3 MPa (b) Injection pressure = 5 Mpa ¹⁴.

Table 4. Simulation Conditions Applied in Figure 21 ¹⁴.

Melt Temperature	3.0 MPa
Die Temperature	25°C
Melt Temperature	
Figure 21(a)	130°C
Figure 21(b)	140°C

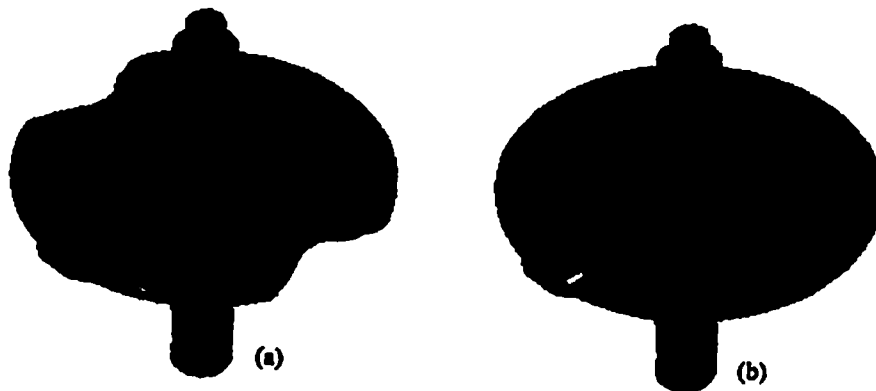


Figure 21. Silhouette of the numerical simulation solutions for two different injection melt temperatures showing that short shot defects are eliminated with increasing injection melt temperature. (a) Injection melt temperature of 130°C (b) Injection melt temperature of 140°C ¹⁴.

- Abrasive contamination
- Contamination from machinery and atmosphere
- Weld lines
- Short shots
- Voids caused by adsorbed water
- Shrinkage voids
- Shrinkage cracks
- Mold ejection defects
- Blistering on mold release
- Delayed failure
- Contamination from the molding machine
- Deformation caused by residual stress relaxation
- Cracking before the softening point is reached
- Bloating
- Slumping
- Cracking caused by thermal degradation of the binder
- Cracks caused by non-uniform polymer removal
- Cracks caused by gravitational effects
- Skin effects
- Residue

The successful development of the ceramic injection molding sequence relies on the careful observation of defects and the diagnostic isolation of their causes. Frequently this involves a stepwise experimental procedure in which processes are interrupted before completion. The major defects associated with the preparation of ceramic molding blends and with mold filling and solidification have to be investigated and their causes understood.

As observed in the discussions in this chapter, the injection pressures and the interfacial heat transfer coefficient, h , at the mold wall play a dominant role in the flow and the solidification of the material in the injection molding processes. It was found that the short shot formation may be minimized by increasing the injection pressure or melt temperature to reduce “hesitancy” and eliminate pre-mature freezing. The interfacial heat transfer coefficient is a function of both material properties and flow properties. It was also found that at low injection pressures, h varies with time as the molded body shrinks away from the wall, but at high injection pressures h can be treated as constant throughout the solidification stage.

CHAPTER 4

PROBLEM STATEMENT

Howmet Corporation would like to increase the yield of green ceramic core parts made by ceramic injection molding process at their Morristown plant. The high injection pressure, the high viscosity of the ceramic/wax mixture and the high injection velocity result in high rate of erosion, or wear, of the internal surfaces of the die. The resurfacing of eroded surfaces of core dies is very costly. It is desirable to increase the productivity of the ceramic injection molding process and at the same time cut back the maintenance costs by evaluating the process performance with computer modeling and simulation to identify means to reduce these problems. In order to achieve this goal, a computer model to be developed to simulate a three-dimensional transient ceramic/wax injection molding process including filling and solidification.

A computer simulation model of the ceramic injection molding process was first done by Strack, Satterfield, and Zeghami ¹⁶ in 1998 in the Advanced Casting Simulation and Mold Design Laboratory at the University of Tennessee; and was later studied by Eric Robbins ¹⁷ in 1999. It is believed that improved predictions over prior models can be achieved through modifications to heat transfer coefficient values. The geometric model of Strack, Satterfield, and Zeghami ¹⁶ with some minor geometric changes will be used in present study. Additionally, to reduce the computational time, a coarser mesh will be used with about half the number of nodes and elements used by Robbins¹⁷. This reduced size model will be used to study the influence of heat transfer coefficient on filling and solidification of the ceramic-wax mixture. Specifically, the following heat

transfer coefficient functions will be considered:

- (a) Constant heat transfer coefficient (h) values of 1400, 1800, and 2200 W/m² K:

These values will enable comparison of the results of the present model with predictions by Robbins¹⁷ and the temperature measurements of Ly²² to determine the effect of mesh-size reduction on filling patterns and temperature distributions.

- (b) Step function for the heat transfer coefficient: This rather simplified model represents a sudden formation of an air gap when the fluid temperature drops below its solidus temperature and the material begins to shrink and breaks away from the mold surface resulting in a sudden drop in the heat transfer coefficient.

- (c) Ramp function for the heat transfer coefficient: This model accounts for a gradual development of an air gap when the fluid temperature drops below its solidus temperature resulting in a linear drop in the heat transfer coefficient

- (d) Variable inlet pressure condition together with ramp function for heat transfer coefficient to model the actual inlet pressure distribution measured by Howmet under production conditions.

CHAPTER 5

MODEL DEVELOPMENT FOR COMPUTER SIMULATIONS

5.1 Introduction

The computer modeling of the injection molding process of a ceramic core was performed in the Advanced Casting Laboratory at UTK. This study addresses filling problems associated with the injection molding of ceramic in the mold and to validate the computer modeling of the ceramic injection process using ProCAST by comparing the modeling results with the experimental data collected by Lewis¹⁸. As mentioned earlier, both the core and the die can be modeled together as a single part with material interfaces between them or they can be modeled individually.

Howmet Casting Support in Morristown, Tennessee has considered the control of the process variables such as velocity, pressure, and temperature. If the steel die is included in the computer model, the total numbers of nodes and elements would rapidly increase resulting in a longer computational time. Secondly, and more importantly, when the die is included together with the ceramic core, there would exist several interfaces between the die and the ceramic core. The heat transfer boundary condition for these interfaces must be assigned prior to the computer simulation. However, these heat transfer coefficients are not a priori known from the ceramic material properties. Furthermore, mass of the die is much greater compared to the mass of a green ceramic core and the filling cycle of the injection is short, therefore the change of temperature of the die is small compared to that of the part and therefore the temperature of the die can

be assumed to be constant. For these reasons, only the ceramic core itself will be modeled in this study.

The software packages that were used in this study from solid model development to thermal-fluid analysis are SolidWorks and ProCAST. A flowchart of the computer modeling process is shown in Figure 22.

5.2 Solid Model Development of SolidWorks

SolidWorks[®] is mechanical design automation software that takes advantage of the familiar Microsoft[®] Windows[™] graphical user interface. This easy-to-learn tool makes it possible for mechanical designers to quickly and accurately sketch out ideas, experiment with features and dimensions, and produce models and detailed drawings¹⁹. The first phase of the whole procedure of this study involved creating a 3-D, solid model of the ceramic core. A 3-D geometry of the ceramic core was built in SolidWorks[®] in spring 1998 by Satterfield, Strack, and Zeghami¹⁶ in the Advanced Casting Simulation and Mold Design Laboratory at the University of Tennessee, Knoxville and is shown in Figure 23.

The dimensions of the actual ceramic core supplied by Howmet Corporation were measured using a dial caliper and micrometer. It should be noted that some inconsistencies existed between the real part and the model due to the difficulty in measuring some of the areas with the available instruments. Several intricate features that existed on the original ceramic core were deemed as negligible and not included in the solid model. These features were considered to have negligible effect on the flow of

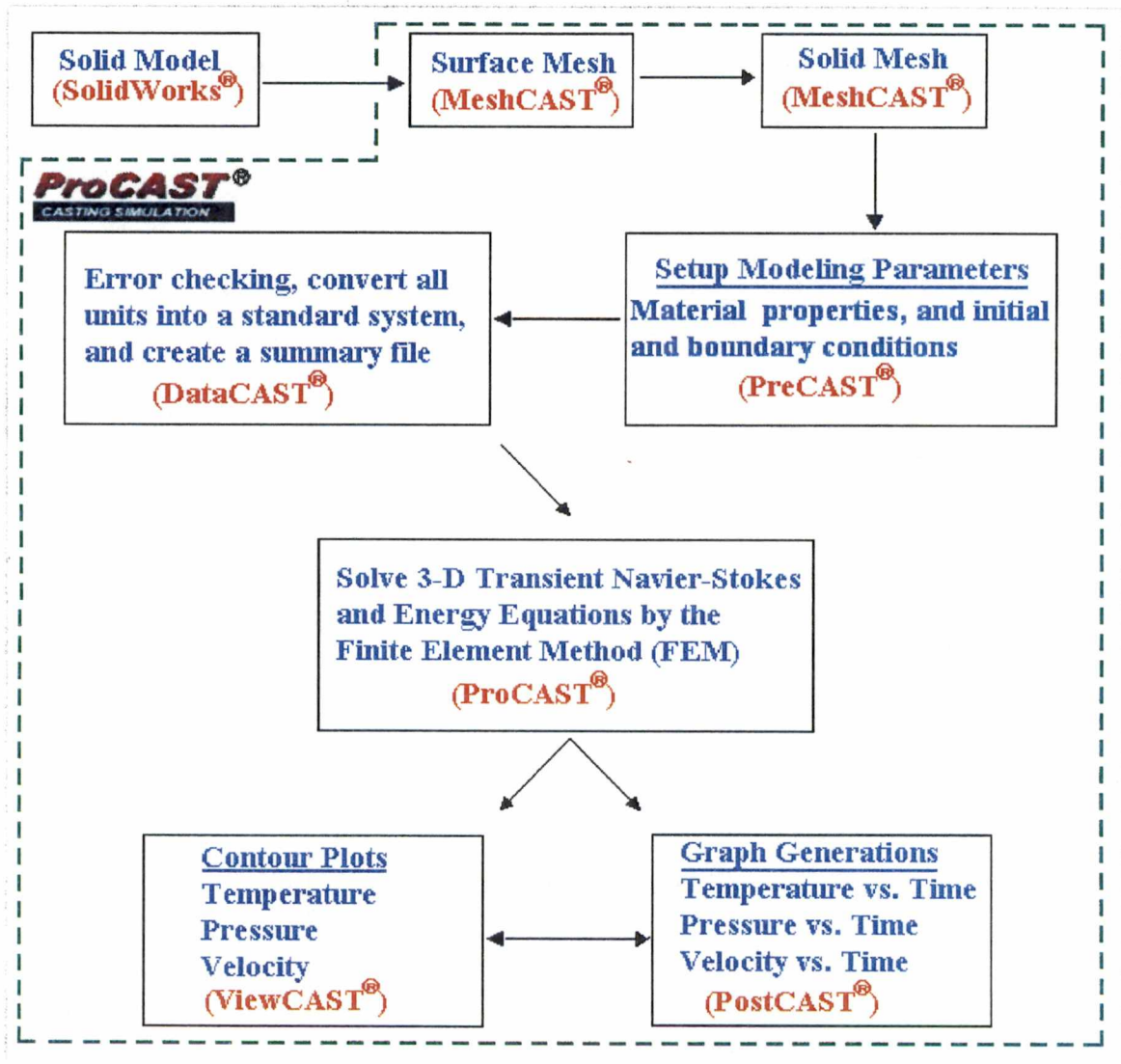


Figure 22. A flowchart of the computer modeling process.

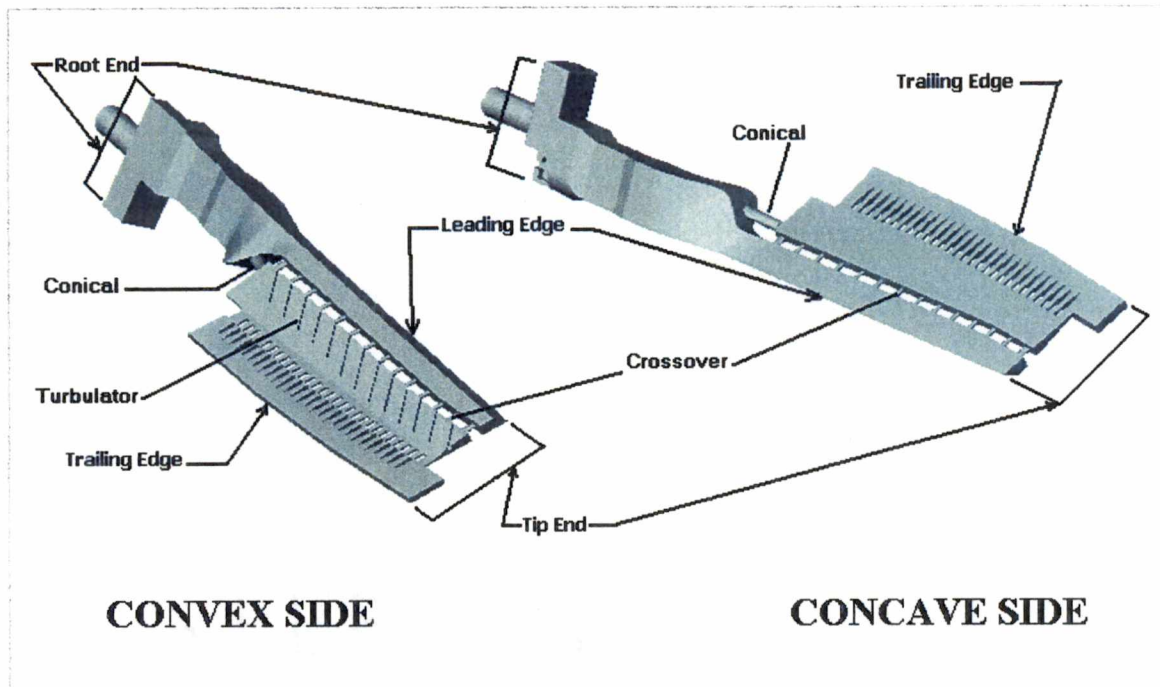


Figure 23. A 3-D solid model of the ceramic core built in SolidWorks®.

material and key thermal features in the problem and were ignored in the computer simulation¹⁶. Furthermore, the inclusion of these intricate features would have significantly increased the number of nodes and elements of the model, which in turn would result in longer computational time. More details of constructing the 3-D of the ceramic model can be found in reference 16. For proprietary reasons, the geometric details of the ceramic core part are not displayed in figures presented in this study. The 3-D solid geometry of the ceramic core constructed by Satterfield, Strack, and Zeghami¹⁶ was used, with some minor changes, in this study. The 3-D solid model of the ceramic core geometry has a surface area of 10.65 in² and a total volume of 0.40 in³.

5.3 Mesh Generation with MeshCAST

The next stage of the computer simulation procedure was the meshing of the solid model of the ceramic core using MeshCAST. MeshCAST²⁰, as the name implies, generates a 3-D tetrahedral mesh of a solid model using the Finite Element Method. A triangular surface mesh of the model is the prerequisite for MeshCAST's "tet mesh" generation. MeshCAST²⁰ is a powerful engineering, design and analytical tool. Some of the features which contribute to the strength MeshCAST include:

- Flexibility
- Rapid mesh generation
- Robust repair and manipulation tools
- Extensive model checking
- The ability to process and produce a variety of input and output file formats.

As seen in Figure 22, the meshing of the solid model of the ceramic core is done in two steps: first a surface mesh is created and, then, this mesh is used to create the solid mesh (or internal mesh).

5.3.1 Surface Mesh of the Core

The geometry of core saved in IGES file format is imported from a local PC system to a remote workstation operating in Unix operating system where ProCAST software package is installed. MeshCAST can process geometries stored in the IGES, PARASOLIDS, or STL formats. The surface mesh of a solid model is the foundation for generating the internal mesh of that model. So, the surface mesh of a model is a very

important part in a thermal-fluid finite element study, thus care must be taken during this surface meshing step. MeshCAST can generate surface meshes, which have different densities on specific surfaces in the model. In this step the Surface Mesh component of MeshCAST is used to group specific edges and/or surfaces and specify unique length values for each group. The Surface Mesh component uses these unique length values to generate the surface mesh. As mentioned earlier, the surface mesh is the foundation of the internal mesh because the number of nodes and elements of the surface mesh will directly control the density of the internal mesh. If the surface mesh is very fine (small mesh size), then the density (nodes and elements) of the internal mesh will increase. This will yield more detailed and accurate results from the computer simulations. However, there is a tradeoff. That is, the benefits of increased detail and accuracy of the computer simulation results also come at a cost of longer computational time. Furthermore, the thermal and fluid equations are solved at each node simultaneously; therefore, the larger the number of nodes and elements of the mesh will result in a longer computational time. If the surface mesh size of the solid model is coarse, the computer simulation results will be less accurate. With this knowledge in mind, when creating the surface mesh for the solid ceramic core model in this study, special attention was paid to the mesh element size. The surface mesh element size was varied depending on the location and size of the different surfaces of the core. The trailing edge has the smallest cross sectional area; therefore the mesh elements at this location were assigned the smallest size. Sizes of the mesh elements were gradually increased from the smallest to the largest cross sectional areas. The mesh element sizes in the triangular pattern ranged from 0.01 inches at the trailing edge connectors to 0.05 inches at the root of the core. The resultant surface mesh

of the ceramic core had 24,372 nodes and 48,908 elements. Overall view of the surface mesh of the ceramic core is shown in Figure 24.

5.3.2 Solid Mesh of the Core

After the surface mesh of the core was created, a 3-D solid (or internal) mesh of the core could begin. In this step, MeshCAST generates the 3-D tetrahedral mesh of the solid core model automatically from the triangular surface mesh of the core model. One consideration addressed while building the solid mesh was avoiding the dead zones in the thin-walled regions. Dead zones are regions where interior nodes do not exist between two opposite boundary nodes although there would be material flow between them. The minimum numbers of nodes in the thin-walled regions are at least three or more in order to avoid the dead zones in those regions. The internal mesh of the solid model of the ceramic core was generated with an aspect ratio of 1. Aspect ratio is a function in MeshCAST that controls the length of the tetrahedral elements generated during the internal mesh. In most cases increasing the aspect ratio will reduce the quality of the internal mesh. After the solid mesh of the core was completely generated, the total nodes increased to 51,115 and the total elements were 227,233 compared to 116,337 nodes and 554,880 elements from model of Robbins ¹¹. At this point, the model may still contain elements having negative Jacobians. The “SMOOTH” and “MINIMIZE” commands in MeshCAST were used to eliminate those errors. An example of the surface mesh of the trailing edge of the core is shown in Figure 25.

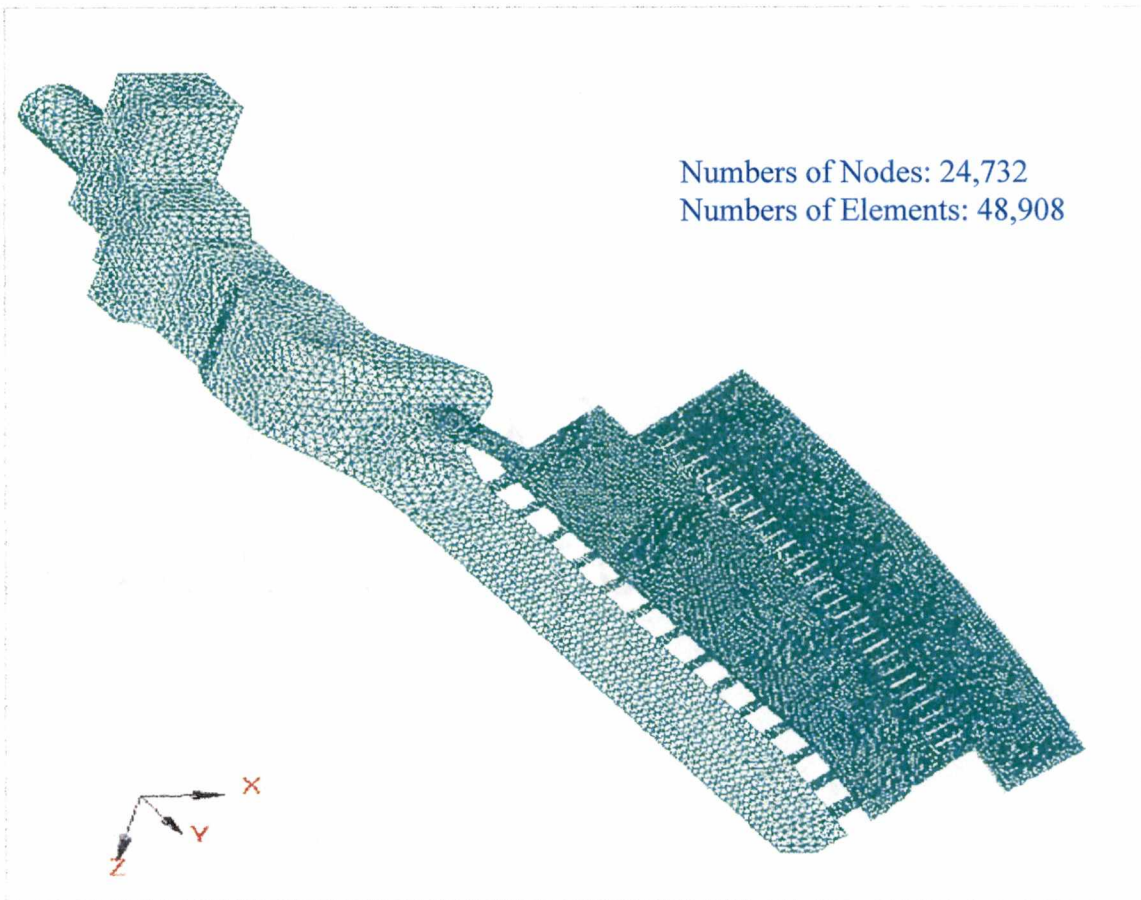


Figure 24. Overall view of the surface mesh of the ceramic core.

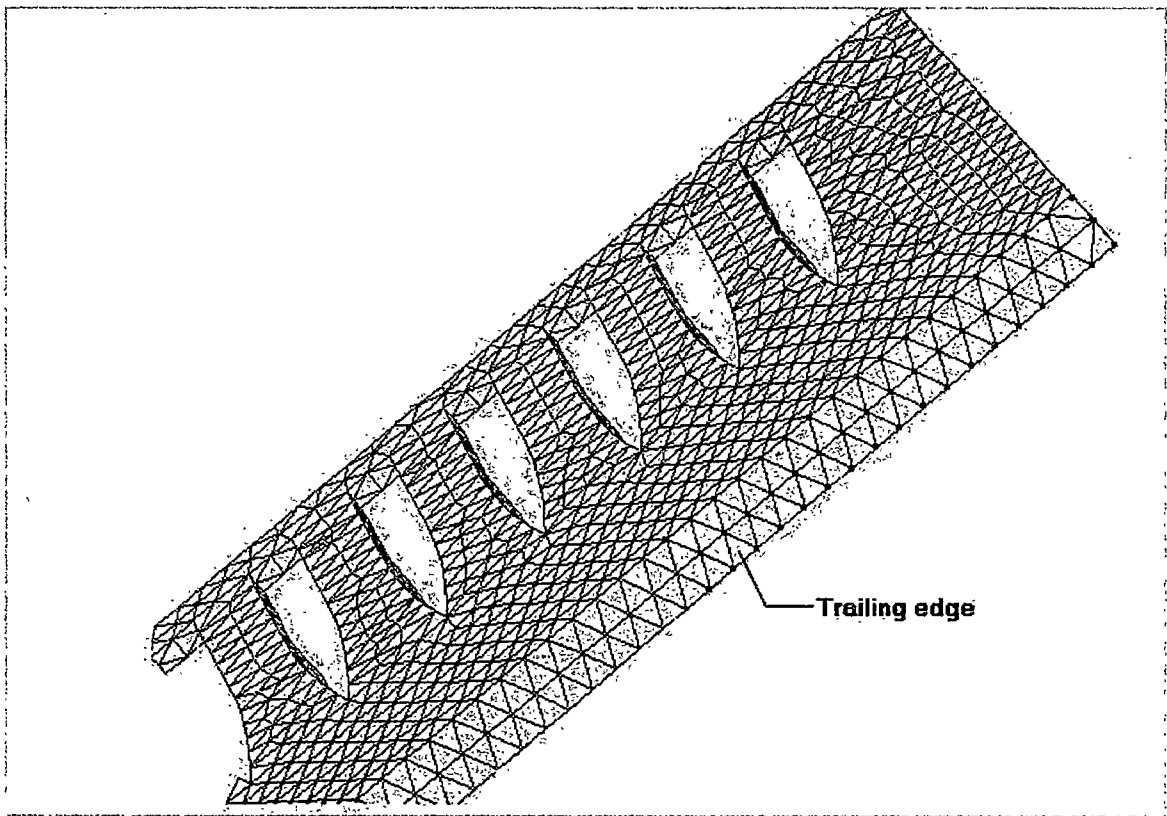


Figure 25. Surface mesh of the trailing edge of the core.

5.4 Thermal-Fluid Model Development

Once the surface mesh and the internal mesh of the solid ceramic model were successfully generated, the next step in the computer simulation procedure is to set up the specification of the thermal-fluid problem with PreCAST, a software package of ProCAST.

5.4.1 Setting All Necessary Parameters for Computer Simulation

PreCAST is used to set-up the thermal-fluid conditions of the problem. This includes specification of material and its thermo-physical properties that are relevant to the problem. Materials, boundary conditions, interfaces, and initial conditions are defined using PreCAST capabilities. Once these components of the model are defined, they may be assigned to specific mesh elements or group of mesh elements.

The material used in this study was a viscous ceramic slurry and wax mixture. The material properties of the ceramic/wax mixture provided by Howmet Corporation were entered into the "MATERIAL DATABASE" library in the PreCAST module for use in the problem setting including solidus and liquidus temperature, viscosity (non-Newtonian), thermal conductivity, density, and specific heat. For proprietary reasons, the material properties will not be disclosed in this thesis. With non-Newtonian flow, the shear rate is a nonlinear function of the strain rate and is represented by the following equation:

$$\tau = \eta \dot{\gamma}$$

where $\dot{\gamma}$ is the strain rate.

Interestingly, ProCAST only models viscous dissipation for the flow of non-Newtonian materials ². It does so through the addition of a dissipation term to the energy equation of the form ²:

$$\phi = 2\eta \left[\left(\frac{\partial \mathbf{u}}{\partial \mathbf{x}} \right)^2 + \left(\frac{\partial \mathbf{v}}{\partial \mathbf{y}} \right)^2 + \left(\frac{\partial \mathbf{w}}{\partial \mathbf{z}} \right)^2 \right] + \left(\frac{\partial \mathbf{v}}{\partial \mathbf{x}} + \frac{\partial \mathbf{u}}{\partial \mathbf{y}} \right)^2 + \left(\frac{\partial \mathbf{u}}{\partial \mathbf{z}} + \frac{\partial \mathbf{w}}{\partial \mathbf{x}} \right)^2 + \left(\frac{\partial \mathbf{v}}{\partial \mathbf{z}} + \frac{\partial \mathbf{w}}{\partial \mathbf{y}} \right)^2$$

The viscosity coefficient, η , of the non-Newtonian material is presented in Carreau-Yasuda form as ²

$$\eta = \eta_{\infty} + (\eta_0 - \eta_{\infty}) \left[1 + \left(\lambda \dot{\gamma} \right)^a \right]^{\frac{n-1}{a}}$$

where

η_0 = zero strain rate viscosity

η_{∞} = infinite strain rate viscosity

λ = phase shift coefficient

a = Yasuda coefficient

n = power law coefficient

The same initial and boundary conditions were used for all simulations performed for this study and they are listed in Table 5. The vent boundary conditions are listed in Table 6. The inlet velocity boundary condition or injection pressure boundary condition and interfacial heat transfer coefficient boundary condition (or film coefficient) are different for each simulation and are listed in Tables 7 and 8. The reasons for specifying

Table 5. Initial and Some Boundary Conditions Common for All Computer Simulations

Initial Conditions	Die Temperature	24°C
	Ambient Temperature	24°C
Boundary Conditions	Inlet Temperature	121°C
	No Slip Velocity	0 in/sec
	Vents	See table 6

Table 6: Summary of Vent Boundary Conditions Common

Diameter	0.01818 in
Length	0.820 in
Roughness	0
Exit Pressure	1 atm

Table 7. Inlet Velocity Boundary Conditions Used in Computer Simulation Cases V-1 through V-5

Simulation Case	Boundary Conditions	
	Inlet Velocity	Interfacial Heat Transfer Coefficient (h)
V-1	130 in/sec	$h = 1400\text{W/m}^2 \text{K}$
V-2	130 in/sec	$h = 1800\text{W/m}^2 \text{K}$
V-3	130 in/sec	$h = 2200\text{W/m}^2 \text{K}$
V-4	130 in/sec	$h = \text{step change function (see Figure 26)}$
V-5	130 in/sec	$h = \text{ramp change function (see Figure 27)}$

Table 8. Injection Pressure Boundary Conditions Used in Computer Simulation Cases P-1 and P-2

Simulation Case	Boundary Conditions	
	Injection Pressure	Interfacial Heat Transfer Coefficient (h)
P-1	See Figure 28	$h = \text{ramp change function (see Figure 27)}$
P-2	See Figure 29	$h = \text{ramp change function (see Figure 27)}$

the step change and ramp change functions for the boundary conditions are discussed in chapter 6. Figures 26 and 27 represent the step change function and ramp change function of the interfacial heat transfer coefficients, respectively. The inlet injection pressure conditions are shown in Figures 28 and 29 for two different computer simulation cases and it should be noted that for convenience the pressure and time scales are presented differently in these figures. With all the initial and boundary conditions defined, the next step is to assign these boundary conditions to individual node or surfaces of nodes using "BOUNDARY" command in PreCAST. Examples of boundary conditions applied to individual node or surfaces of nodes in red color are shown in Figures 30-34. As seen in Figure 31, the inlet velocity boundary condition was applied only to the interior nodes of the injection surface whereas the outer nodes (on the circle) have to satisfy the no-slip boundary condition. The inlet temperature boundary, however,

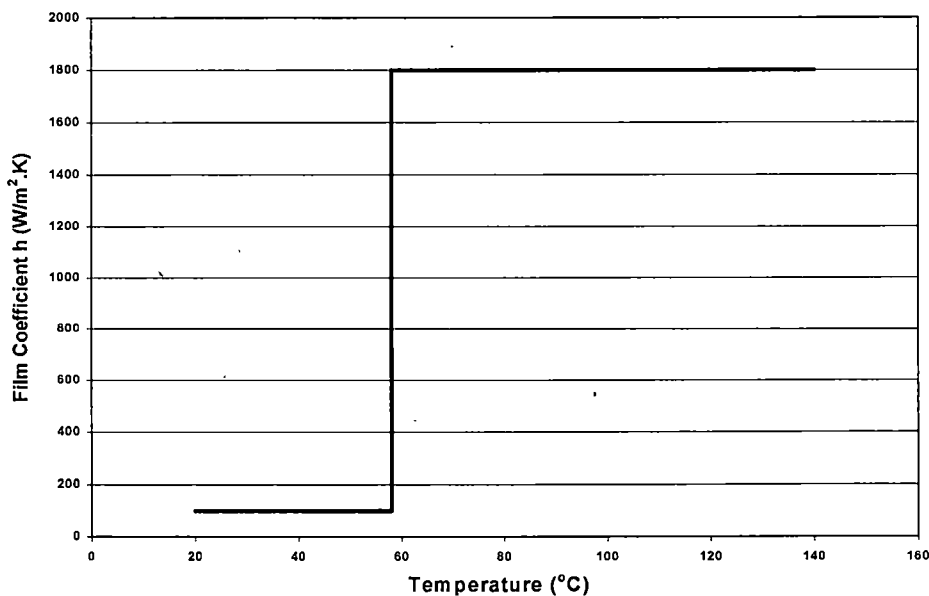


Figure 26. Time step change function of the film coefficient h.

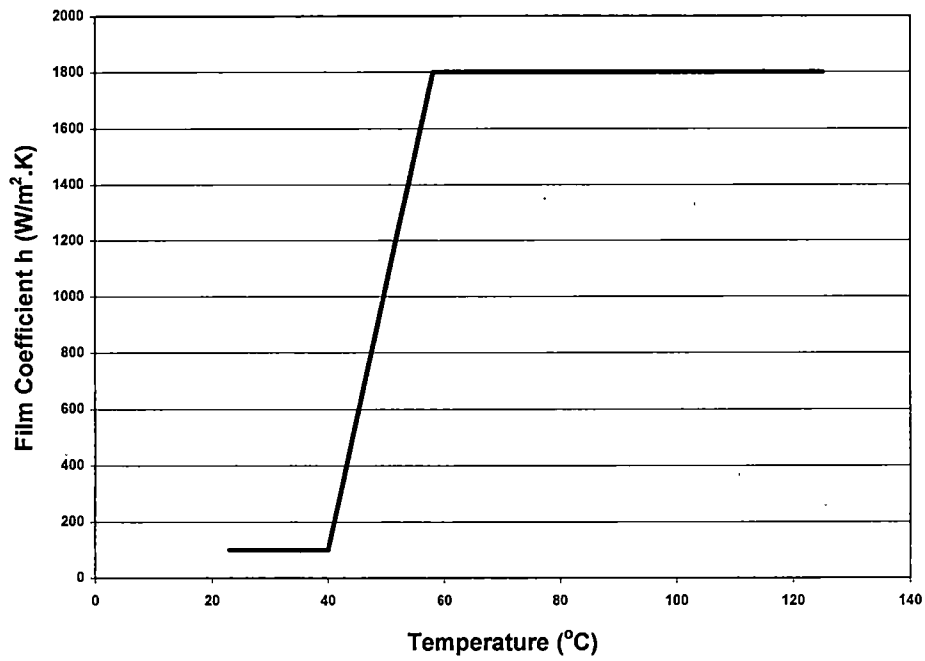


Figure 27. Time ramp change function of the film coefficient h.

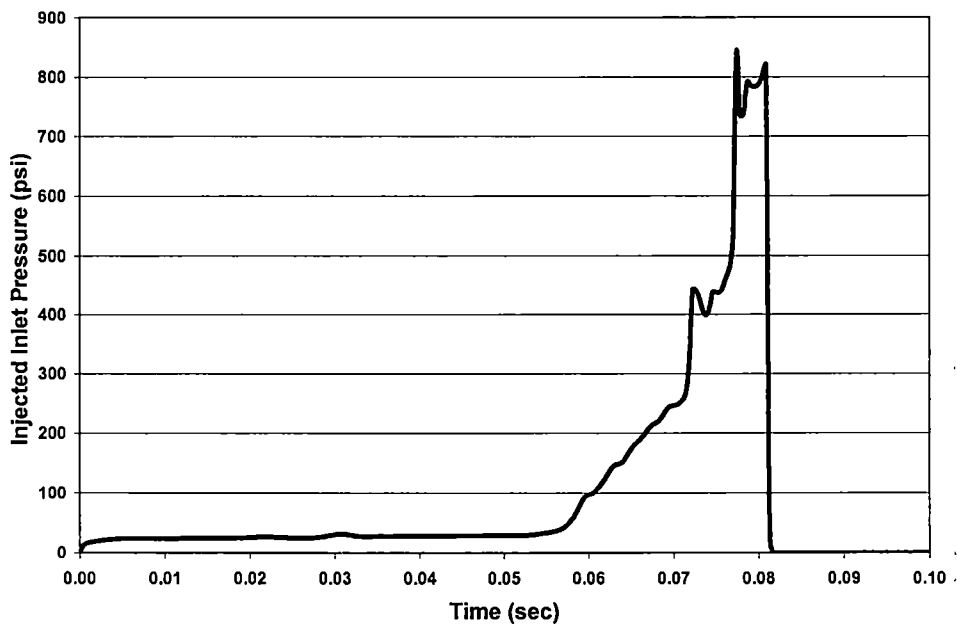
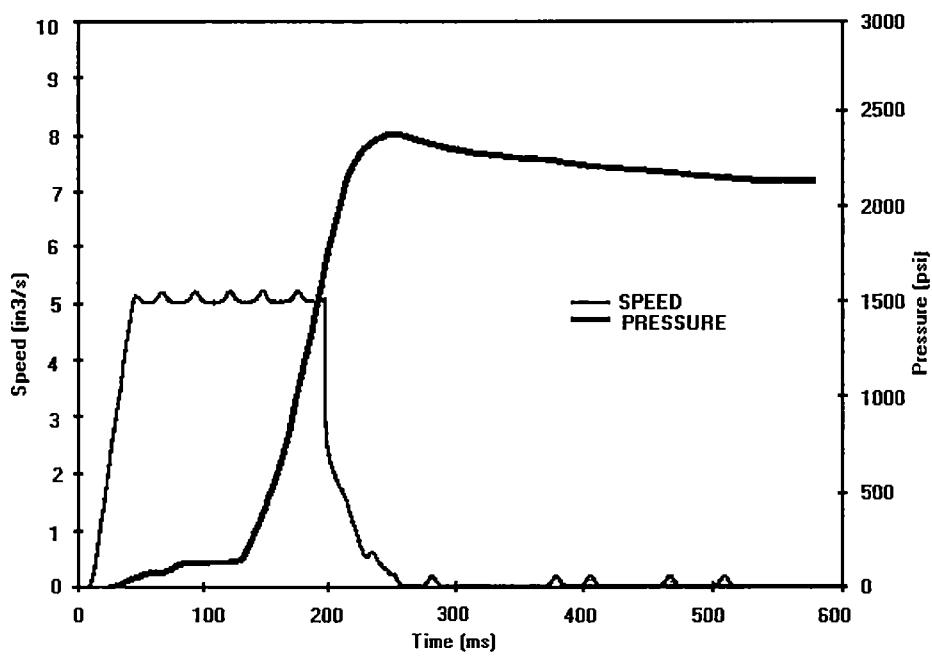


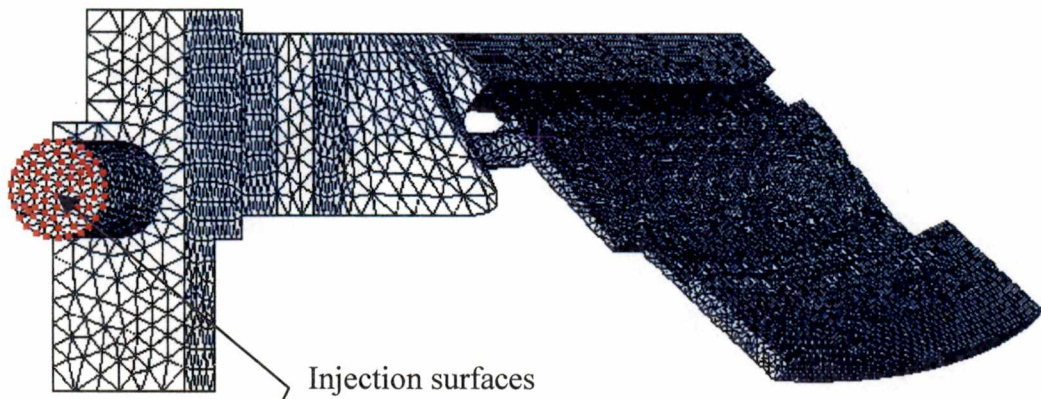
Figure 28. Injection inlet pressure used for computer simulation case P-1.



(Courtesy of Howmet Corporation)

Figure 29. Injection inlet pressure used for computer simulation case P-2.

(a) Overall view



(b) Enlarged view

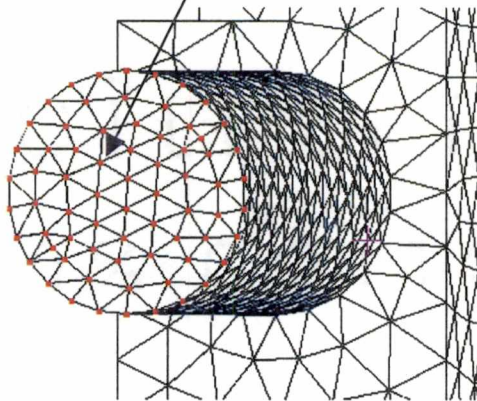
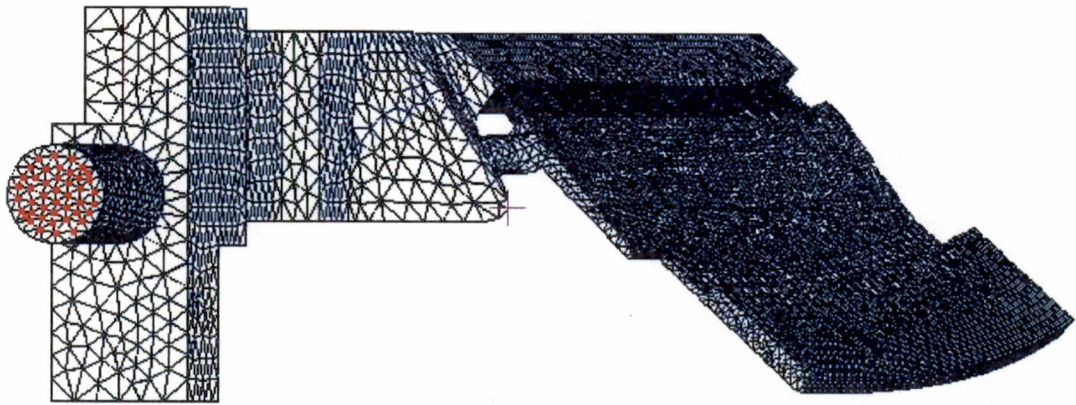


Figure 30. Inlet temperature applied to all nodes of the injection surface.

(a) Overall View



(b) Enlarged View

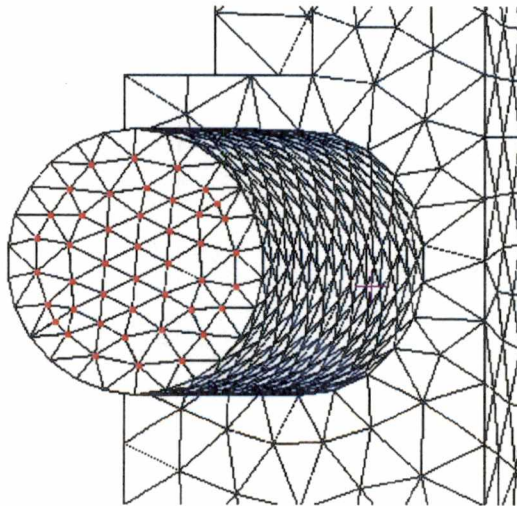


Figure 31. Inlet velocity applied to all interior nodes of the injection surface.

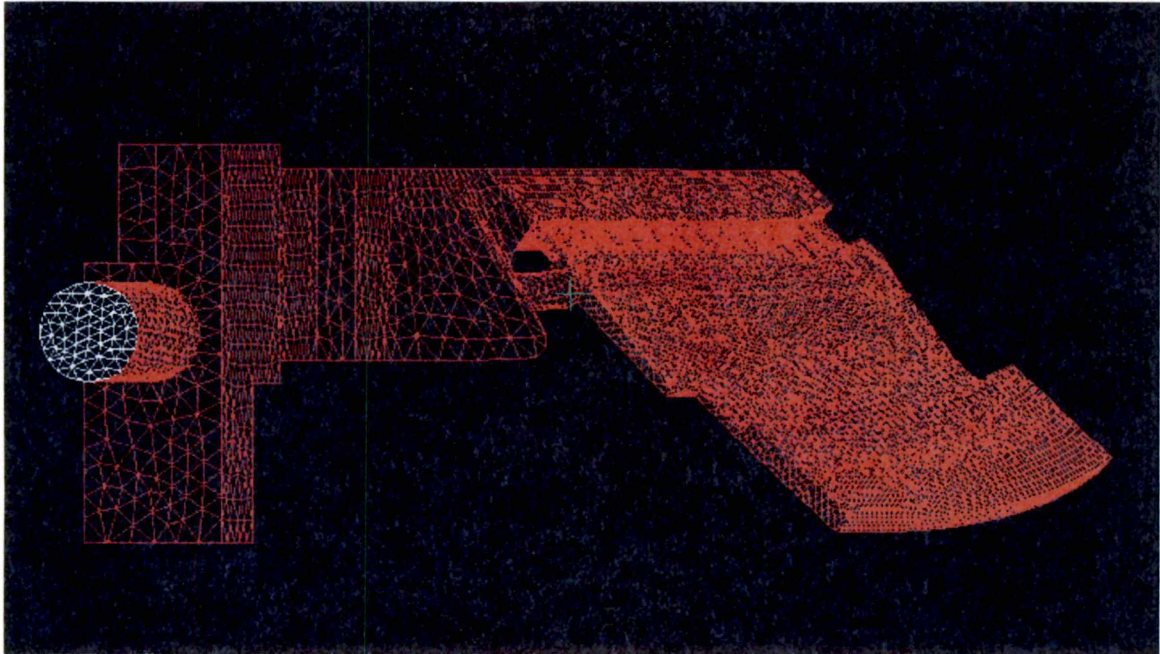


Figure 32. Heat transfer coefficient assigned to all surfaces of nodes except injection surface.

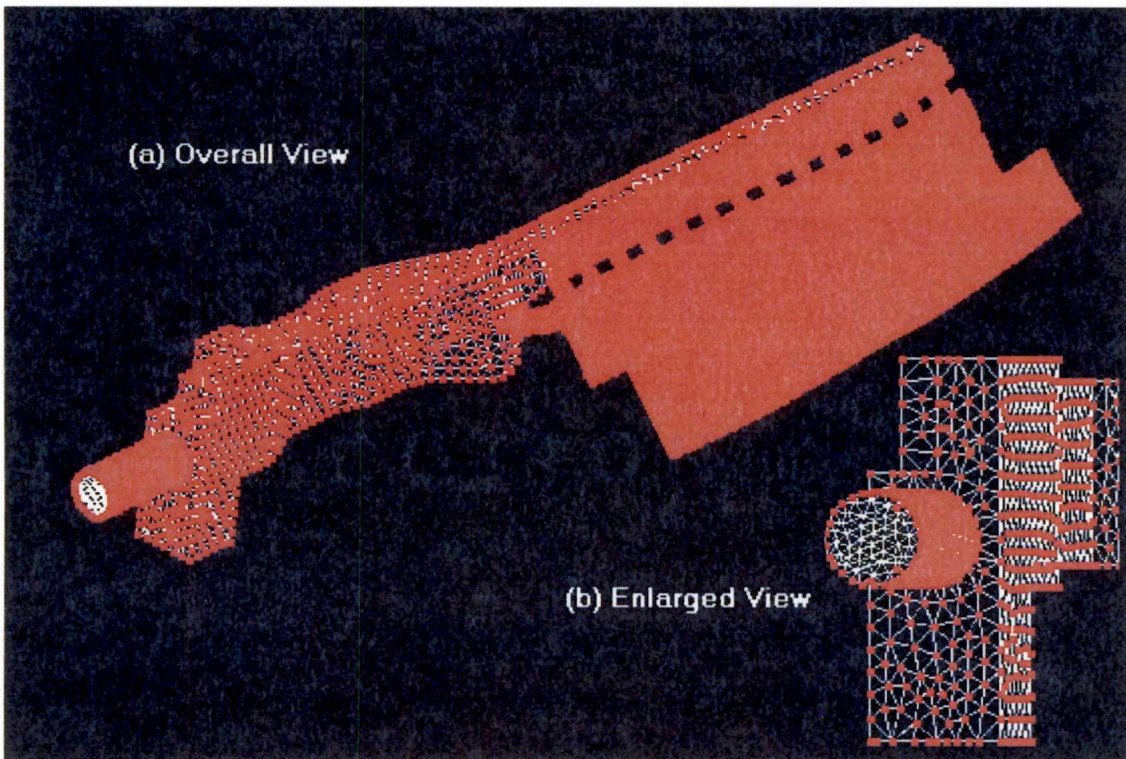
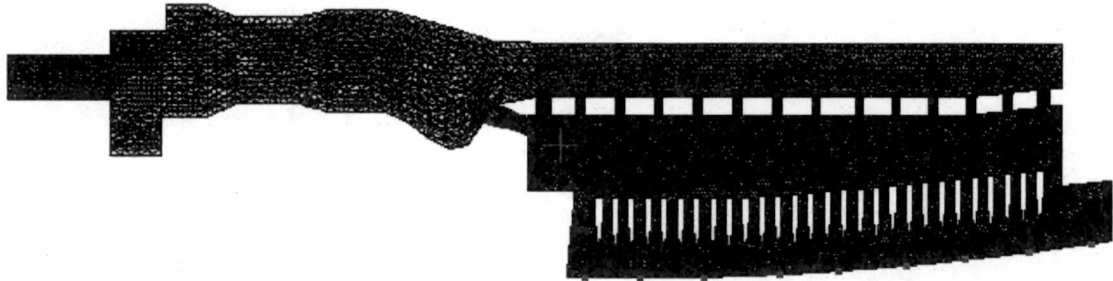


Figure 33. No-slip velocity assigned to all surfaces of nodes except injection surface.

a) Overall View



(b) Enlarged View

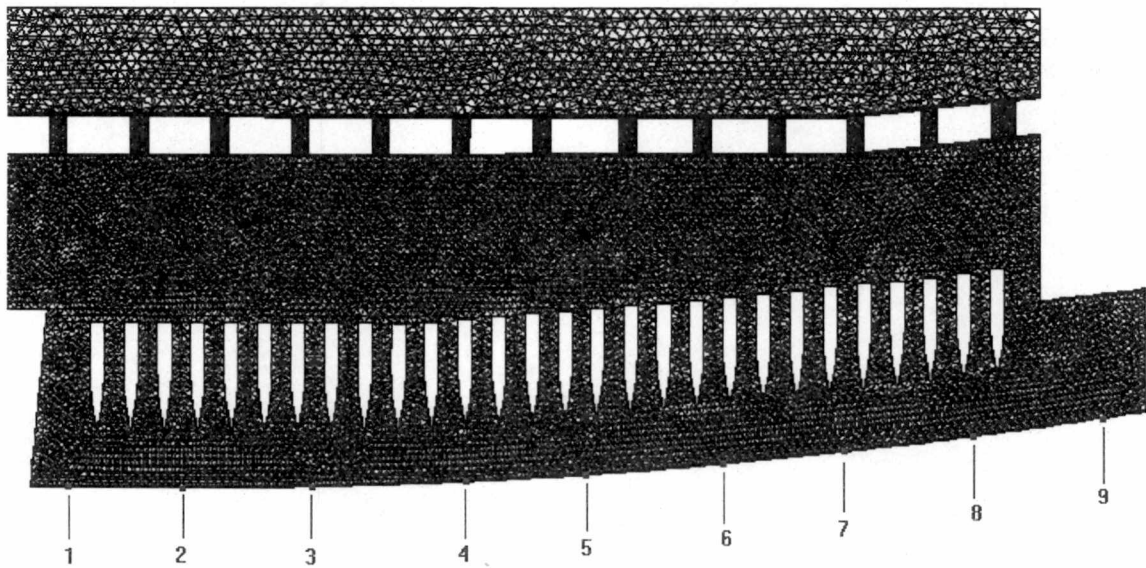


Figure 34. Vent boundary conditions assigned to nodes along the trailing edge at nine locations with properties listed in Table 6.

was applied to the entire injection surface as shown in Figure 30. The default run parameters of PreCAST were used with the exceptions that governing equations are coupled, the model is set to solve fluid equations during filling, but switch over to thermal only analysis when the level surface fill limit is reached, and the data is saved after every time step.

Once all the applicable initial and boundary conditions had been assigned to the nodes and elements in PreCAST, the next step is to check the setup for inconsistencies or other errors.

5.4.2 Error Checking with DataCAST

DataCAST was used after the completion of model setting up in PreCAST. DataCAST, a software module of ProCAST, reviews the total FEA model set-up created in PreCAST. It performs an extensive error checking of the FEA model, and converts all the units into standard CGS. DataCAST also creates a summary file that describes the complete analysis model. When DataCAST has completed its error checking, it creates various binary files, which will be read by ProCAST as the simulation input. If there are no errors, then the model is ready for the ProCAST step.

5.4.3 Performing Simulation Analysis with ProCAST

The software module ProCAST performs the finite element analysis for the computer simulation of the casting process. ProCAST uses the initial and boundary conditions to calculate the physical properties between each internal and external node of the part, solves the coupled governing equation for mass, momentum, and energy, and

then generates the simulation results. In this study, the simulation of the ceramic core model was run on an Ultra 5 Sun Microsystems computer with Unix operating system. The computational time took an average of 35 hours of the CPU time to complete the FEA simulation of the ceramic core model composed of 51,115 nodes and 227,233 elements. There is a small utility program, called ProSTAT, which can be run to report the status of any ProCAST analysis which is currently running or which has completed its processing. ProSTAT will provide information about the simulation which includes: number of time steps completed, total simulated time, current time step size, percent filled, solid fraction, cycle number, elapsed CPU time, and elapsed wall clock time. An example of a ProSTAT Report is shown in Figure 35.

5.5 Post Processing of Results

Once the ProCAST analysis of the ceramic core model is complete, the results can be viewed on the computer in ViewCAST. PostCAST can be used to extract the results of the computer simulations for further analysis and validation with experimental data.

```
NUMBER OF STEPS = 700
SIMULATED TIME = 1948.959473 SECONDS
TIME STEP = 5.000000 SECONDS
PERCENT FILLED = 98.000000 %
SOLID FRACTION = 100.000000 %
CYCLE 1 IS 0.000000 % COMPLETE
CPU TIME = 128069.812500 SECONDS
SYSTEM TIME = 65.180000 SECONDS
WALL CLOCK TIME = 128548 SECONDS
STEP COMPLETED ON Oct 21 2000 AT 23:57:22
```

Figure 35. Example of a ProSTAT Report².

5.5.1 Visualization of Casting Process with ViewCAST

ViewCAST provides the capability to visualize the results of the simulation. ViewCAST generates contour plots of the results based upon the user defined time step intervals. "For example, the temperature contours can be plotted at every time step automatically, giving an animated effect"². ViewCAST enables users to tailor the visualization of results to best suit their analysis requirements by selecting the desired steps, parameters, and materials for viewing. ViewCAST also enables users to select the category of analysis results from ProCAST simulation to be viewed, such as thermal contour, fluid contour, radiation contour, and stress contour, etc. ViewCAST was used to generate thermal and fluid contours in this study. An example of ViewCAST of the temperature contour plot of the casting process of the ceramic core is shown in Figure 36. More thermal and fluid contour plots can be seen in Appendices.

5.5.2 Extraction of Time-Temperature Data from Computer Simulation

PostCAST, another post-processor of ProCAST, was used to graphically display temperature, velocity, pressure, fraction solid, and stress versus time results at any individual node of the solid model. PostCAST provides the post-simulation capability to view X-Y plots, calculate derivative results, and selectively extract data from the simulation results files and format this data for further processing, analysis, and viewing. Time-temperature data extracted by PostCAST at specified locations from the simulation will be used for computer model validation by comparing with the experimental data. Figure 37 shows the selected locations on the ceramic core model that best represent the locations of thermocouples placed on the die cavity, which can be seen in Figure 38, used

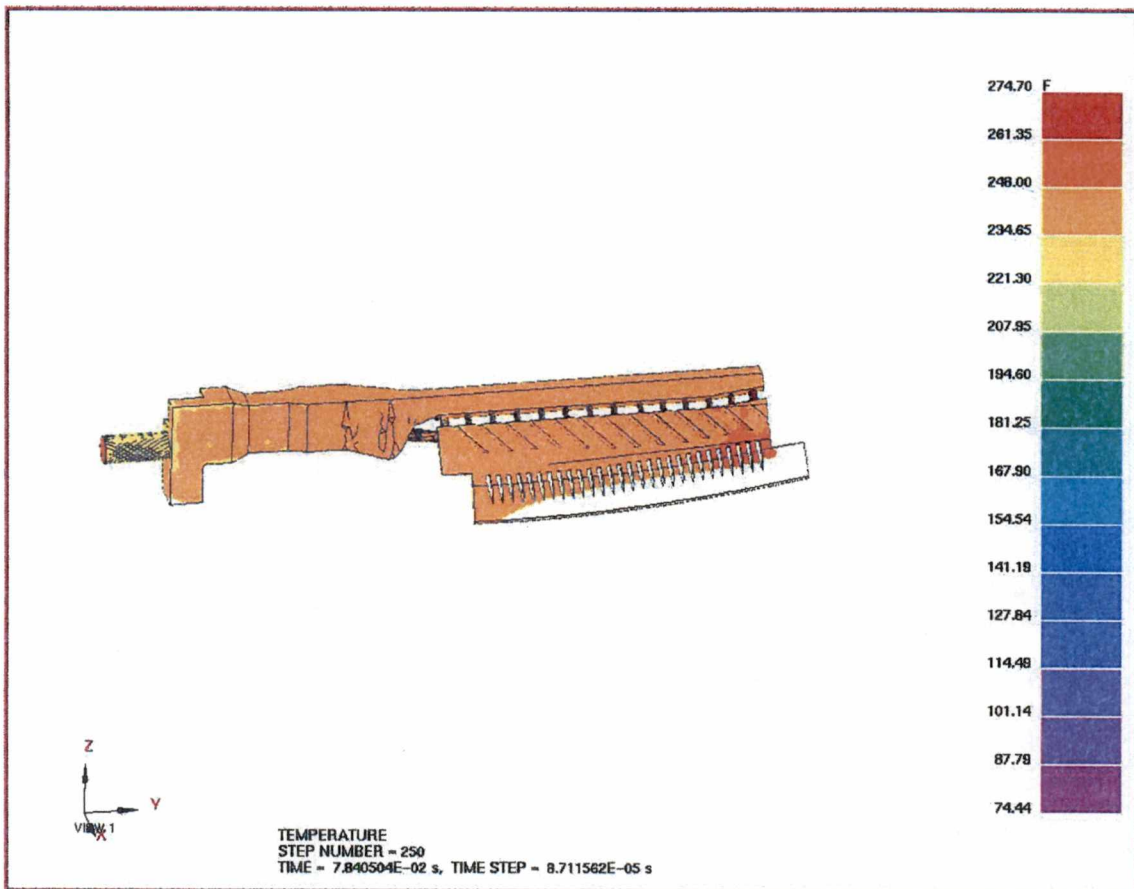


Figure 36. An example of ViewCAST of the temperature contour plot of the injection molding process of the ceramic core.

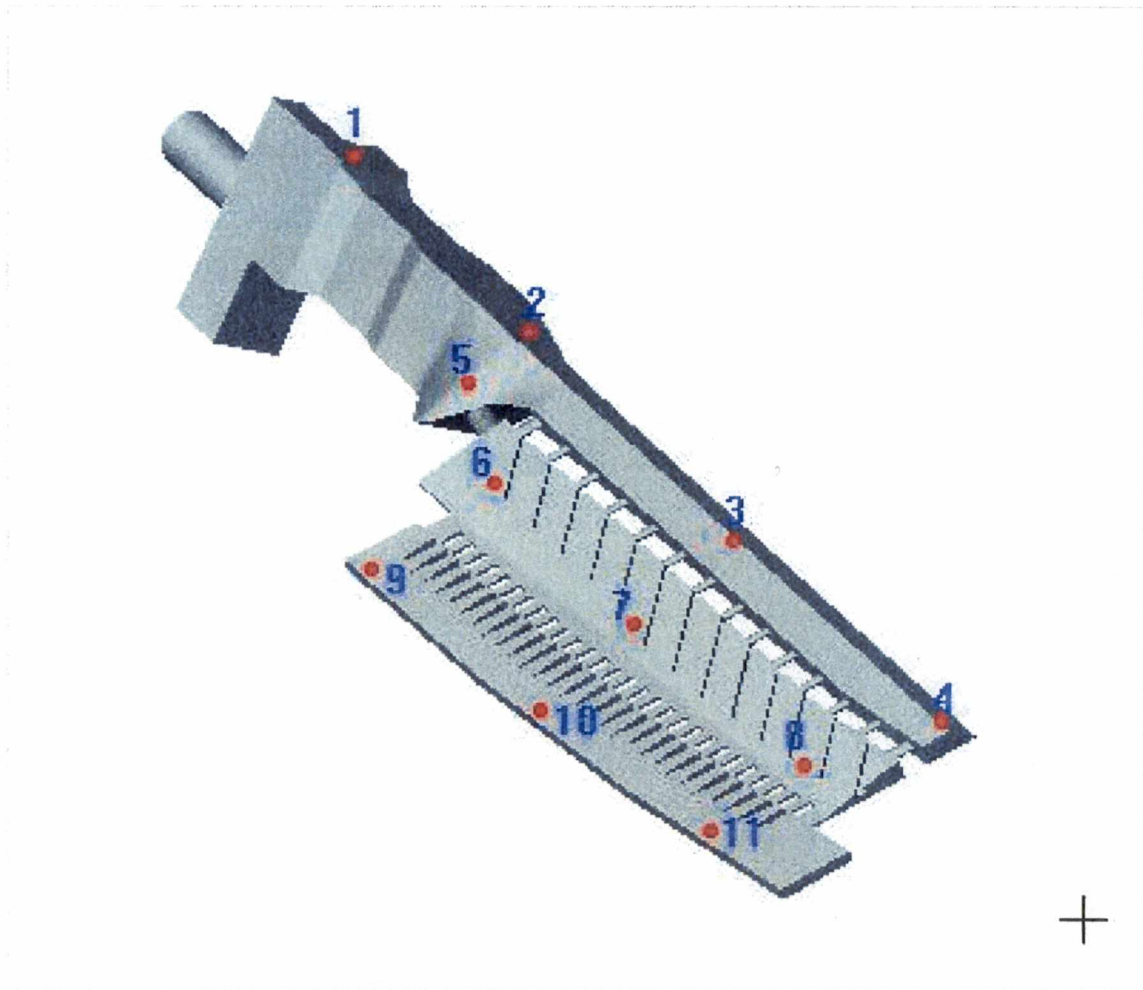
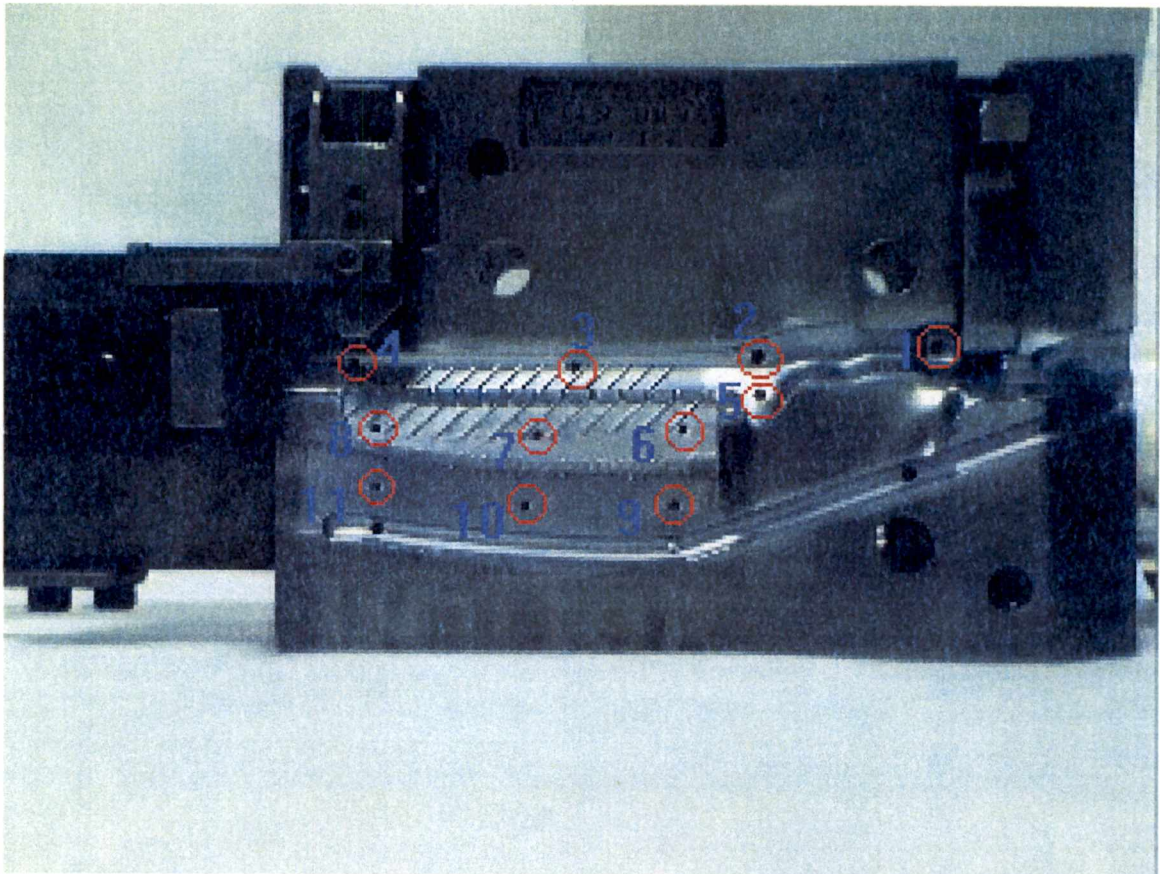


Figure 37. Selected locations on the ceramic core model that best represent locations of thermocouples on die cavity.



(Courtesy of Howmet Corporation)

Figure 38. Die cavity and thermocouples locations.

in the experiment, by Lewis ¹⁸, to measure the temperature of the ceramic slurry during the injection molding process. These thermocouples are identified by channel numbers. The numbers from 1 to 11 represent the channel number of locations of thermocouples placed on the die. The node identification number of each channel on the ceramic core model is given in chapter 6.

5.6 Experimental Objective and Criteria

The main objective of the experiments at Howmet Casting Support was to provide time-temperature data at eleven locations as shown in Figure 37. The experimental data is used to validate the ProCAST simulation analysis of the ceramic core injection molding process. Once confidence is established in the model, engineers can redesign the injection process by choosing the correct injection speed and pressure to reduce die wear, prolong the die, and to have better quality molded products. However, the use of ProCAST in optimizing the injection molding process would not be acceptable without the experimental validation. Therefore, experiments are carried out to ensure the credibility of the model predictions from ProCAST and their reliability.

The details of the experiments are left to Lewis ¹⁸. However, a brief overview of the experiment is given here. The die cavity provided by Howmet was used to conduct the experiments under production conditions at Howmet Casting Support in Morristown, Tennessee. Eleven thermocouples were placed through the ejector-pin holes to measure the temperature of the ceramic slurry at these locations of the die. The locations of thermocouples on the die cavity and their identification numbers can be seen in Figures 37 and 38.

The time-temperature data of the injected ceramic material at each of these eleven locations was collected using a National Instruments SCXI-2000 12-bit data acquisition and control unit. Several runs were made to ensure the availability and quality of these sets of data. These data were then reduced for the validation of the ProCAST simulation analysis.

CHAPTER 6

RESULTS AND DISCUSSIONS

6.1 Comparison of Experimental and Simulation Results

Seven computer simulations of the injection molding process of the ceramic core were run on the Ultra 5 Sun Microsystems in the Advanced Casting Simulation and Mold Design Laboratory at UTK with different boundary conditions as listed in Table 5. The predicted results from the computer simulations were then validated by comparing with the temperature measurements from the experiments. Experiments have been conducted to validate ProCAST model predictions with experimental measurements.

Thermocouples used in the experiments measured and collected time-temperature data of the fluid during each injection molding cycle with a sampling rate of 10 ms at eleven different locations as seen in Figure 38. The injection molding process experiment was repeated ten times to ensure the reliability of the data. At each time, the sampled temperatures from the ten runs were averaged to generate the experimental time-temperature data; and average temperature values were determined for all time steps. An error band was also constructed¹⁸ by calculating the minimum and the maximum temperatures of all ten runs at each time step.

For the model, at time greater than zero, the ceramic begins to flow across the inlet area. Whereas in the production runs, the flow will cross the inlet area after a slight delay following the press of the "Start" button of the injection machine. This delay was found to be different for each run. To account for these differences and to put the experimental results and the model predictions on a common time basis, the results were

plotted from the time the injected ceramic first reached each thermocouple. Specifically, this was implemented by shifting the start time of both the measured and predicted temperatures by using the following for the time axis:

$$\mathbf{Time} - \mathbf{Time} @ \text{maximum_temperature}$$

It is also convenient to nondimensionalize the comparison for the generalization of the results. Nondimensionalization of data allows it to be compared to any other data with different units of measurement or different initial and ambient temperatures. The formula used to nondimensionalize the temperature data from the average experimental data and the model simulation data is shown below ²¹:

$$\theta = \frac{\mathbf{T} - \mathbf{T}_{\text{ambient}}}{\mathbf{T}_{\text{initial}} - \mathbf{T}_{\text{ambient}}}$$

Only data sets of four thermocouples were used in the validation of the computer simulation. These thermocouples are named channels 3, 7, 9, and 11 in Figure 37. According to Lewis ¹⁸, these four thermocouples yielded the most reliable and repeatable data sets compared to the others. The average time-temperature data of the experimental channels 3, 7, 9, and 11 in dimensional form can be seen in Figure 39. The locations of nodes on mesh of the solid core model were selected to best represent the locations of these four thermocouples on the actual die. They are node numbers 10554, 29541, 25798, and 49704 and known as model channels 3, 7, 9 and 11, respectively. Locations of these four nodes were selected because they are close to the physical locations of thermocouples on the die. Locations of these four nodes can be seen in Figure 40.

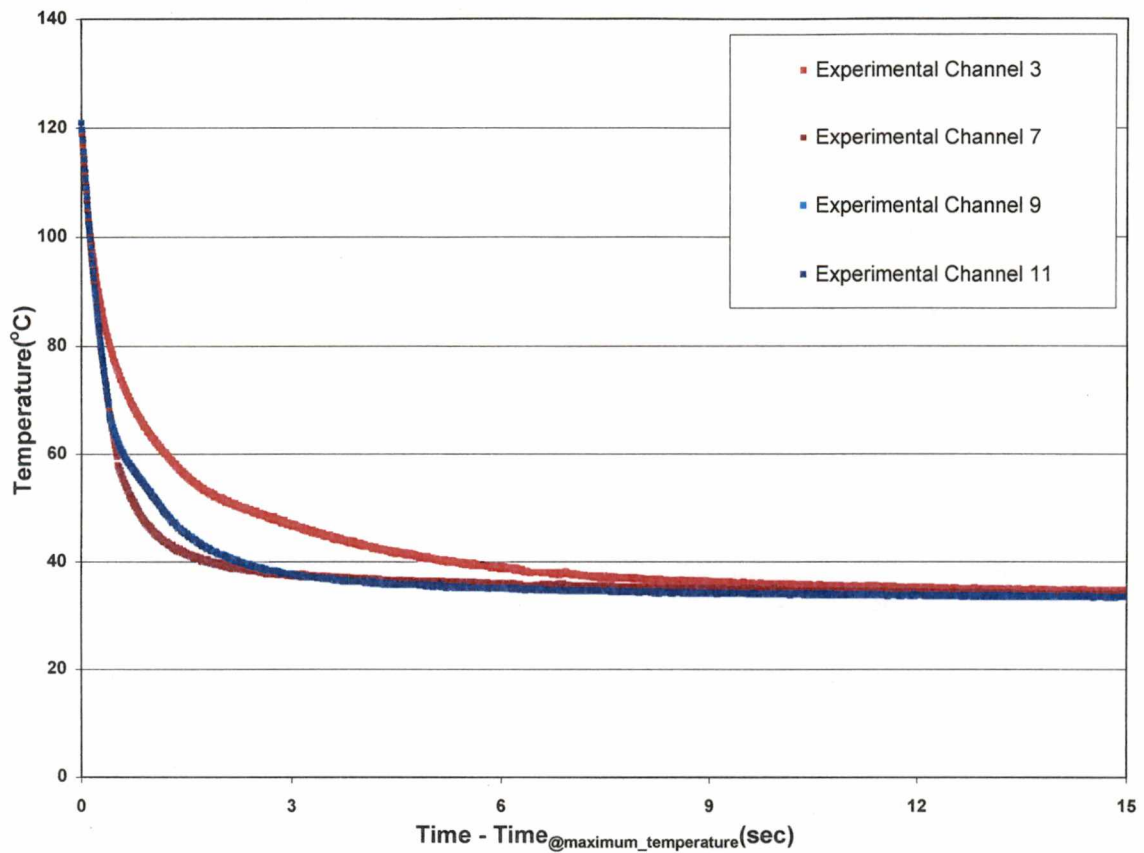


Figure 39. Average time-temperature of experimental channels 3, 7, 9, and 11 in dimensional form with the start-time shifted. Note the overlap of measured temperatures for channels 9 and 11.

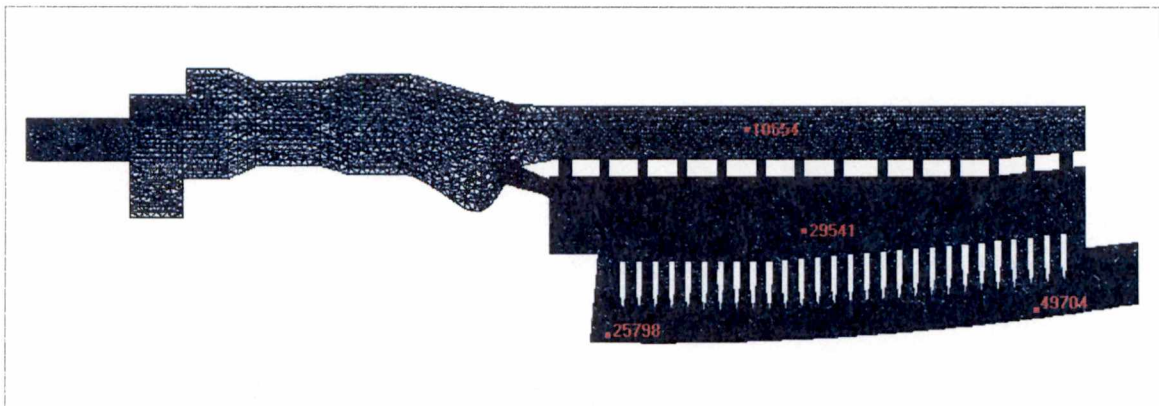


Figure 40. Locations of nodes selected on mesh of the solid core model.

The computer simulation of the injection molding process of the ceramic core is a free surface flow model. As a reminder, the interfacial heat transfer coefficient or film coefficient (h) was not known for this material, the values previously identified by Ly²² for this process were used as a guide. As a result, the computer simulation case V-1 in this study was started with the interfacial heat transfer coefficient h of $1400 \text{ w/m}^2 \text{ K}$ ¹⁷ because it matched the experimental data collected by Ly²² in spring 1999.

6.1.1 Constant Heat Transfer Coefficient (Cases V-1, V-2, and V-3)

The result of this computer simulation for case V-1 is shown in Figures 41 to 56. The filling pattern started at the root end of the core as shown in Figures 41 and 42. The material then flowed to the leading edge and filled it as shown in Figures 43 to 46. At the same time, a small amount of the molten material also went through the conical section of the core to the thin section that lies between the leading edge and the trailing edge as seen in Figures 46 - 48. Once the leading edge was completely filled, the material was forced to flow through a series of narrow passages having elliptical cross section to get to the other end of the thin section. It then passed through another series of narrow passages having a rectangular cross section to reach the trailing edge and finally filled the trailing edge at its tip end. In Figures 49 to 53, it is shown that the material in the last elliptical cross section has the highest temperature range compare to any other locations of the core. This was a result of the shear heating. When a highly viscous material was forced to flow from an area with a larger cross section (leading edge) to the smaller cross section (elliptical crossover) its velocity gradients increase rapidly resulting in shear heating caused by viscous dissipation. Such localized regions of high shear rate will have a more

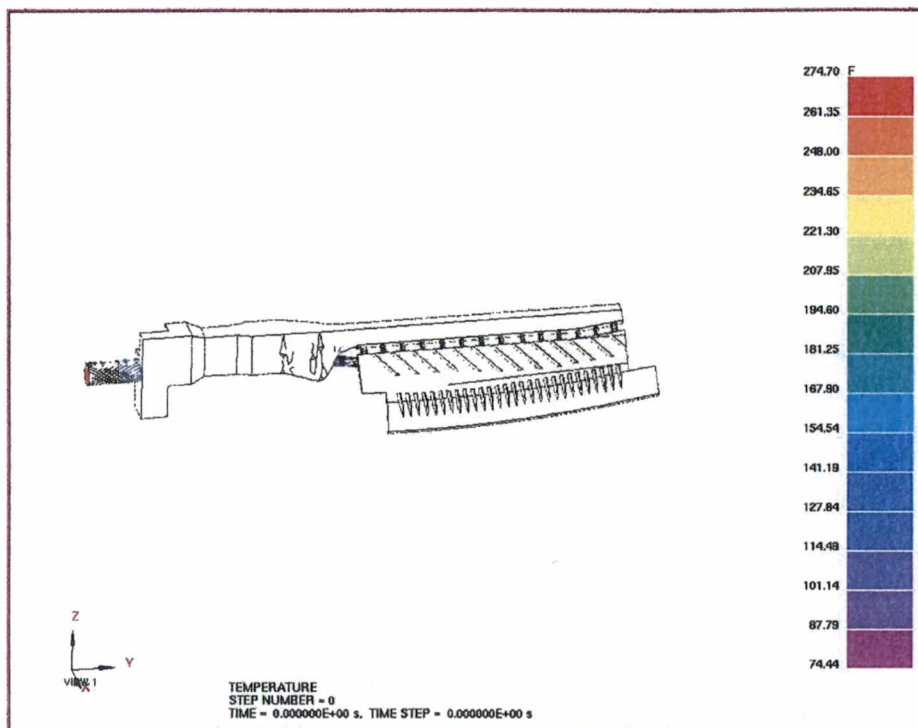


Figure 41. Filling pattern of computer simulation case V-1 at time of 0.0 ms

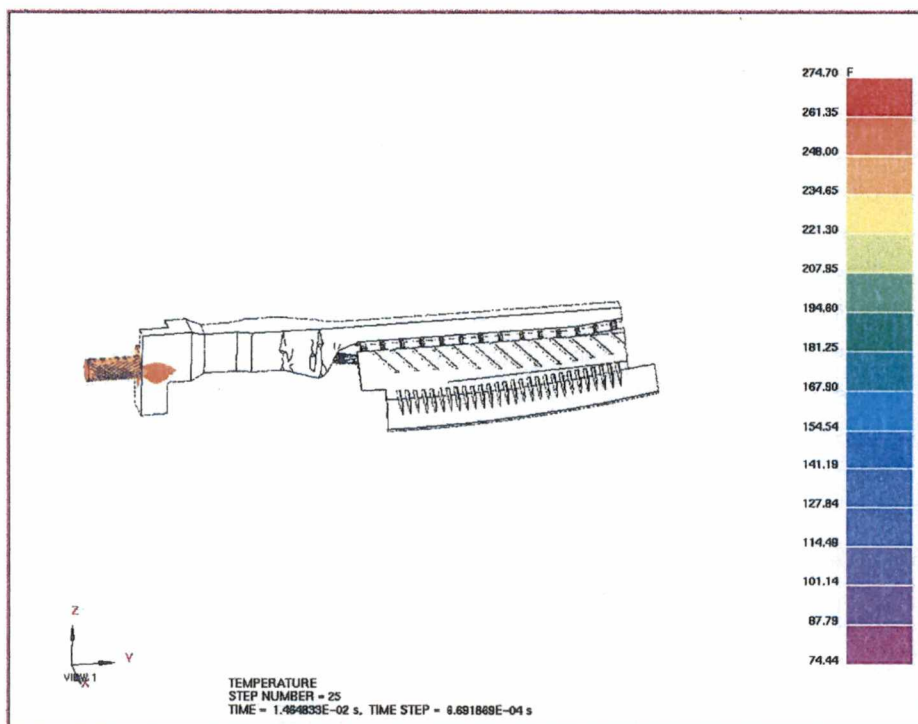


Figure 42. Filling pattern of computer simulation case V-1 at time of 14.6 ms

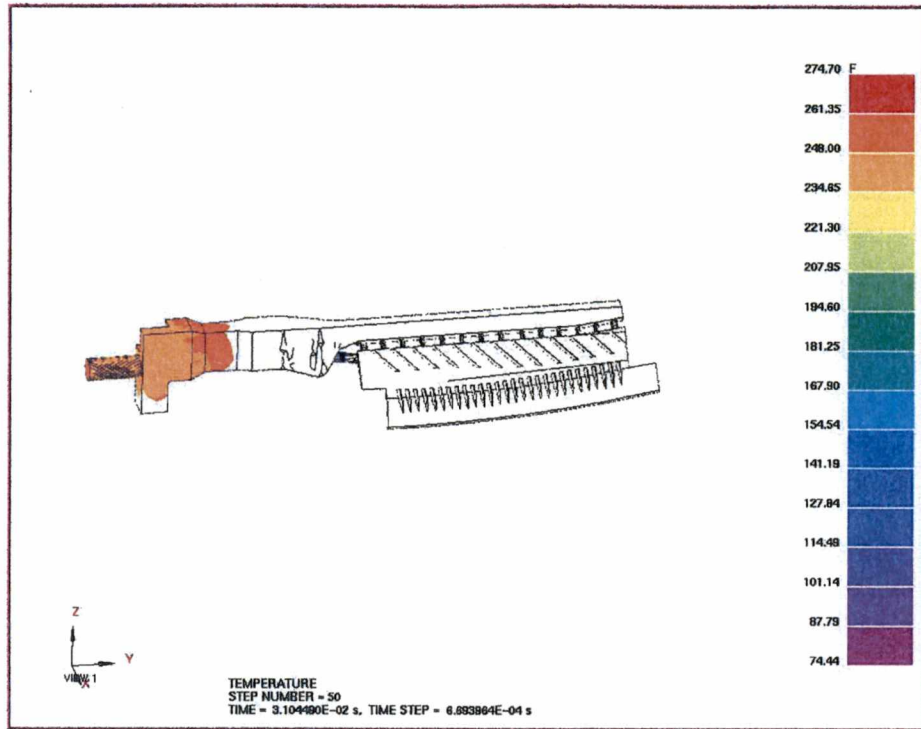


Figure 43. Filling pattern of computer simulation case V-1 at time of 30 ms

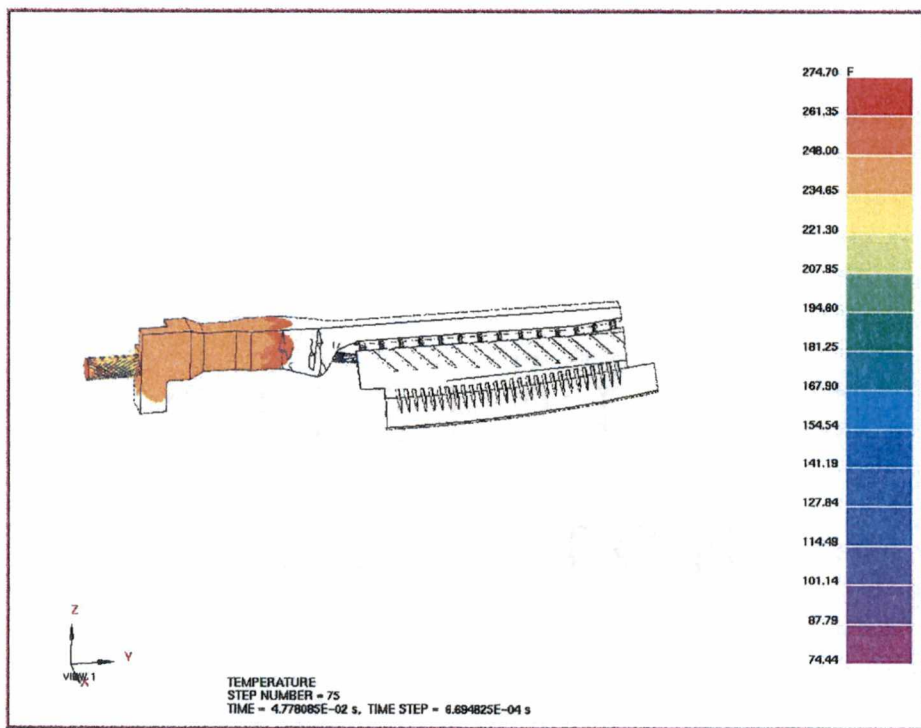


Figure 44. Filling pattern of computer simulation case V-1 at time of 47.8 ms

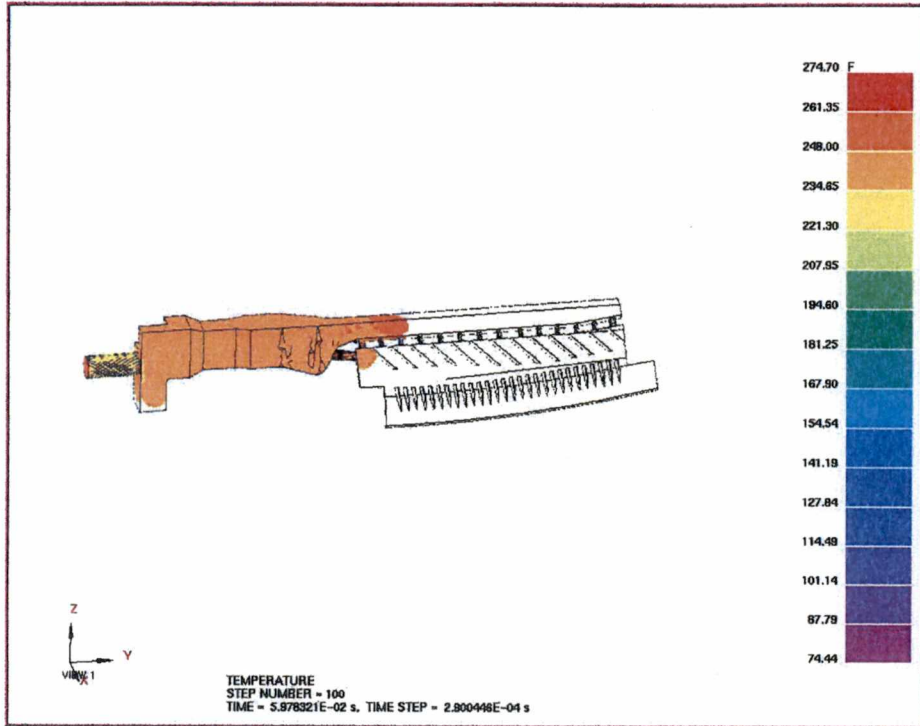


Figure 45. Filling pattern of computer simulation case V-1 at time of 59.8 ms

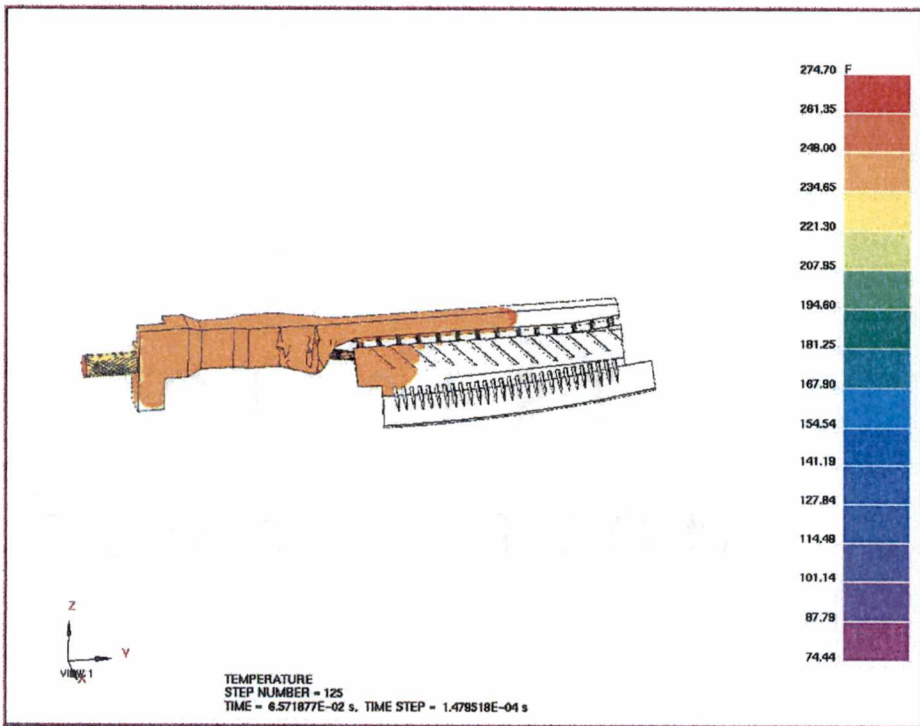


Figure 46. Filling pattern of computer simulation case V-1 at time of 65.7 ms

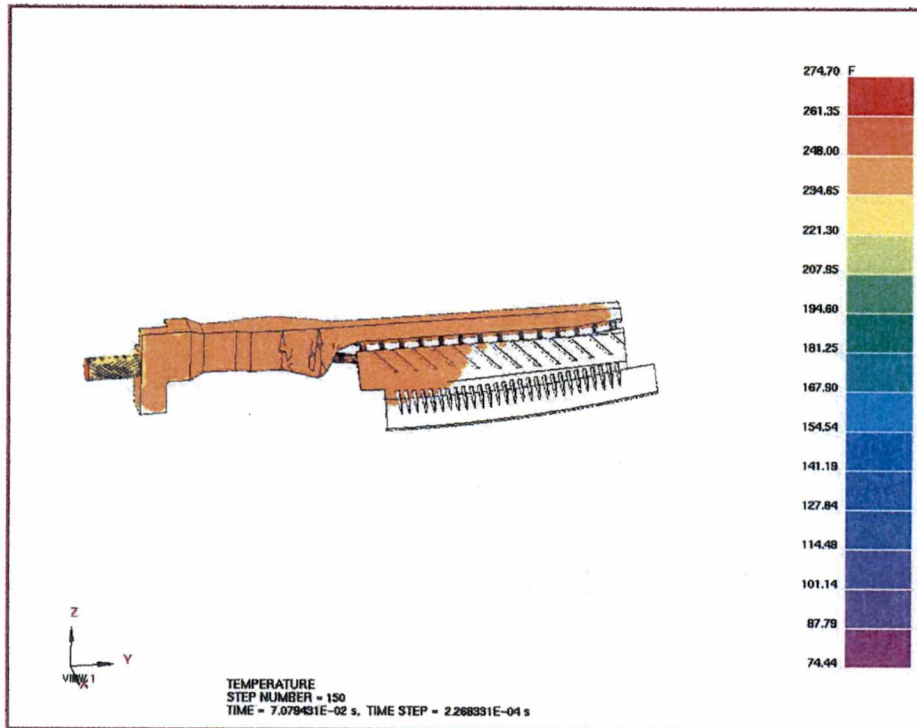


Figure 47. Filling pattern of computer simulation case V-1 at time of 70.8 ms

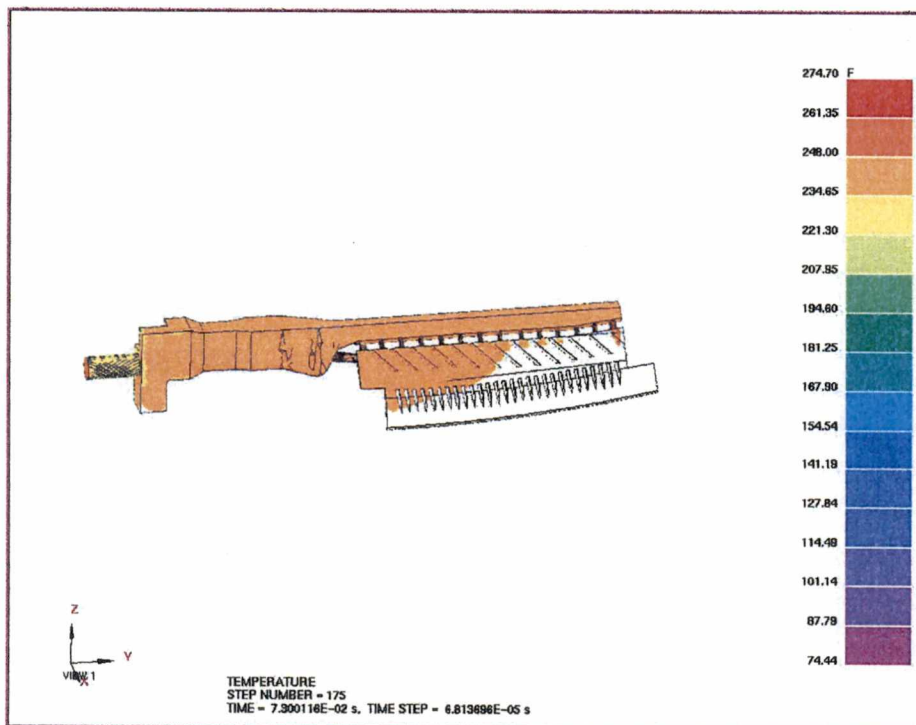


Figure 48. Filling pattern of computer simulation case V-1 at time of 73.0 ms

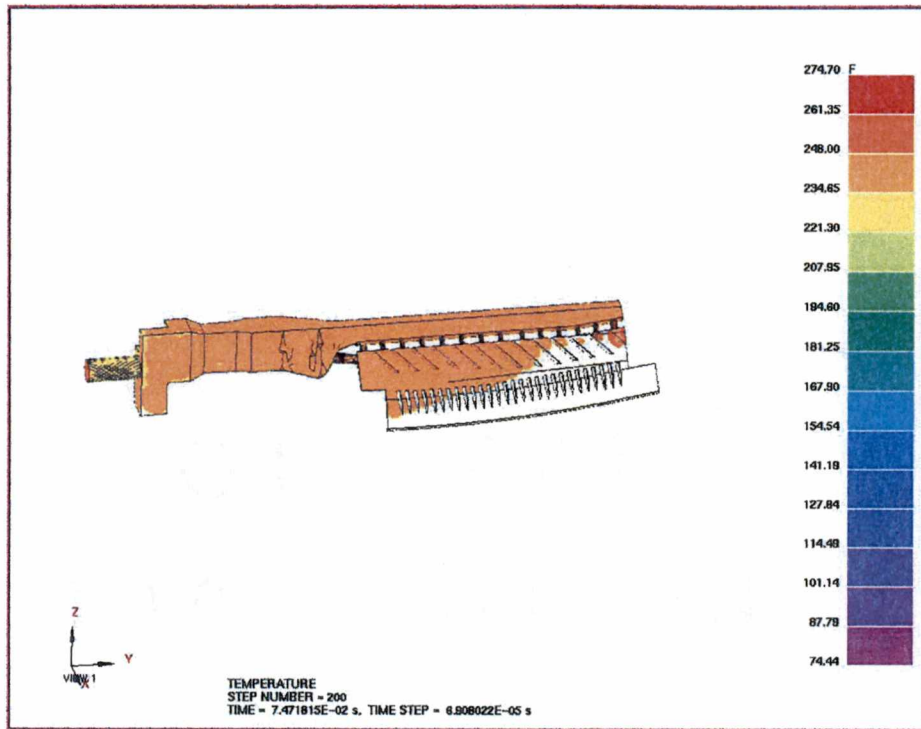


Figure 49. Filling pattern of computer simulation case V-1 at time of 74.7 ms

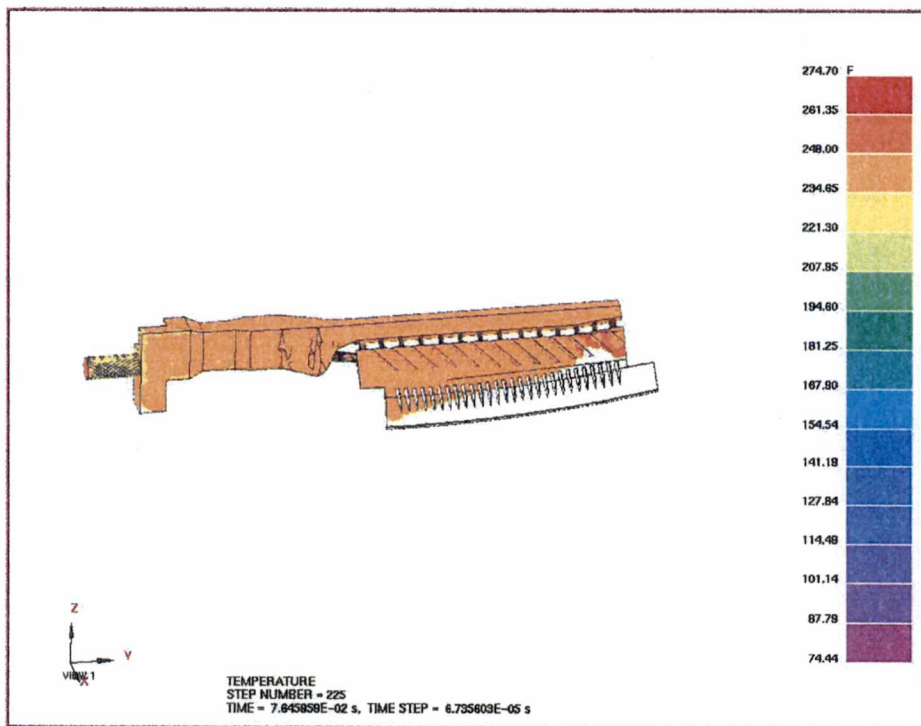


Figure 50. Filling pattern of computer simulation case V-1 at time of 76.5 ms

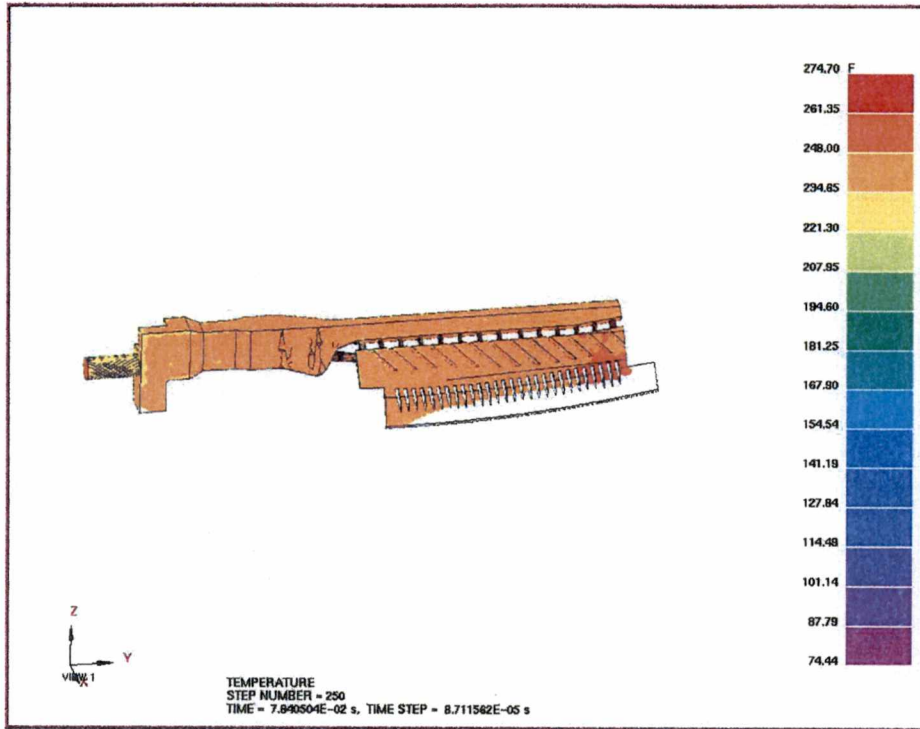


Figure 51. Filling pattern of computer simulation case V-1 at time of 78.4 ms

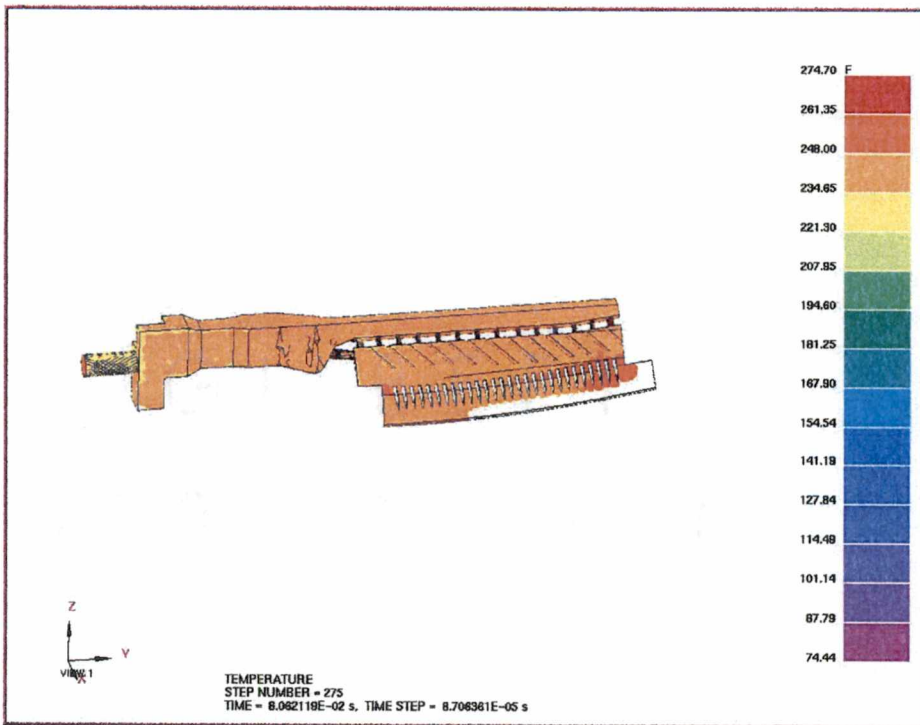


Figure 52. Filling pattern of computer simulation case V-1 at time of 80.6 ms

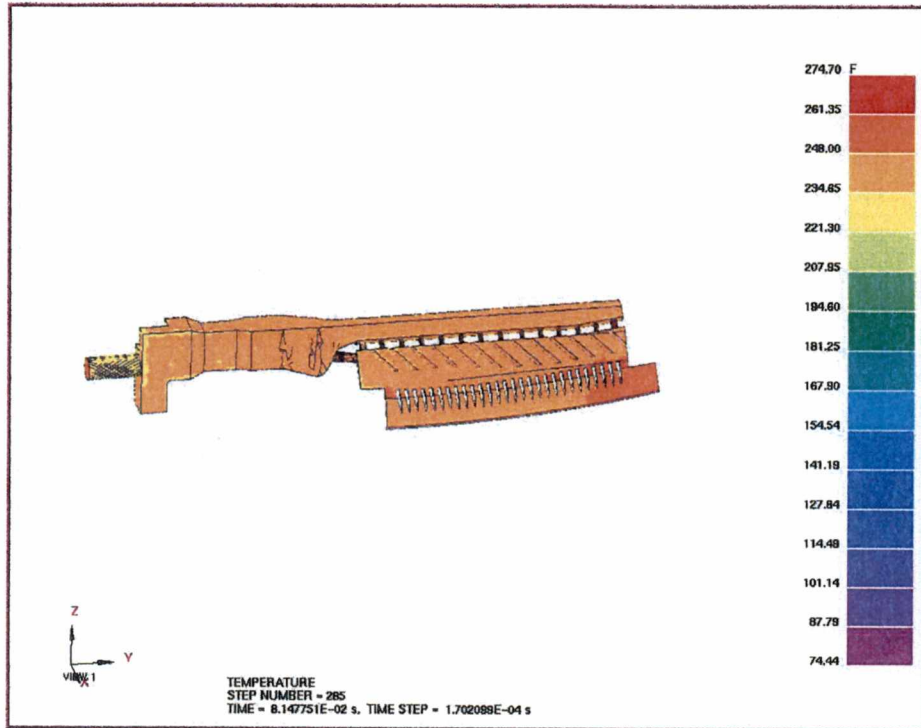


Figure 53. Filling pattern of computer simulation case V-1 at time of 81.5 ms

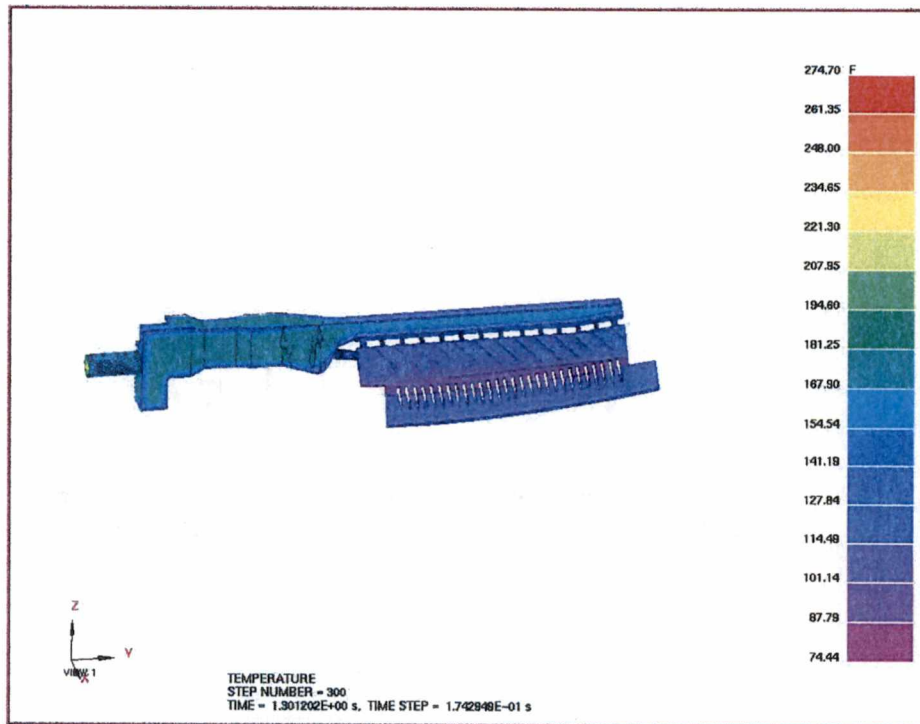


Figure 54. Filling pattern of computer simulation case V-1 at time of 1.3 sec

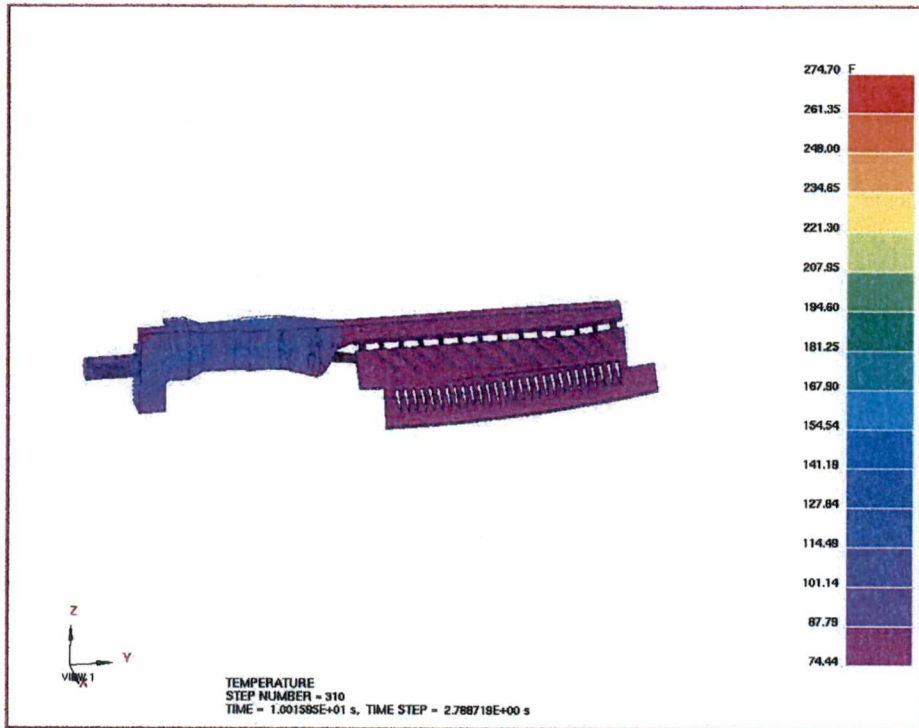


Figure 55. Filling pattern of computer simulation case V-1 at time of 10 sec

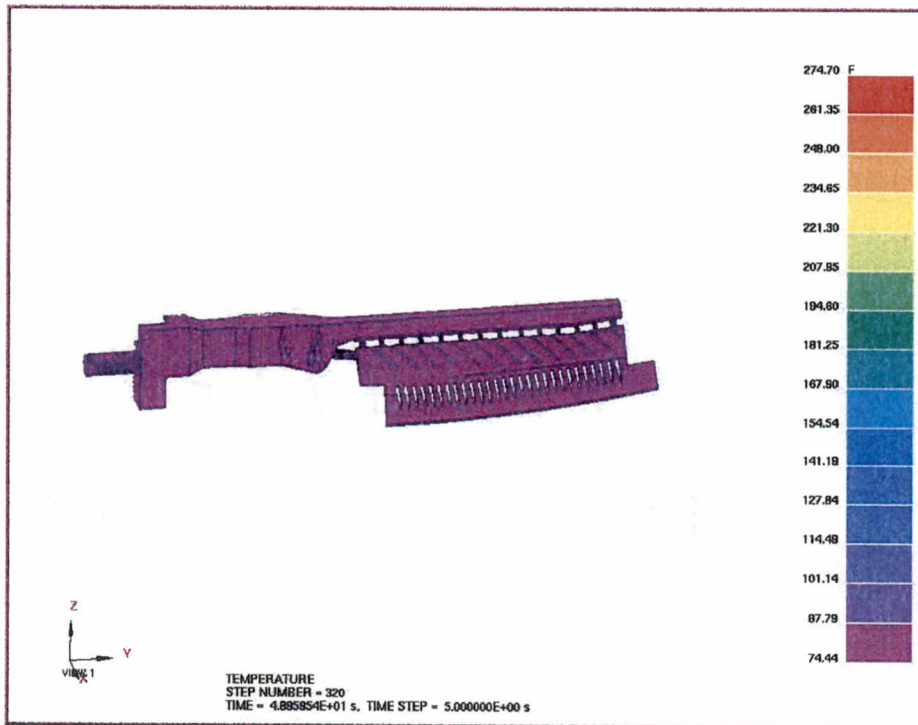


Figure 56. Filling pattern of computer simulation case V-1 at time of 49 sec

rapid wear of the die relative to regions of low shear rates. The temperature contours on the surface of the core are shown in Figures 54 to 56, representing the post-filling cooling patterns on the surface of the core.

The predicted temperatures in dimensional form of all four channels from the computer simulation corresponding to four experimental thermocouples are shown in Figure 57. From this Figure, it is observed that once the die cavity is filled, the injected material in the thin region (where thermocouple channels 7, 9, and 11 are located) cools faster than the injected material at thermocouple channel 3 located in the thick region. The predicted temperature distributions of these four channels from the computer simulation case V-1 were not in good agreement with the experimental data as shown in Figure 57.

The results from the computer simulation cases V-2 and V-3 with the interfacial heat transfer coefficients of $1800 \text{ W/m}^2 \text{ K}$ and $2200 \text{ W/m}^2 \text{ K}$, respectively, showed the same filling patterns as in case V-1. Therefore, filling pattern results for these cases are not included. The predicted temperature distributions for case V-2, as shown in Figure 58, were in good agreement with measurements for cooling down to about 60°C and below this temperature the model over predicts the cooling rate. The predicted temperature distributions for case V-3, as shown in Figure 59, were in good agreement with measurements for cooling down to only about 70°C and below this temperature the model over predicts the cooling rate. The increase in value of heat transfer coefficient for this case relative to case V-2 results in a higher cooling rate and is responsible for more deviation from the measurements. Results for case V-2 are in better agreement (down to 60°C) with the measurements than those of V-1 or V-3. In Figure 60, the predicted

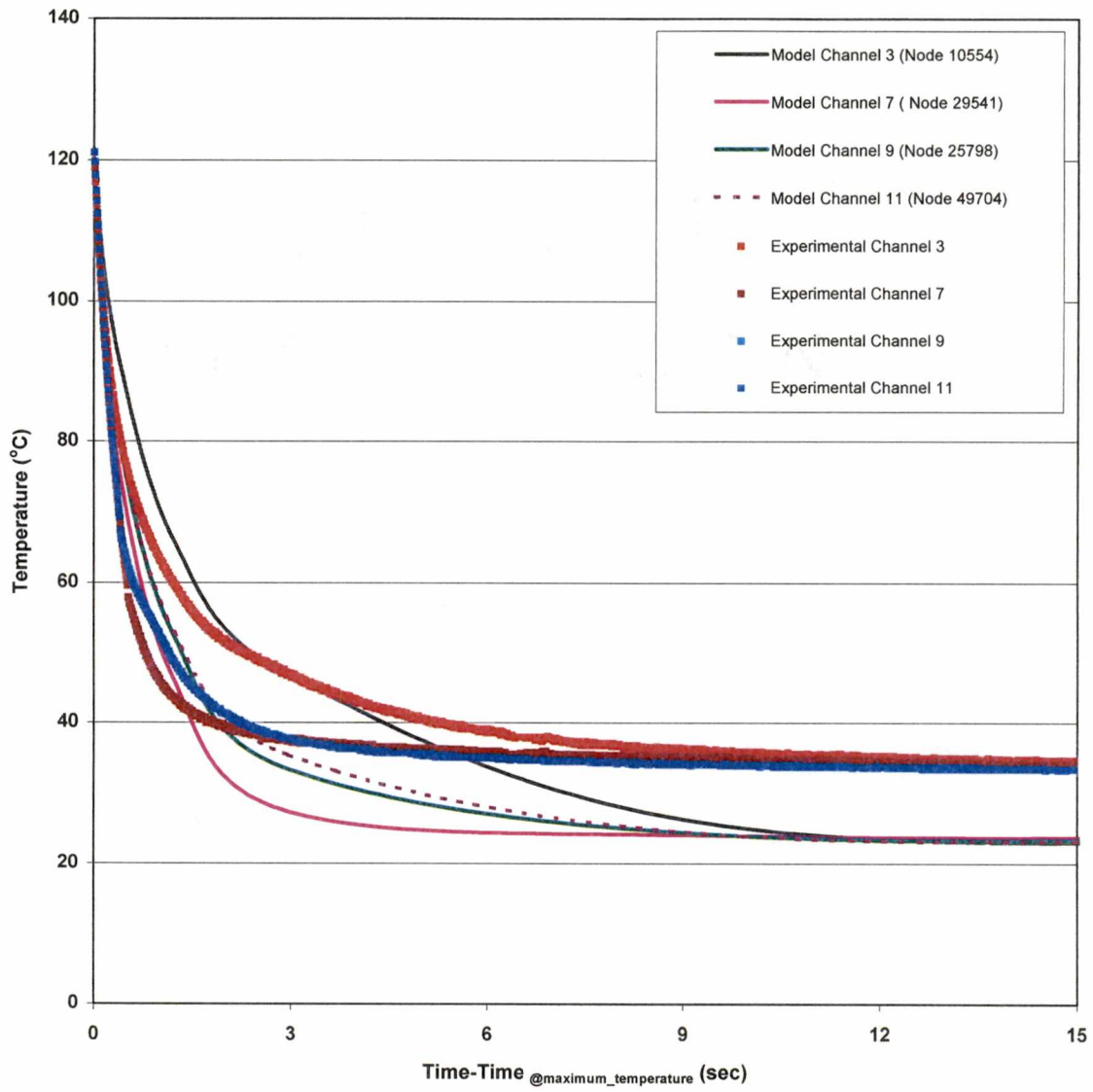


Figure 57. Comparison of case V-1 ($h = 1400 \text{ W/m}^2 \text{ K}$) model predictions with experimental measurements of temperature distributions at four locations. Note the overlap of measured temperatures for channels 9 and 11.

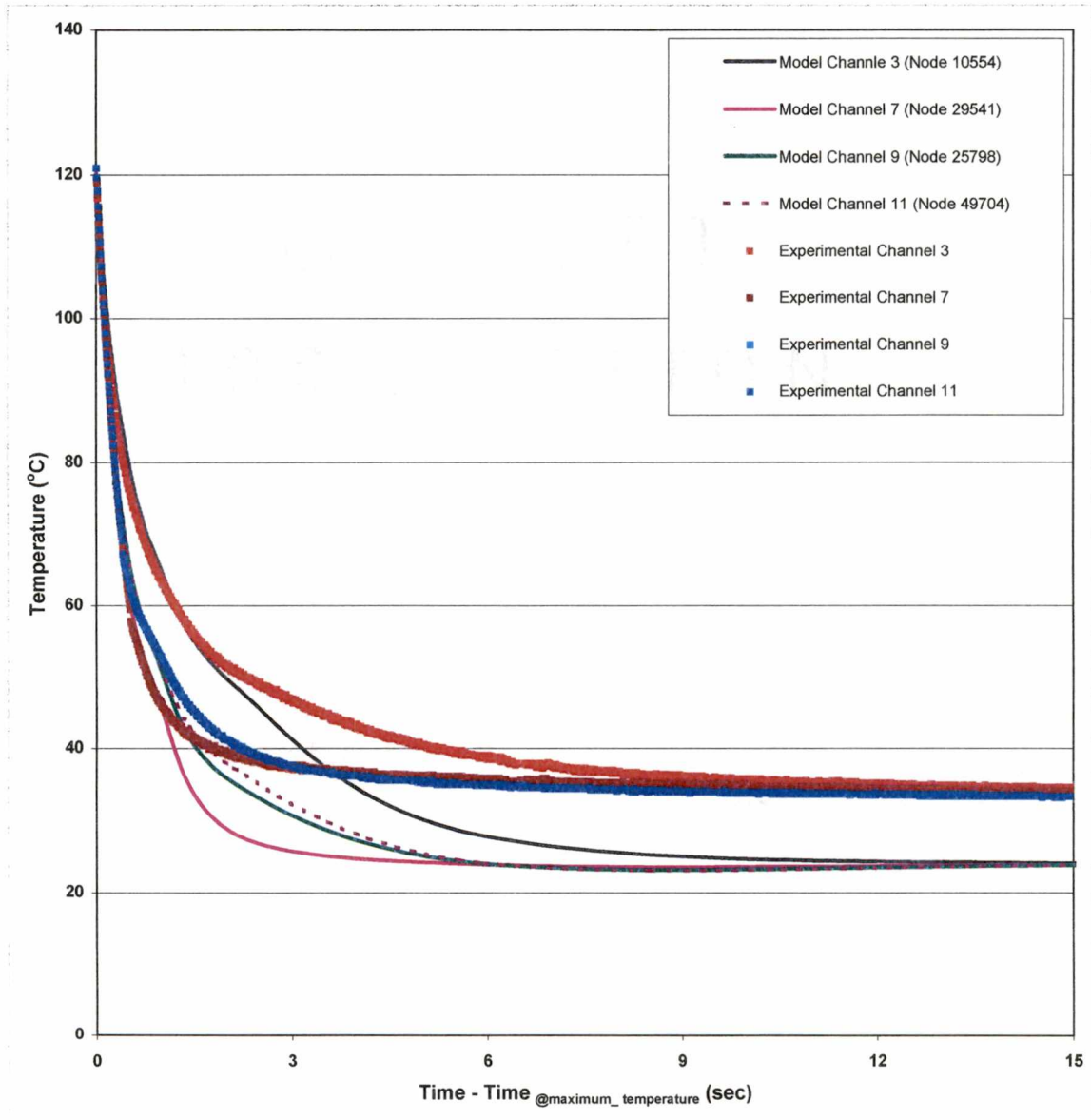


Figure 58. Comparison of case V-2 ($h = 1800 \text{ W/m}^2 \text{ K}$) model predictions with experimental measurements of temperature distributions at four locations. Note the overlap of measured temperatures for channels 9 and 11.

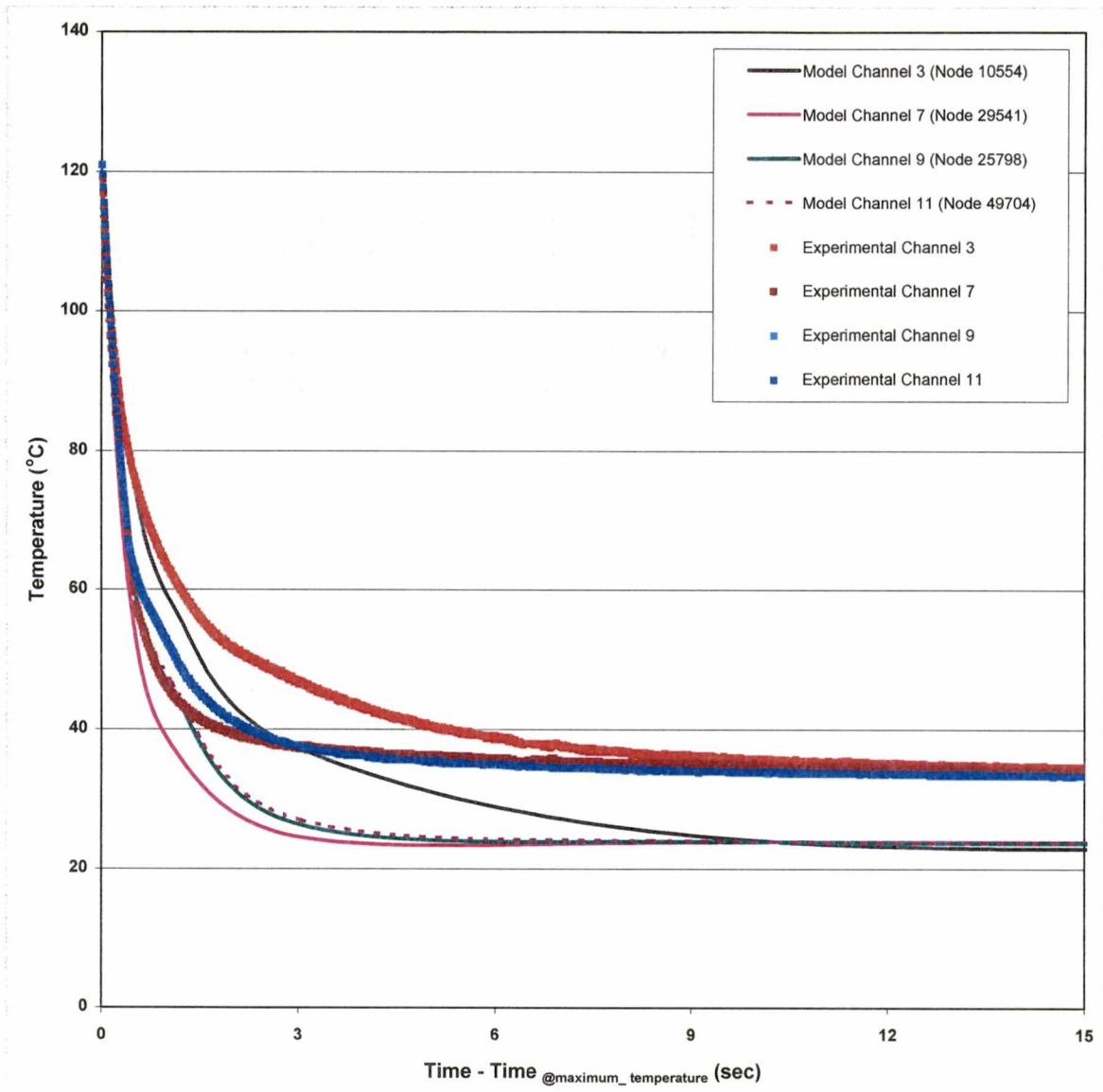


Figure 59. Comparison of case V-3 ($h = 2200 \text{ W/m}^2 \text{ K}$) model predictions with experimental measurements of temperature distributions at four locations. Note the overlap of measured temperatures for channels 9 and 11.

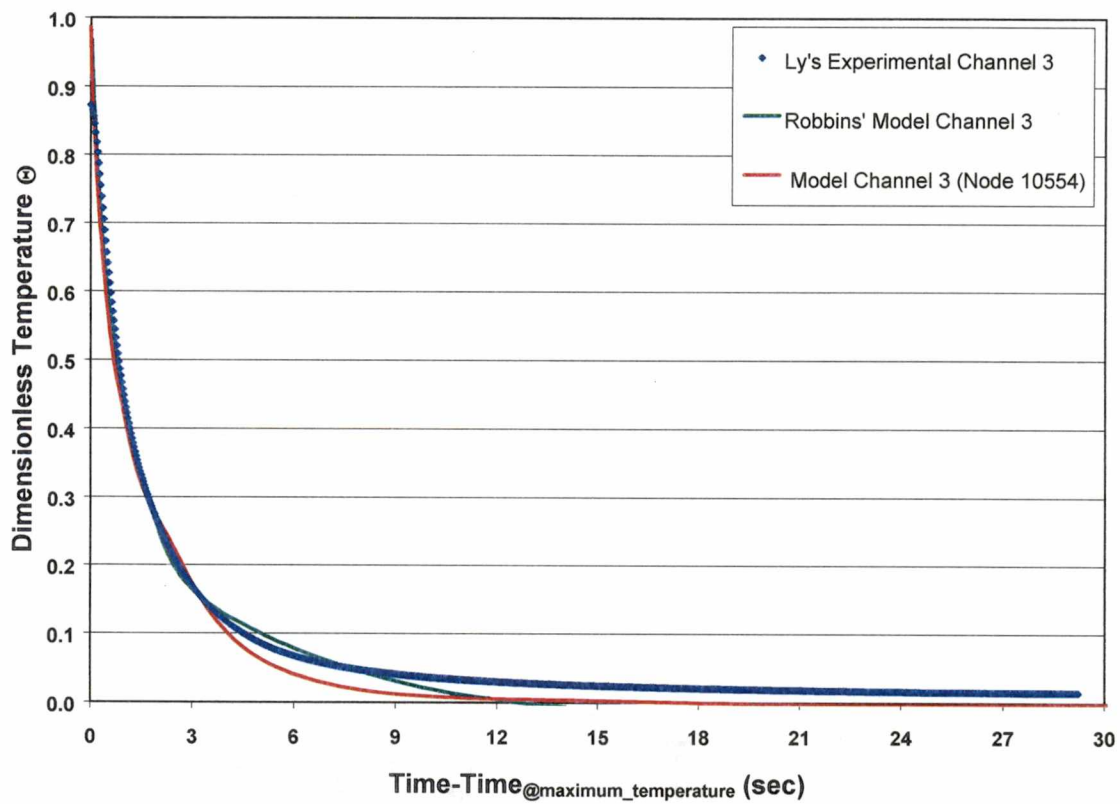


Figure 60. Comparison of predicted temperature distributions for channel 3 of case V-2 ($h = 1800 \text{ W/m}^2 \text{ K}$) with predictions by Robbins¹⁷ and measurements by Ly²².

temperature distributions of case V-2 for channel 3 are also compared to the modeling results of Robbins¹⁷ and experimental results of Ly²² and for the first three seconds (adjusted time) the agreement is very good. From this comparison, it is concluded that reducing the total numbers of nodes and elements of mesh in this study (about one-half compared to Robbins' model¹⁷) yielded a faster turn around of the results by reducing the computational time without sacrificing the accuracy of the results. It should be pointed out that Ly²² and Robbins¹⁷ had measured temperature for a single channel, channel 3.

6.1.2 Step Function Model (Case V-4)

For the temperature less than about 60°C, the results of cases V-1, V-2, and V-3 were not found to be in good agreement with the measurements and cooling rate within the model appear to be too high. The liquidus and solidus temperatures of the material are 58.1°C and 58°C, respectively. When the medium solidifies, shrinkage begins and the medium can begin to separate away from the wall of the die. The resulting gap dramatically reduces the heat transfer coefficient to that of natural convection in a gaseous medium. To represent these effects in the model, a step function for interfacial heat transfer coefficient was considered for the next run labeled case V-4. The step change function of the interfacial heat transfer coefficient is shown in Figure 26 and is described below:

$$\text{For } 120^{\circ}\text{C} \geq T \geq 58^{\circ}\text{C}, \quad h = 1800 \text{ W/m}^2 \text{ K (Liquid state)}$$

$$\text{For } 58^{\circ}\text{C} \geq T \geq 23.9^{\circ}\text{C}, \quad h = 100 \text{ W/m}^2 \text{ K (Solid state)}$$

The filling pattern from the computer simulation case V-4 is found to be the same as those in the previous cases. The results of the temperature distributions in dimensional from of all four model channels for this V-4 case are shown in Figure 61. From this figure it can be seen that, for the temperature range below 58°C, the predicted temperatures for all model channels are not in good agreement with the experimental data. Temperature of the injected material rapidly dropped down from the initial temperature of 121.1°C to 58°C and then linearly decreased to ambient temperature due to the low value of the interfacial heat transfer coefficient.

6.1.3 Ramp Function Model (Case V-5)

From the results of the computer simulation case V-4, it is evident that the assigned interfacial heat transfer coefficient of 1800 W/m² K was reasonable in the temperature range form 121°C to 58°C because the temperature distributions of all for channels of the model and the experiment matched well in this temperature range. So, in the next computer simulation, case V-5, the interfacial heat transfer coefficient, h , was assigned a value of 1800W/m² K in the temperature range of 121°C to 58°C. For temperatures below 58°C, the transition state of the injected material is taken into account. When the material starts to solidify, portions of it solidify and the remaining continues to be in a liquid state. Therefore, the interfacial heat transfer coefficient was decreased linearly from 1800 W/m² K to 100 W/m² K as temperature decreased from 58°C to 40°C as shown as a ramp function in Figure 27. For the temperature range from 40°C to ambient temperature, the heat transfer coefficient was assigned a constant value of 100 W/m² K as in case V-4. The step change function of the interfacial heat transfer

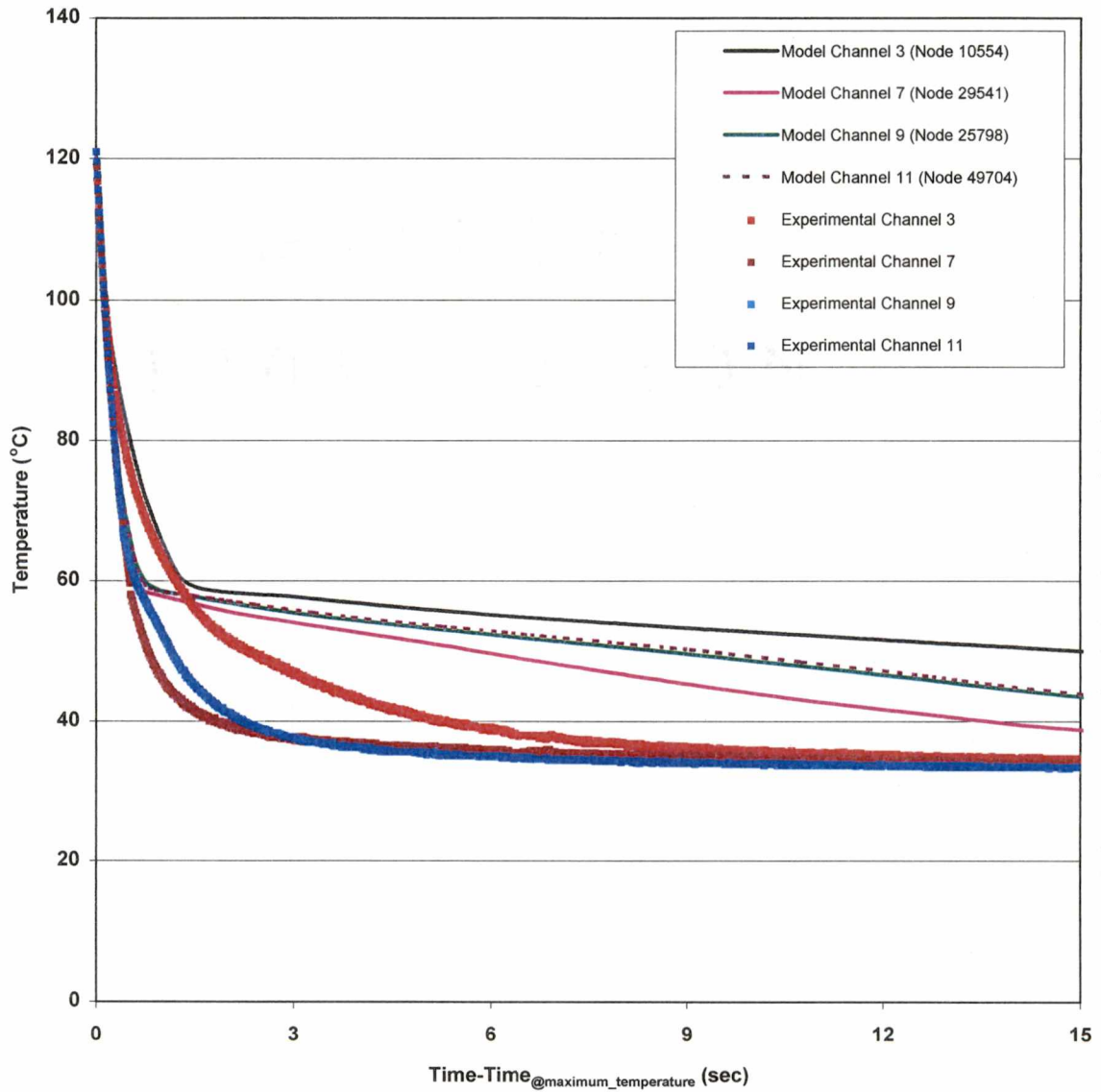


Figure 61. Comparison of case V-4 (step change) model predictions with experimental measurements of temperature distributions at four locations. Note the overlap of measured temperatures for channels 9 and 11.

coefficient is summarized below:

For $120^{\circ}\text{C} \geq T \geq 58^{\circ}\text{C}$,	$h = 1800 \text{ W/m}^2 \text{ K}$ (Liquid state)
For $58^{\circ}\text{C} \geq T \geq 40^{\circ}\text{C}$,	$h = a \cdot T + b$ (Transition state)
For $40^{\circ}\text{C} \geq T \geq 23.9^{\circ}\text{C}$,	$h = 100 \text{ W/m}^2 \text{ K}$ (Solid state)

where a and b are constants.

The computer simulation for case V-5 showed that the filling patterns of this case were the same as those for cases V-1 through V-4 as shown in Figures 41 to 56. The filling patterns and pressure gradients of case V-5 are included in Appendices A and B, respectively. The significance of the results of case V-5 is that the temperature distributions of all model channels are closer to the experimental results than any of the previous cases, cases V-1 through V-4, as shown in Figure 62. In Figures 63 through 66 the temperature distribution at each channel location from the model and the measurements, including the error bands, are presented in dimensionless form for direct comparison. When error bands associated with the measurements are taken into account, the agreement is even better than that indicated by Figure 62.

6.1.4 Results of Computer Simulation Case P-1

Howmet Casting Support in Morristown, Tennessee has been interested in controlling pressures and temperatures in their ceramic injection molding process. Therefore, the next computer simulation was modeled with a variable inlet pressure condition instead of constant inlet velocity condition. In the first case, case P-1, the variable pressure profile at the inlet determined from the computer simulation case V-5 results was applied to case P-1 to verify that the results obtained from ProCAST for case

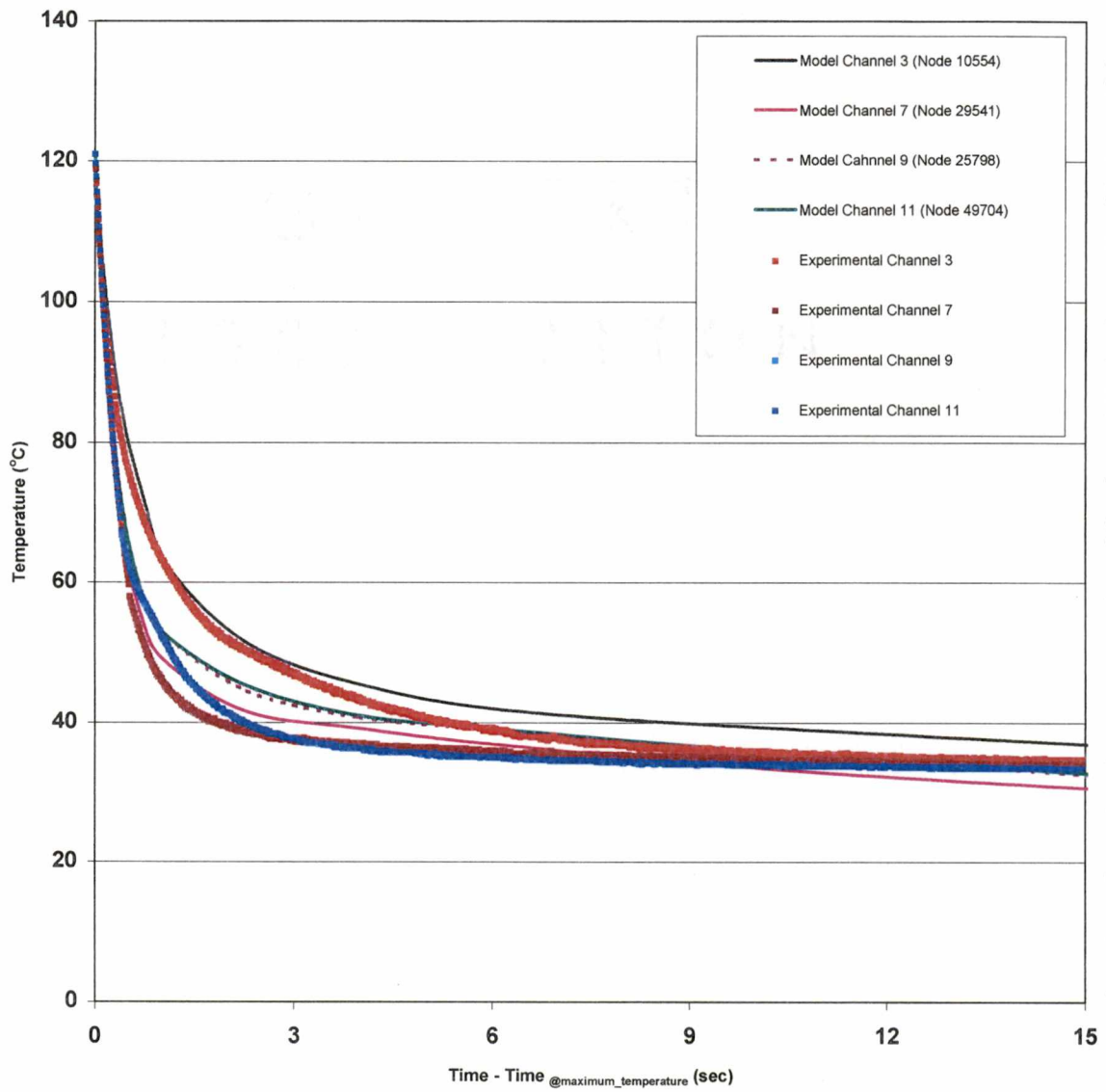


Figure 62. Comparison of case V-5 (ramp function) model predictions with experimental measurements of temperature distributions at four locations. Note the overlap of measured temperatures for channels 9 and 11.

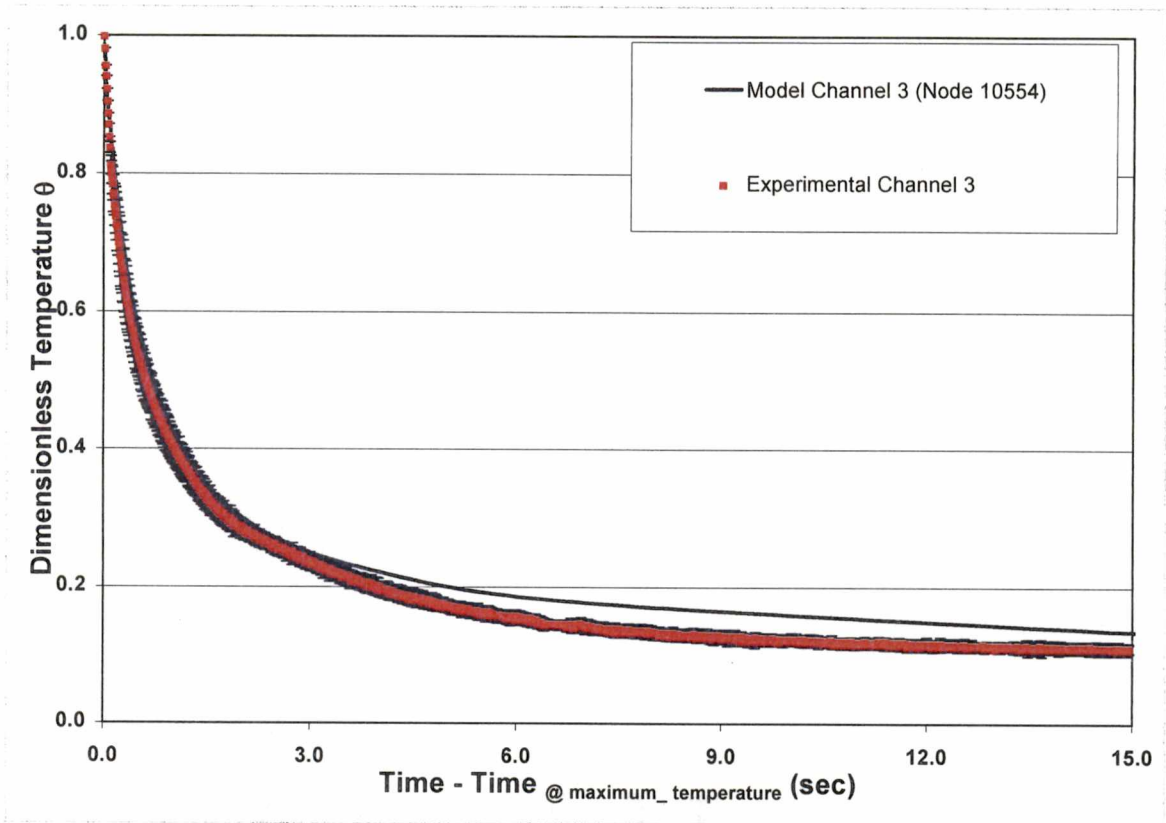


Figure 63. Dimensionless temperature distributions of channel 3 of both model simulation and experiment of case V-5 (ramp function).

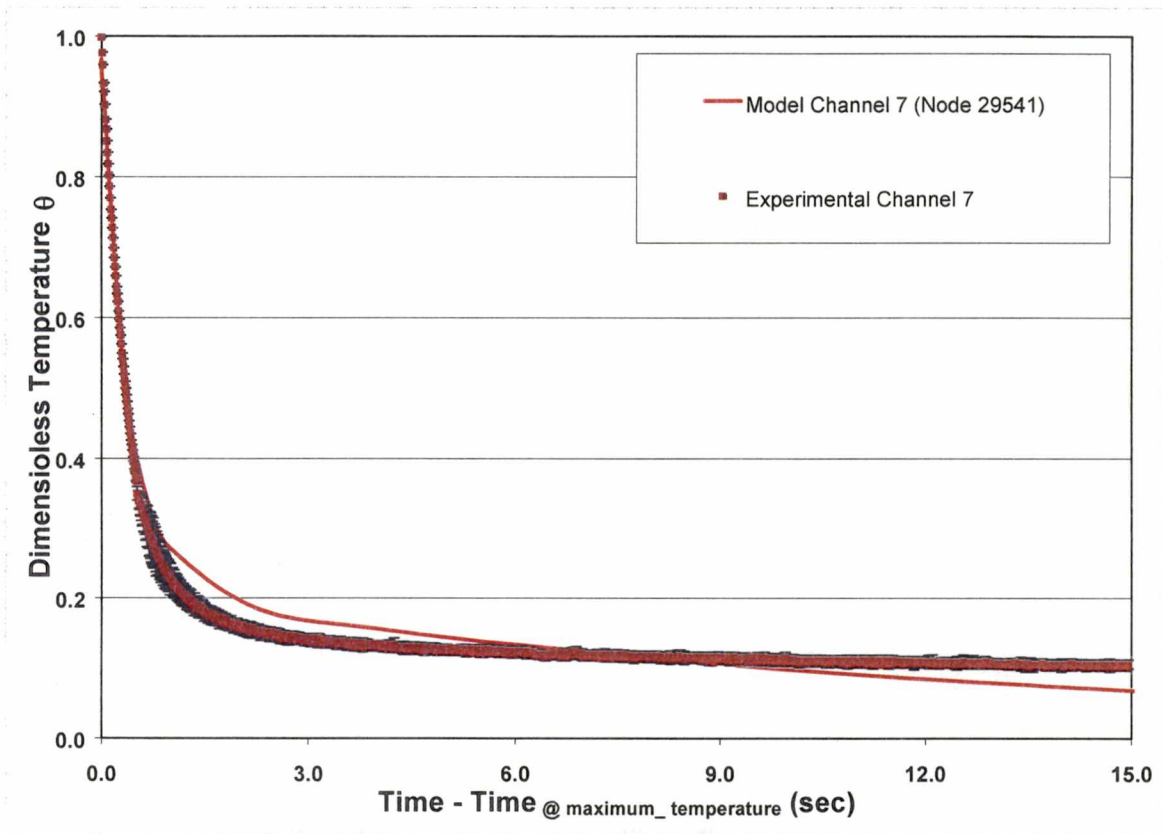


Figure 64. Dimensionless temperature distributions of channel 7 of both mode simulation and experiment of case V-5 (ramp function).

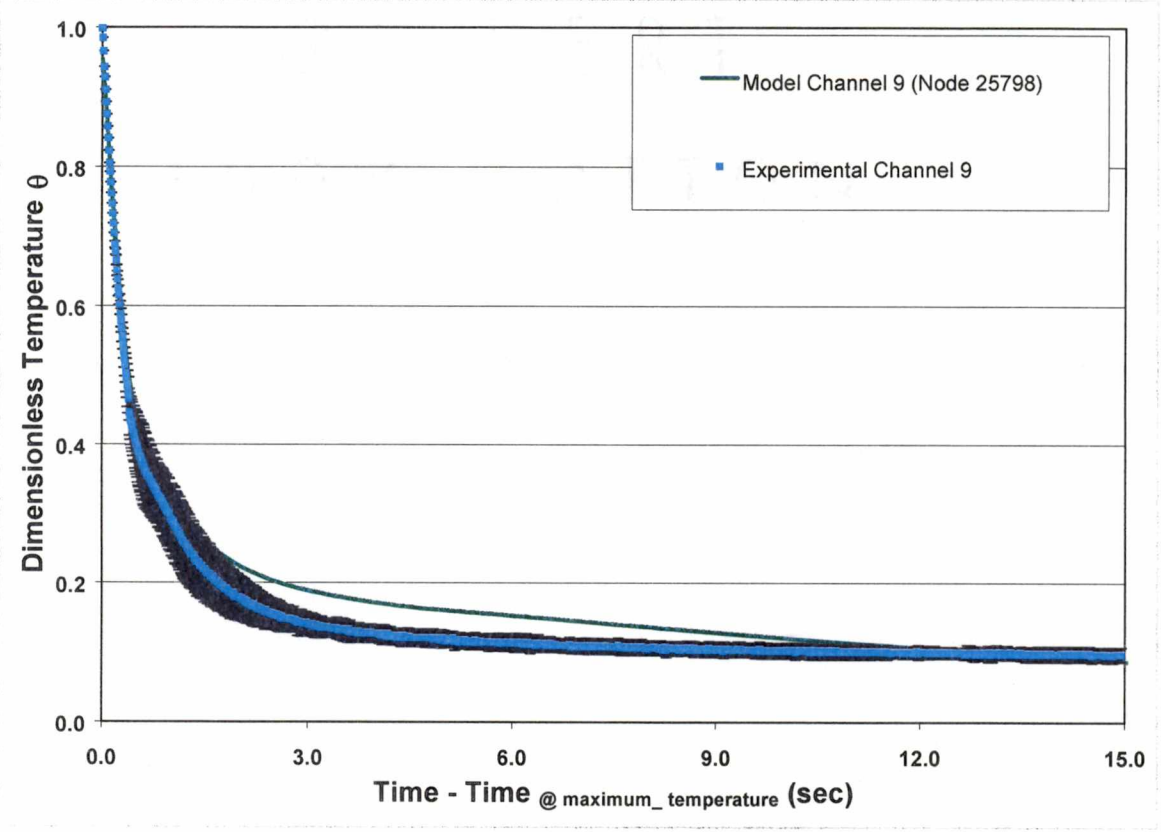


Figure 65. Dimensionless temperature distributions of channel 9 of both model simulation and experiment of case V-5 (ramp function).

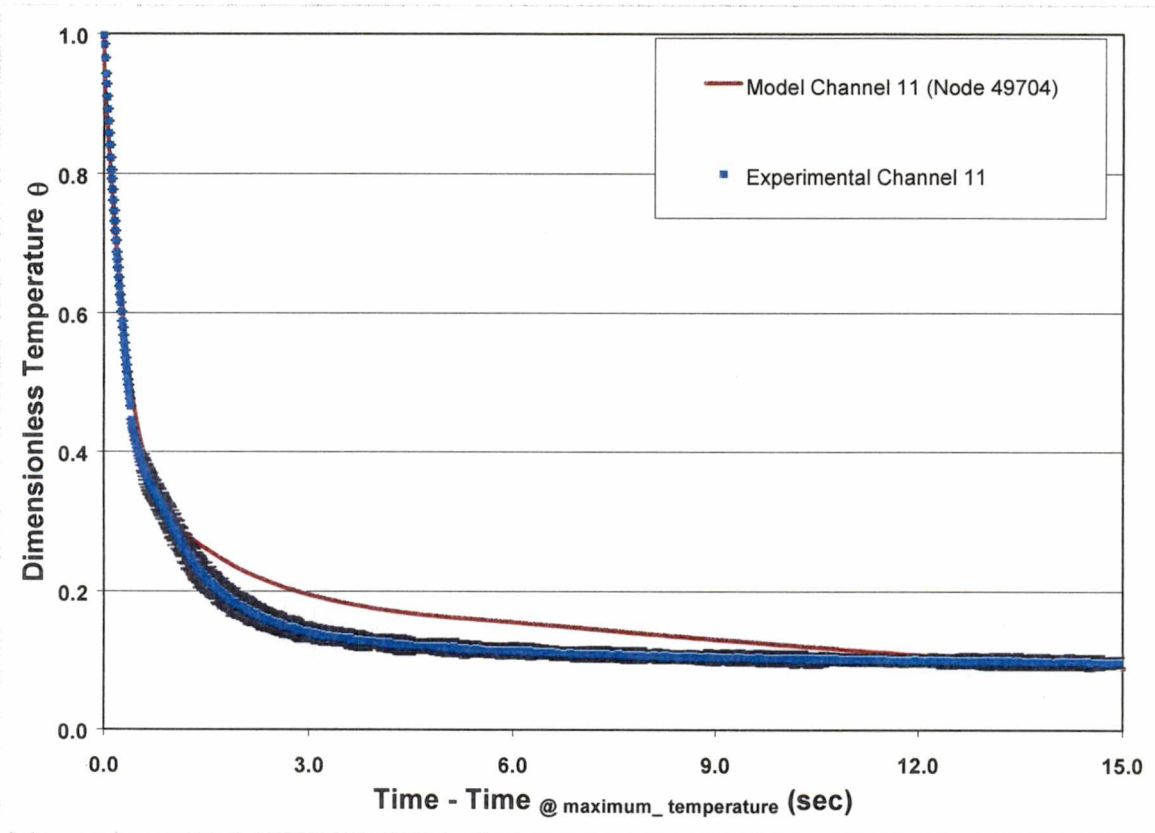


Figure 66. Dimensionless temperature distributions of channel 11 of both model simulation and experiment of case V-5 (ramp function).

P-1 would be consistent with those of case V-5. Note that cases P-1 and V-5 are otherwise similar in all respects. However, controlling inlet injection pressure in practice makes case P-1 a more realistic simulation of production conditions. The ramp change function of the interfacial heat transfer coefficient (Figure 27) was also used in the case. The computer simulation case P-1 yielded identical results with case V-5 as expected. Since the results of the computer simulation case P-1 are identical to case V-5, they are not included in this study and can be referred to the results of computer simulation case V-5.

6.1.5 Result of Computer Simulation Case P-2

The last computer simulation case was case P-2 with the injection pressure boundary conditions provided by Howmet Corporation plotted in Figure 29 and an interfacial heat transfer coefficient of a ramp change function as seen in Figure 27. The computational time for this case was twice as long as any other cases. The results of this computer simulation showed the filling time to be twice that of the other cases. The filling pattern was different from the previous cases. The injected material filled the root end and the tip end of the trailing edge before they met at the center section of the trailing edge as seen in Figure 67. Complete filling patterns of the injected material of the computer simulation case P-2 can be seen in Appendix C. Pressure distributions of the computer simulation can also be seen in Appendix D. The predicted temperature distributions for all channels of case P-2 were plotted along with the temperature distributions of case P-1 and experimental temperatures in Figures 68 to 71 in dimensionless form.

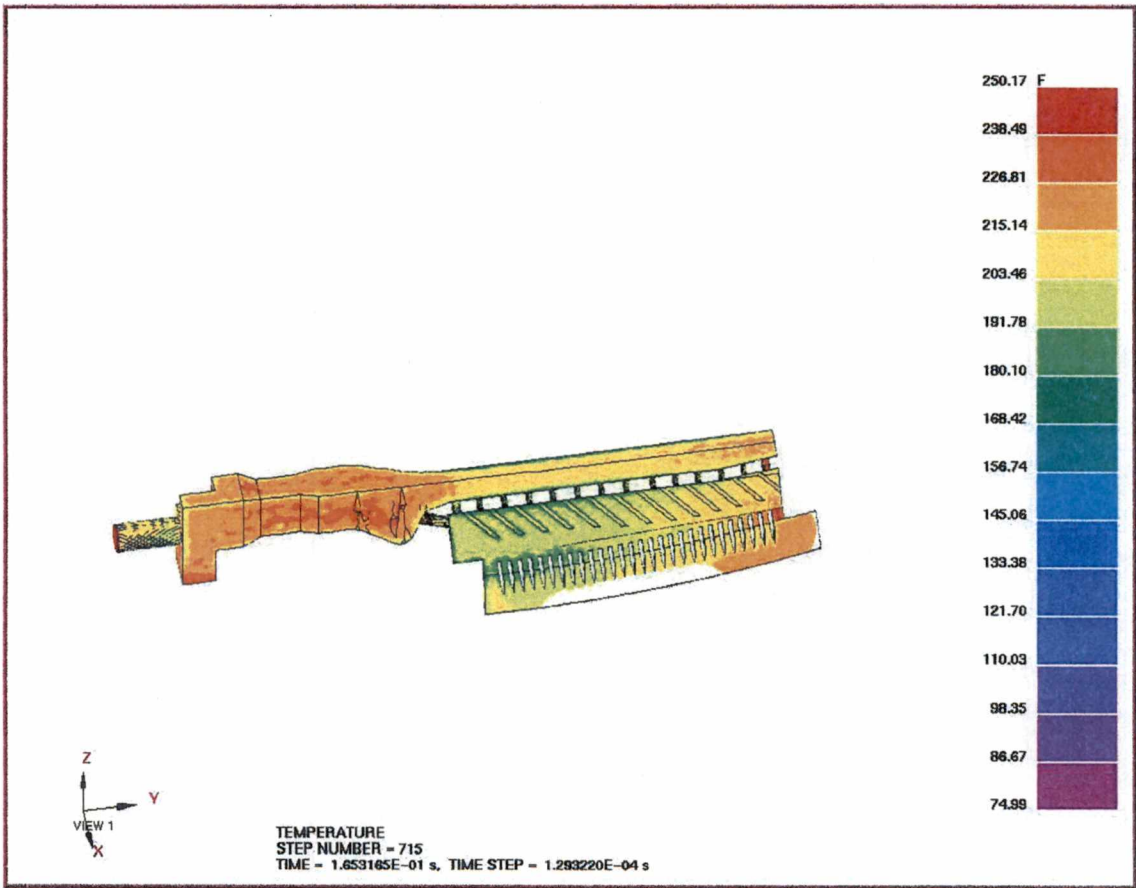


Figure 67. Filling pattern of computer simulation case P-2 at time of 163.3 ms

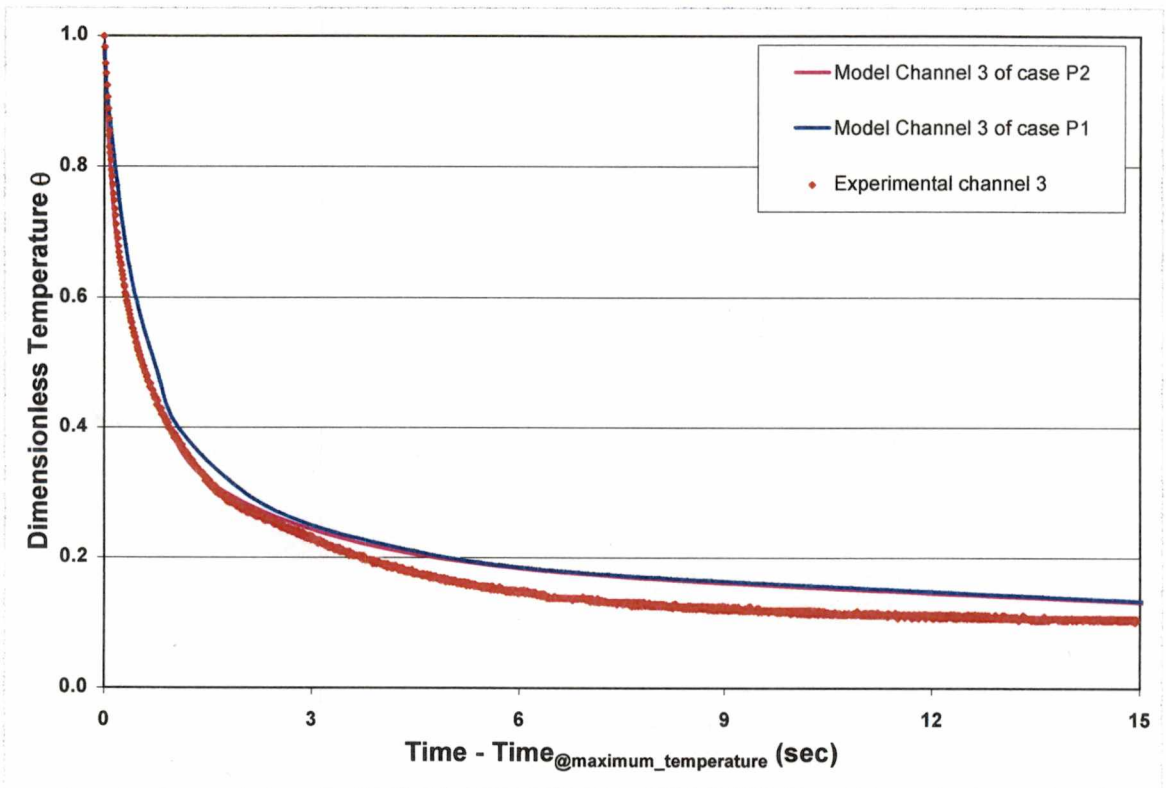


Figure 68. Comparison of experimental and predicted temperatures as a function of time for channel 3 of computer simulation cases P-1 and P-2 (Node 10554).

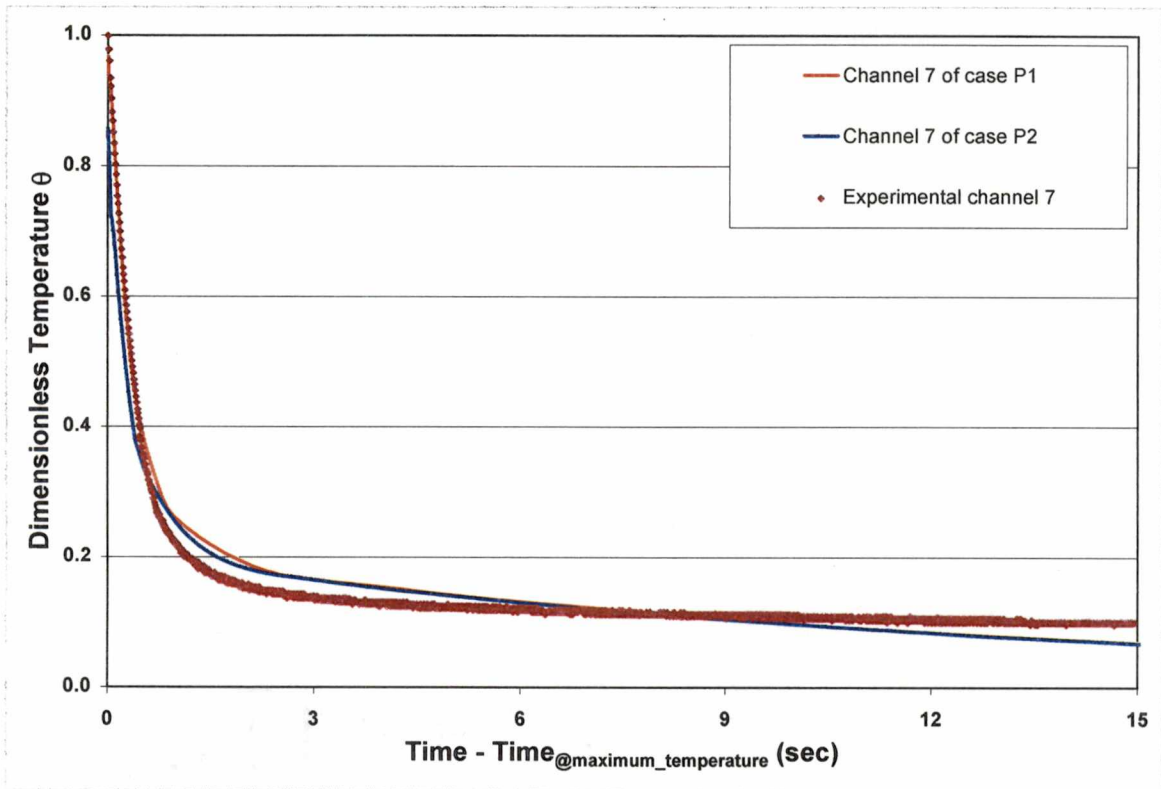


Figure 69. Comparison of experimental and predicted temperatures as a function of time for channel 7 of computer simulation cases P-1 and P-2 (Node 29541).

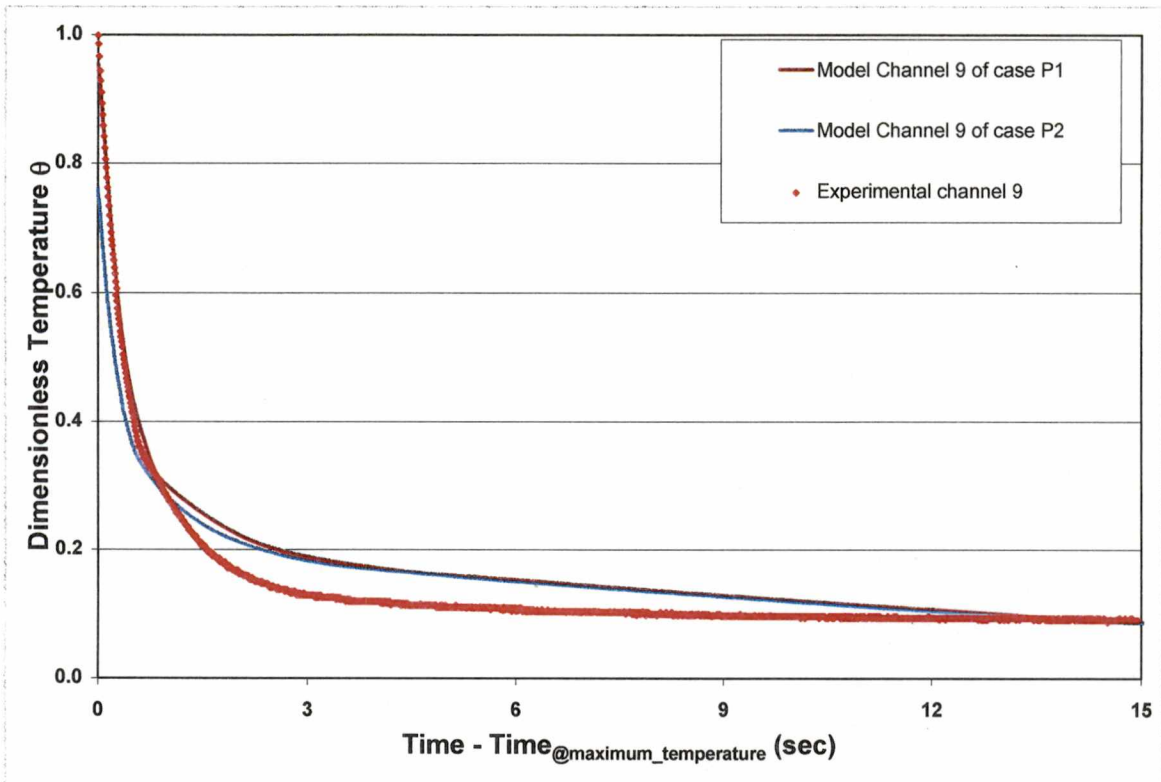


Figure 70. Comparison of experimental and predicted temperatures as a function of time for channel 9 of computer simulation cases P-1 and P-2 (Node 25798).

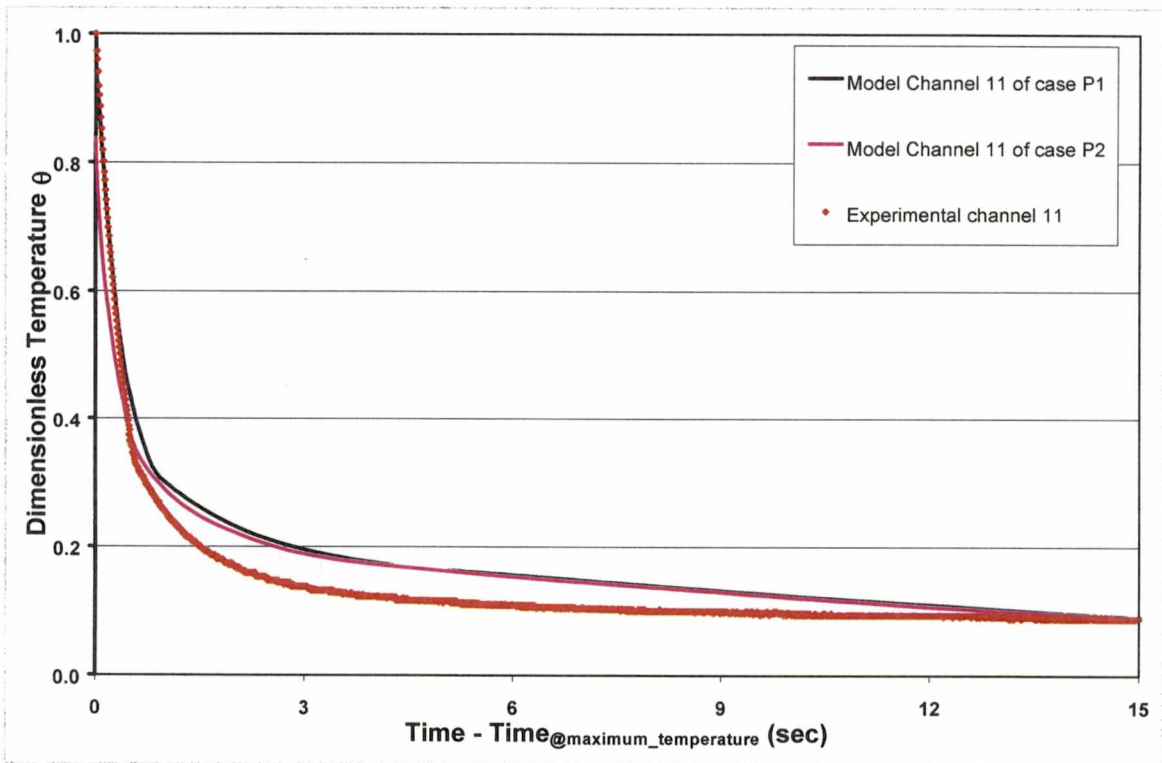


Figure 71. Comparison of experimental and predicted temperatures as a function of time for channel 11 of computer simulation cases P-1 and P-2 (Node49704).

6.2 Summary of Results

It was shown by computer simulation results that the case V-5 (or case P-1) with the ramp function change of the interfacial heat transfer coefficient had the best predicted temperature distributions of all four channels 3, 7, 9, and 11 of all computer simulation cases. These predicted temperature distributions of case V-5 (or case P-1) were in good agreement with the experimental temperatures. The predicted temperatures of the model channels fall in the error bands of the experimental data from the injected temperature to the solidifying temperature. From the solidifying temperature down to the ambient temperature, the predicted temperatures deviated from the experimental values in a narrow margin of about 5%. The deviation was small and acceptable. The filling pattern of the ceramic core in the injection molding process was a desirable pattern. With this filling pattern, the weld line would no longer be a problem in the injection molding process because the injected material filled the trailing edge of the core from the root end to the tip end, instead of filling both root end and tip end first, and then meet at the center section of the core trailing edge. The results of the predicted temperatures of four channels from the computer simulation case P-2 also showed good agreement between its temperature distributions and the temperature distributions from case P-1 or case V-5 as seen in Figures 68 to 71. The maximum temperature of each channel of the computer simulation case P-2 was lower compared to the maximum temperatures of case P-1 (or case V-5). The longer filling time associated with case P-2 results in lower inlet velocity, and lower shear rates in the die cavity compared to case P-1 (or case V-5). Therefore, lowering injection velocity reduces die wear. Furthermore, the filling pattern of the ceramic core of this computer simulation case was not preferable because it would

introduce the weld line to the final products. In conclusion, the simulation case V-5 (or case P-1) represented the best estimate of the interfacial heat transfer coefficient of the injected material, and yielded reasonable temperature distributions of all channels, and preferable filling pattern of the injection molding process of the ceramic core.

CHAPTER 7

CONCLUSIONS AND RECOMMENDATIONS FOR FUTURE WORK

7.1 Conclusions

The main objective of this study was to develop a computer model in ProCAST to simulate the ceramic core injection molding process of a production ceramic core and validate the results. In the thermal-fluid specification of the model, the main challenge turns out to be the identification of the effective heat transfer coefficient at the surface of the part such that the resulting temperature distributions at four selected points in the flow region are in agreement with the measured temperature profiles.

This objective was successfully met within the accuracy of the experimental results. The model predictions of case V-5 (or case P-1) were in good agreement with the time-temperature data collected at four locations with thermocouples under industrial production conditions of the injection molding process. In case V-5 the heat transfer coefficient represented a high value while the fluid remained above the solidus temperature and decreased linearly as the material is cooled below that temperature as shown below:

$$h = \begin{cases} 1800 \text{ W/m}^2 \text{ K} & T \geq 58^\circ \text{C} \\ a * T + b & 58^\circ \text{C} \geq T \geq 40^\circ \text{C} \\ 100 \text{ W/m}^2 \text{ K} & 40^\circ \text{C} \geq T \geq 23^\circ \text{C} \end{cases}$$

In addition, it also yielded a very desirable filling pattern that would avoid the introduction of weld line into the quality of the final product. Overall, the model

developed was shown to predict successfully the thermal characteristics of the core filling process.

7.2 Recommendations for Future Work

For future work, it would be highly beneficial to transfer electronically geometric data of parts and die between Howmet Research Corporation and the Advanced Casting Laboratory at the University of Tennessee, Knoxville. The thermal analysis developed in this study could be used to model new geometries and new ceramic core materials provided by Howmet Research Corporation. The effects of process parameters on filling and solidification patterns of ceramic core should be studied for quality improvement.

◦

LIST OF REFERENCES

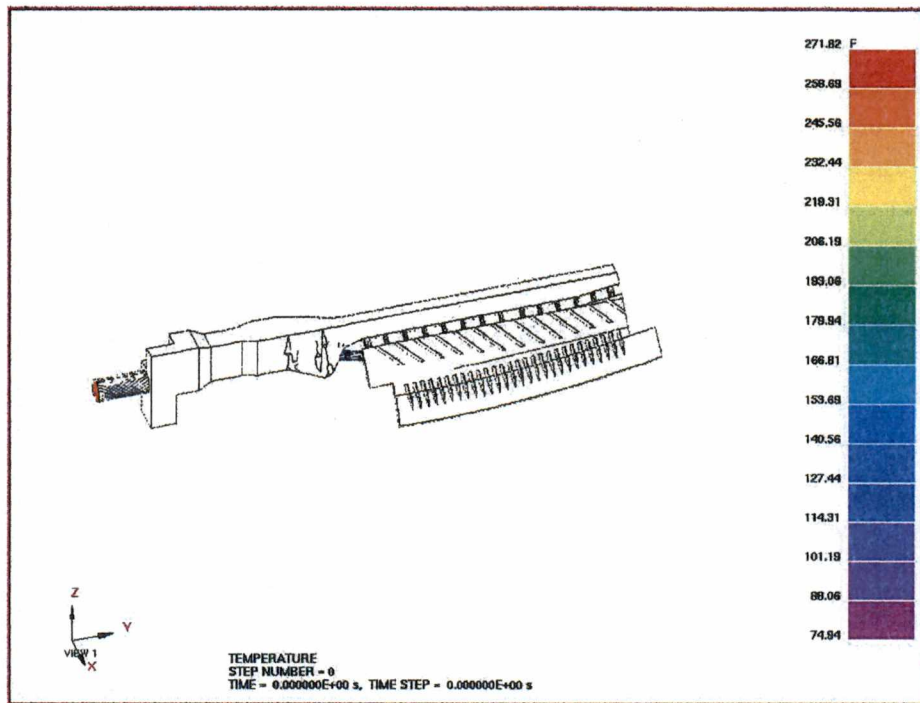
1. Kumar, N., Besant, C.B., and Ristic, M., "Process Variables Determining the Dimensional and Metallurgical Properties of Directionally Solidified, Cored Turbine Blades Produced by Investment Casting of Supper-Alloys", The International journal, advanced manufacturing technology, Vol. 3, No. 2, 1988, pp. 3-19.
2. ProCAST® User's Manual, Version 3.1.0, UES Software, Inc., Annapolis, MD, 1996.
3. Milne, J., "Casting Techniques Make Turbines More Efficient", Metallurgia, Vol. 61, Nov 1994, pp. 331.
4. <http://www.howmet.com/homepage.nsf>
5. Mangels, J. A., "Ceramic Components by Injection Molding", Advances in Ceramics, Vol. 9, 1984, pp. 220-33.
6. Mutsuddy, B. C., "Past, Present, and Future of Ceramic Injection Molding", Journal of the Australasian Ceramic Society, Trans Tech Publications, Vol. 26, No. 2, 1990, pp. 93-126.
7. Evans, R. J., "Ceramic Injection Molding and Related Process", Ceramic Technology International, Sterling Publications, London, 1992, pp. 171-175.
8. Tu, J.S., Foran, R.K., Hines, A.M., and Aimone, P.R., "An Integrated Procedure for Modeling Investment Castings", JOM Journal, Vol. 47. No. 10, 1995, pp. 64-68.
9. Zhang, T., and Evans, J.R.G., " Calculation of Temperature Distributions During the Solidification Stage in Ceramic Injection Molding," Journal of American Ceramic Society, Vol. 75, No. 8, 1992, pp. 2260-67.

10. Hunt, K.N., and Evans, J.R.G., "Computer Modelling of the Origin of Defects in Ceramics Injection Moulding I. Measurement of Thermal Properties," Journal of Materials Science, Vol. 26, 1991, pp. 285-291.
11. Hunt, K.N., and Evans, J.R.G., "Computer Modelling of the Origin of Defects in Ceramics Injection Moulding II. Shrinkage Voids," Journal of Materials Science, Vol. 26, 1991, pp. 292-300.
12. Nogueira, R.E.F.Q., Edirisinghe, M.J., and Gawne, D.T., "Selection of a Powder for Ceramic Injection Moulding," Journal of Materials Science, Vol. 27, 1992, pp. 6525-31.
13. Kostic, B., Zhang, T., and Evans, J.R.G., "Measurement of Residual Stress in Injection-Molded Ceramics," Journal of the American Ceramic Society, Vol. 75, No. 10, 1992, pp. 2773-78
14. Wang, C.M., Carr, K.E., and McCabe, T.J., "Computer Simulation of the Powder Injection Molding Process," Advances in Powder Metallurgy & Particulate Materials, 1994: Proceedings of the 1994 International Conference & Exhibition on Powder Metallurgy & Particulate Materials, Vol. 4, May 1994, pp. 15-25.
15. Zhang, J. G., Edirisinghe, M. J., and Evans R. J., "Catalog of Ceramic Injection Molding Defects and Their Causes", Industrial Ceramics, Faenza, Italy, 1989, Vol. 9, No. 2, pp. 72-82.
16. William, S., Strack, C., and Zeighami, R., "Computer Simulation of the Ceramic Injection Molding Process," University of Tennessee, Knoxville, May 11, 1998.

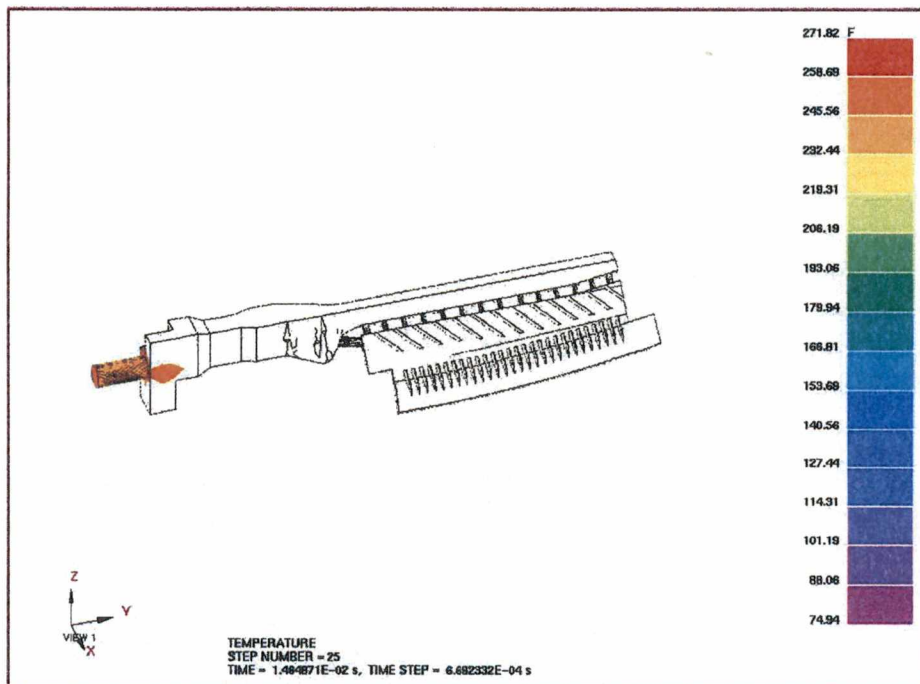
17. Robbins, E., "Model Development and Validation of a Ceramic Core Injection Molding Process," MS Thesis in Preparation, University of Tennessee, Knoxville, 2001.
18. Lewis, M., "Measurement of Fluid Temperature Variations in an Industrial Setting During a Ceramic Core Injection Molding Process," MS thesis in Preparation, University of Tennessee, Knoxville, 2001.
19. SolidWorks® 98 User's Guide, SolidWorks Corporation, 1998.
20. MeshCAST® User's Manual, Version 1.3.0, UES Software, Inc., Annapolis, MD, 1996.
21. Incropera, F.P., and DeWitt, D.P., Fundamentals of Heat and Mass Transfer, 4th Ed., John Wiley and Sons, New York, 1996.
22. Ly, A., "Experimental Validation of Computer Simulations of Ceramic Core Injection Process," MS Thesis, University of Tennessee, Knoxville, Dec 2000.

APPENDICES

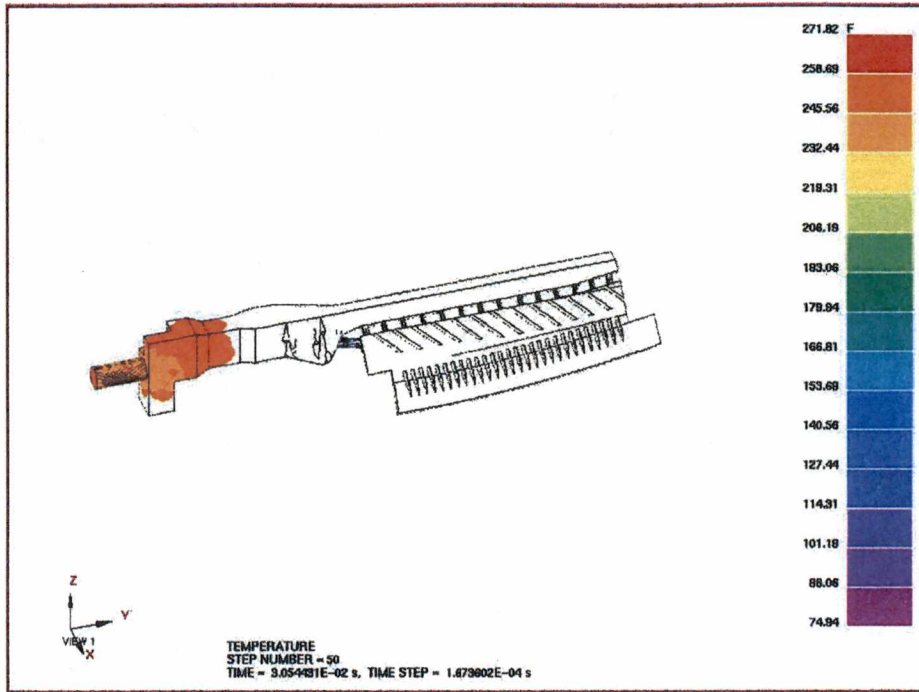
APPENDIX A



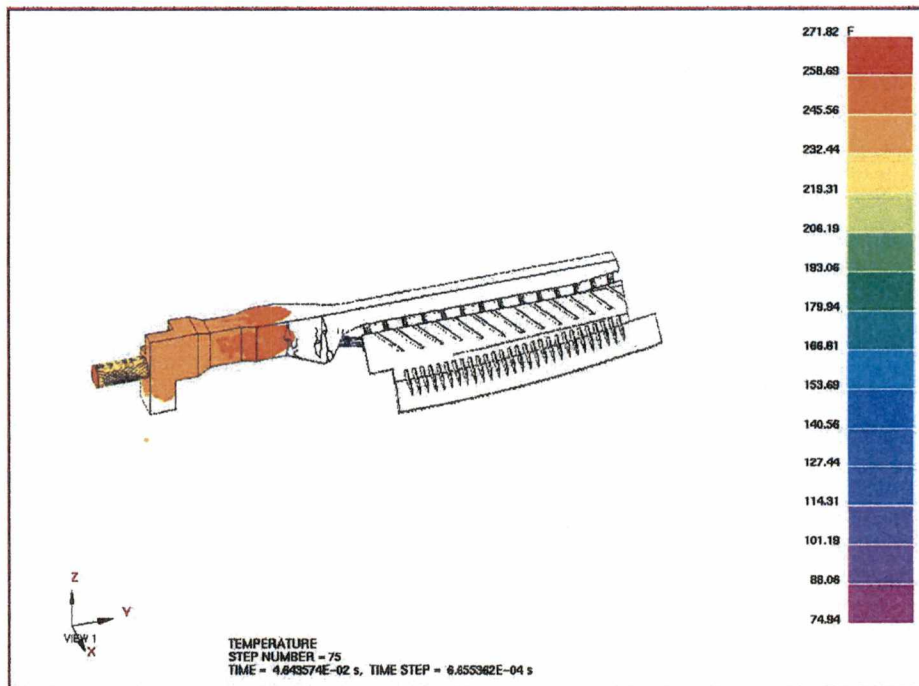
A.1 Temperature contour plot of the case V-5 at time of 0.0 ms



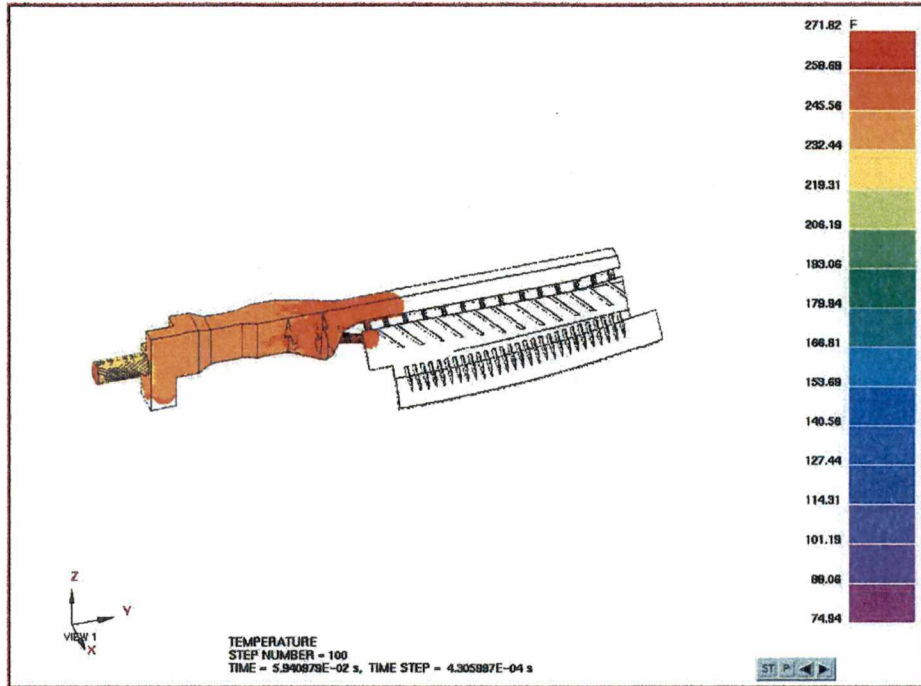
A.2 Temperature contour plot of the case V-5 at time of 14.6 ms



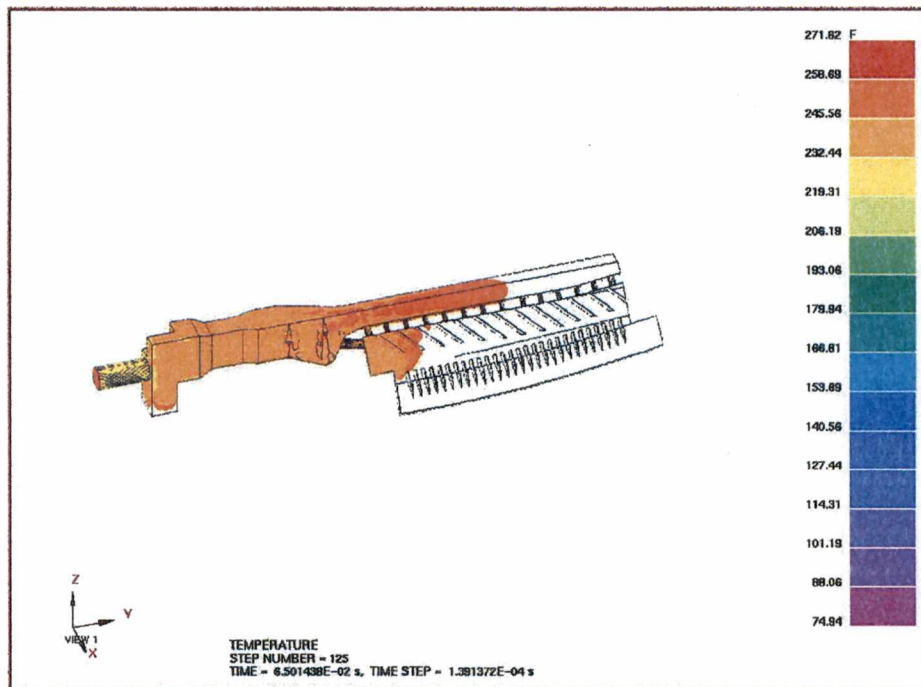
A.3 Temperature contour plot of the case V-5 at time of 30.5 ms



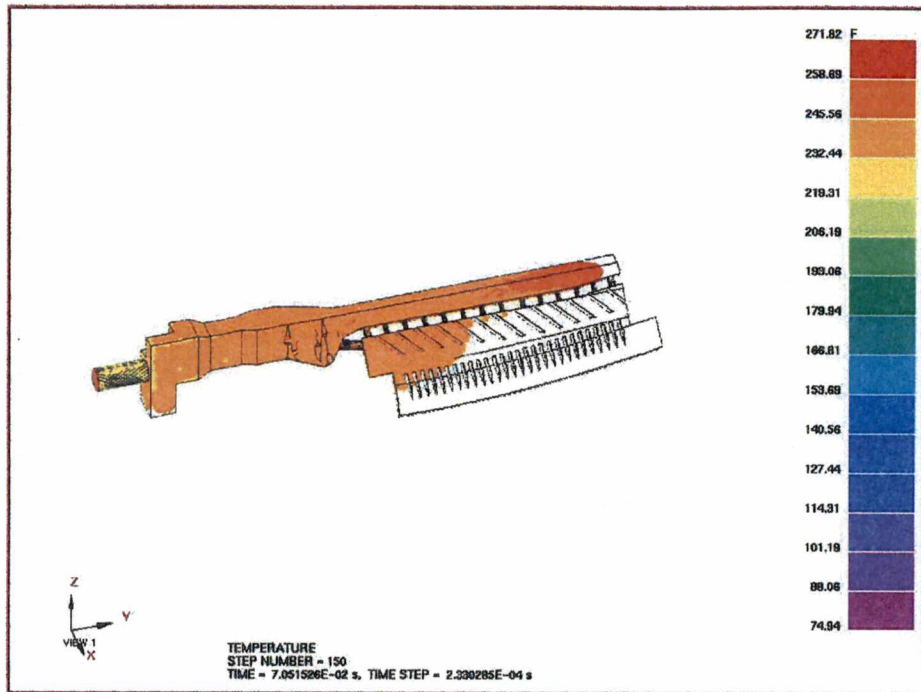
A.4 Temperature contour plot of the case V-5 at time of 46.4 ms



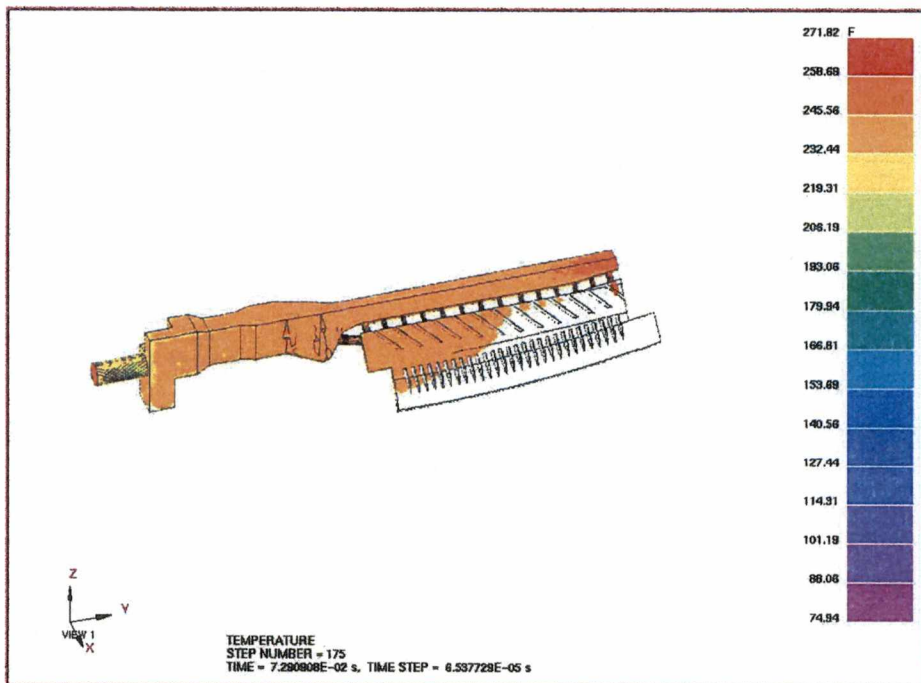
A.5 Temperature contour plot of the case V-5 at time of 59.4 ms



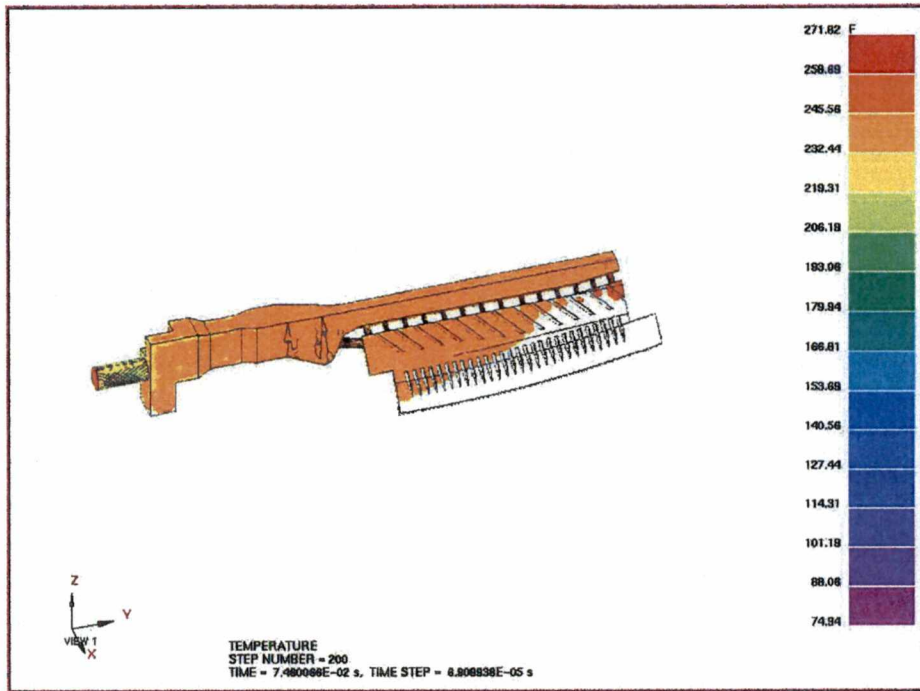
A.6 Temperature contour plot of the case V-5 at time of 65.0 ms



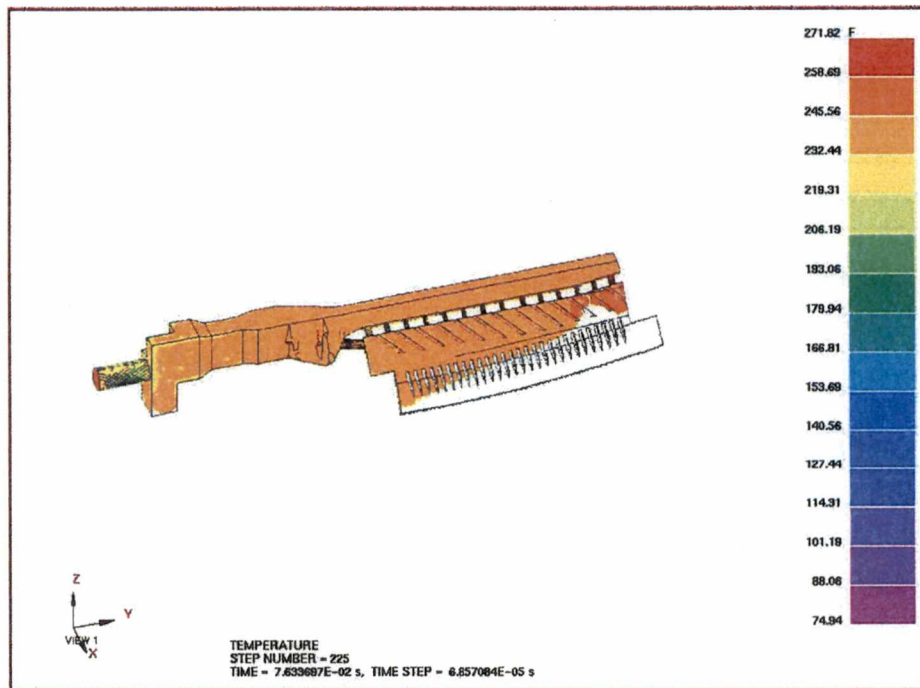
A.7 Temperature contour plot of the case V-5 at time of 70.5 ms



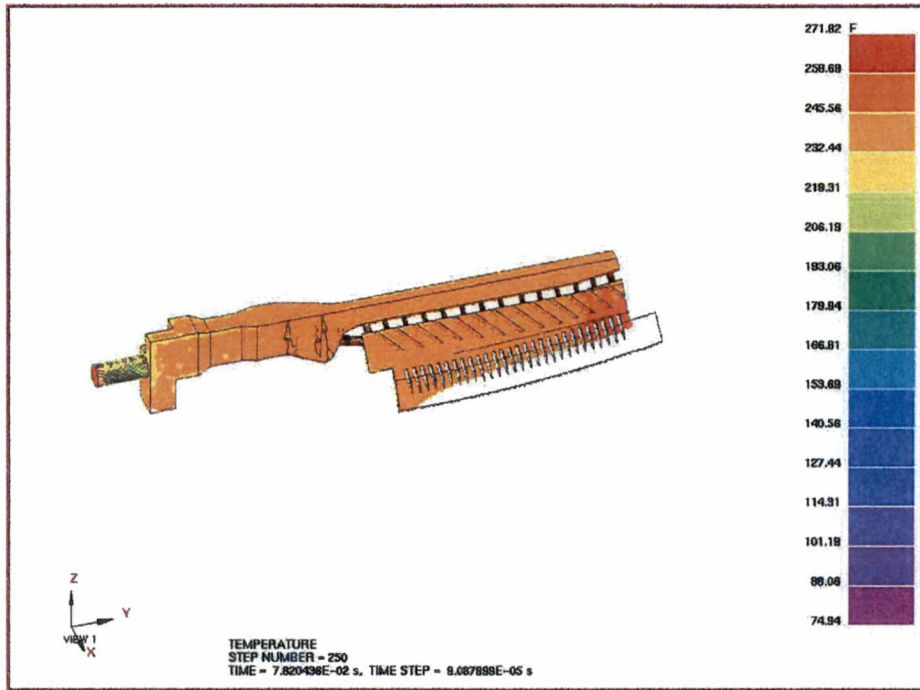
A.8 Temperature contour plot of the case V-5 at time of 72.9 ms



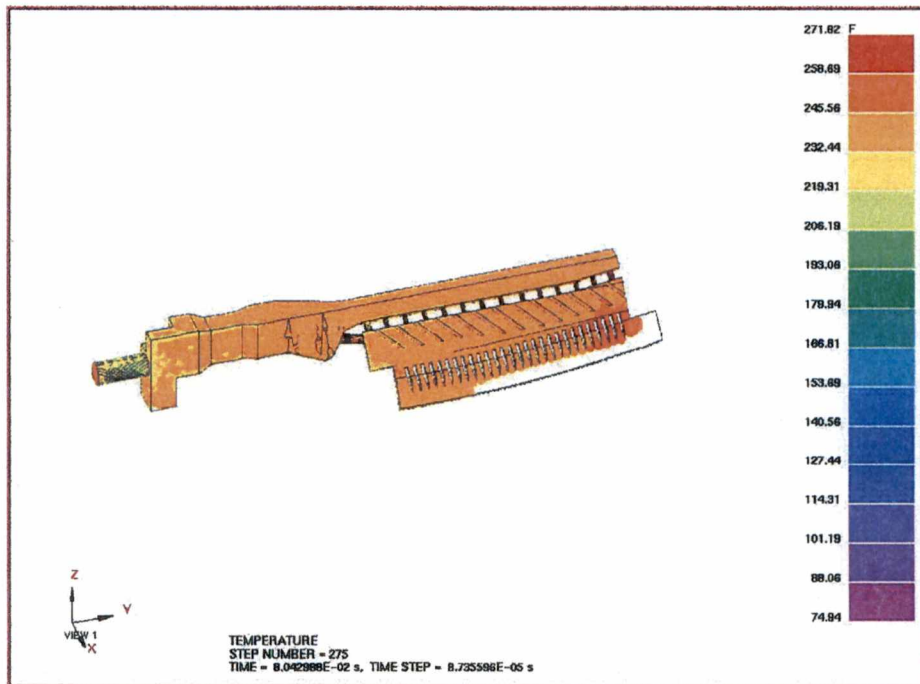
A.9 Temperature contour plot of the case V-5 at time of 74.6 ms



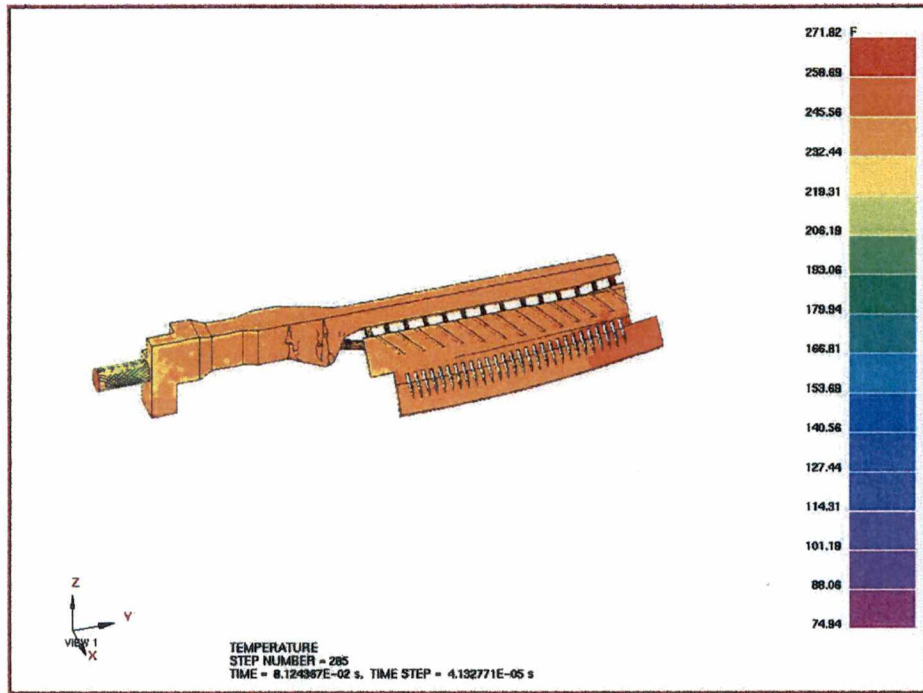
A.10 Temperature contour plot of the case V-5 at time of 76.3 ms



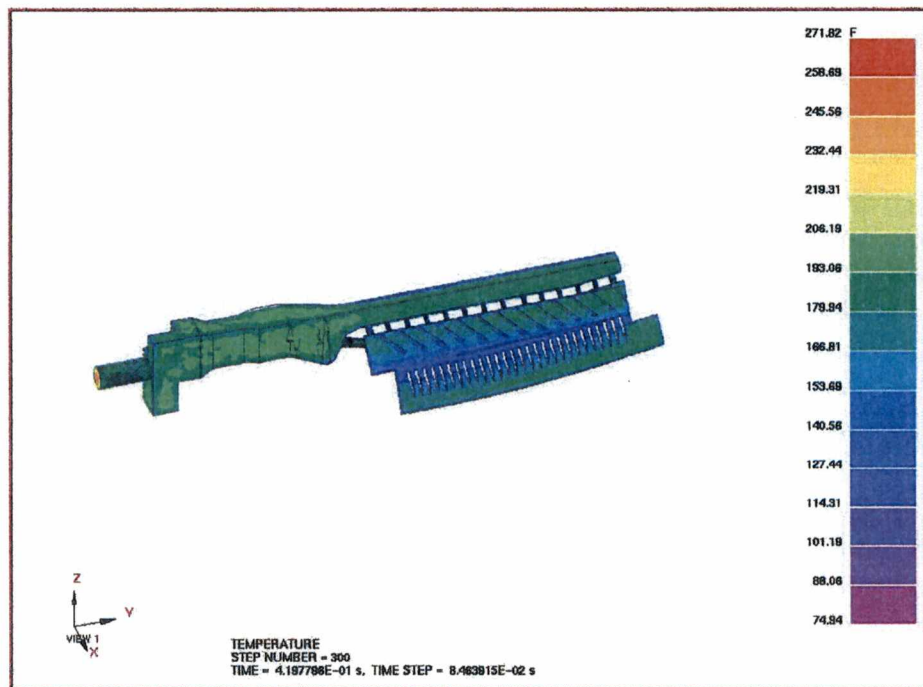
A.11 Temperature contour plot of the case V-5 at time of 78.2 ms



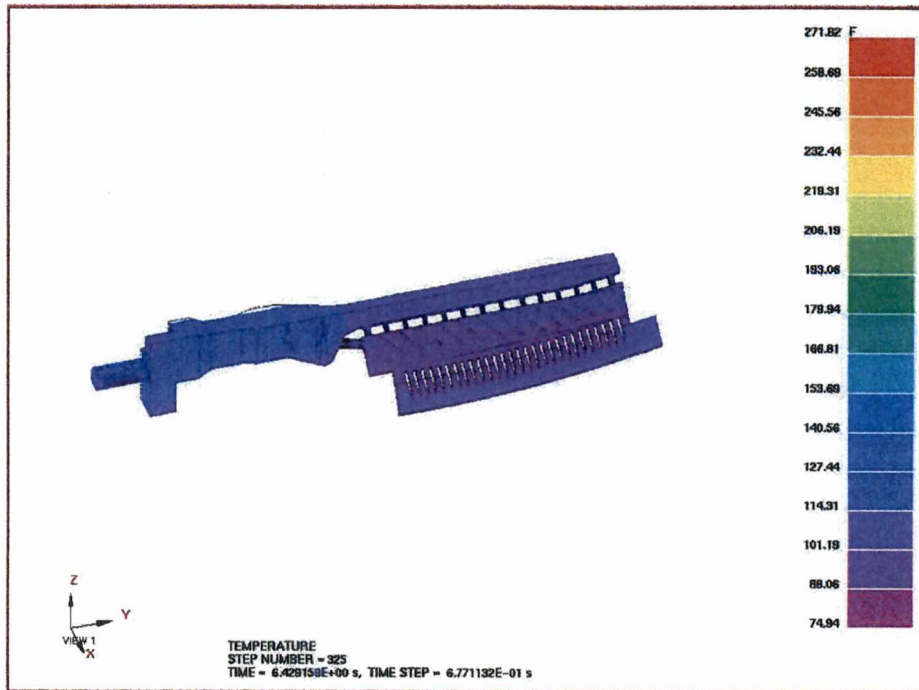
A.12 Temperature contour plot of the case V-5 at time of 80.4 ms



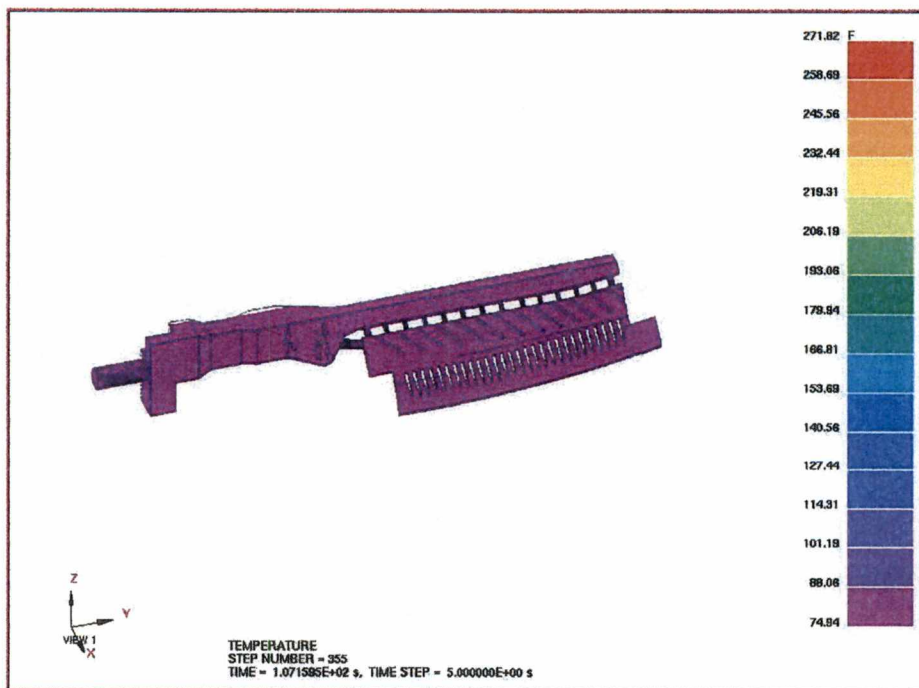
A.13 Temperature contour plot of the case V-5 at time of 81.2 ms



A.14 Temperature contour plot of the case V-5 at time of 0.49 sec

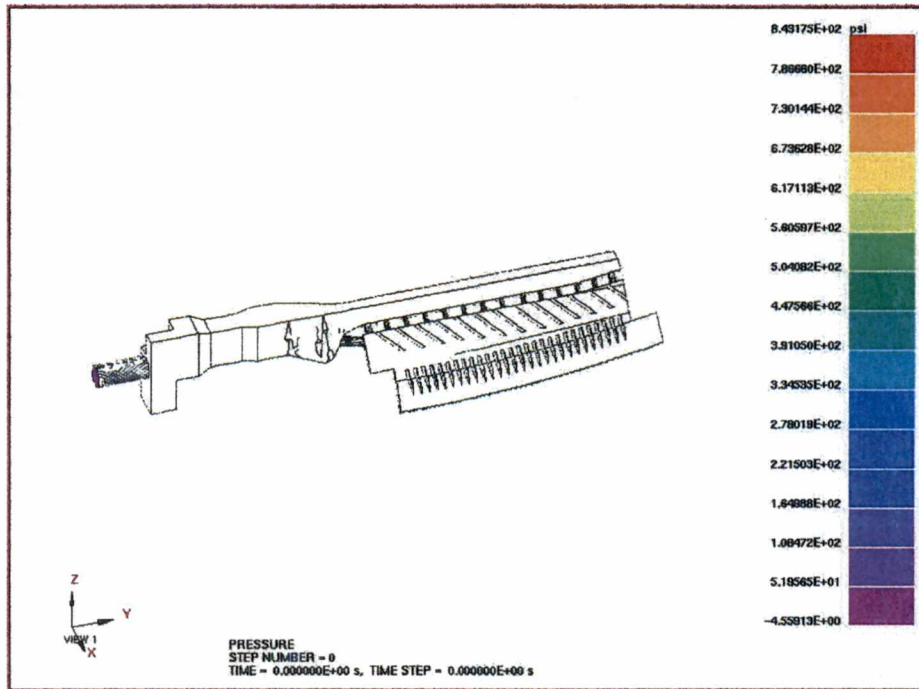


A.15 Temperature contour plot of the case V-5 at time of 6.43sec

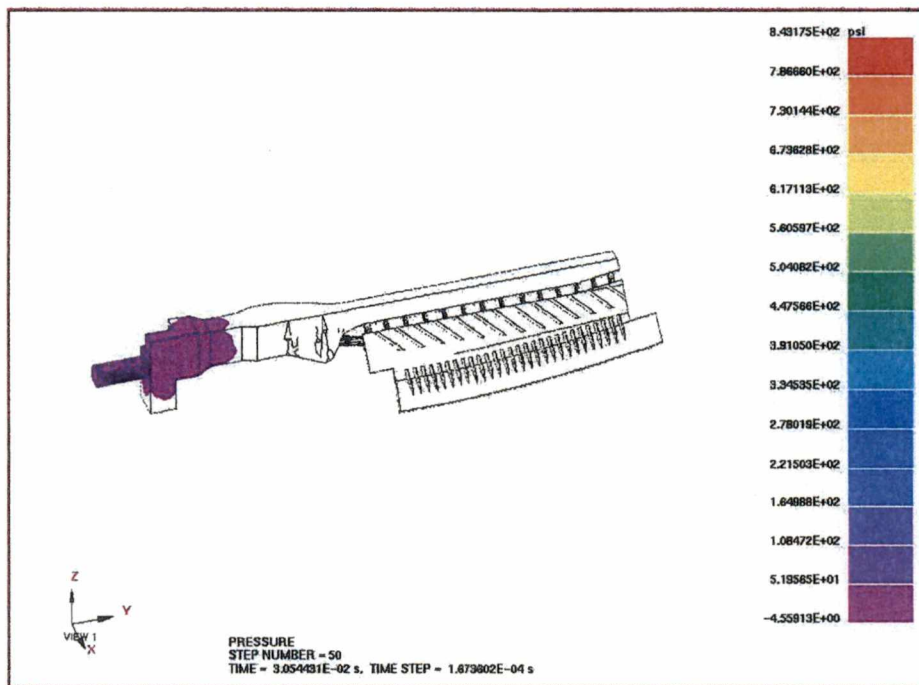


A.16 Temperature contour plot of the case V-5 at time of 107 sec

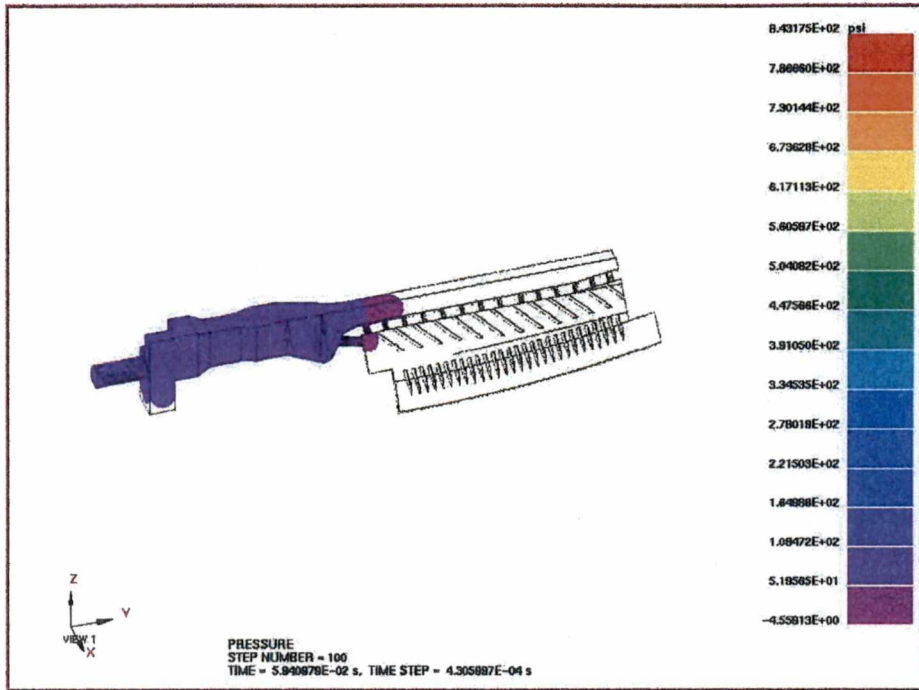
APPENDIX B



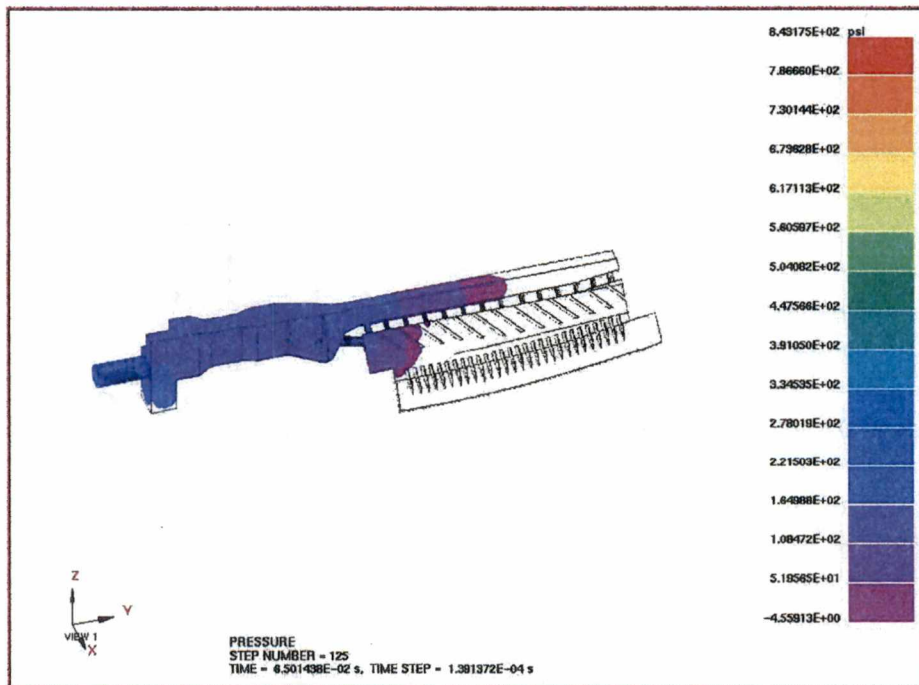
B.1 Pressure contour plot of the case V-5 at time of 0.0 ms



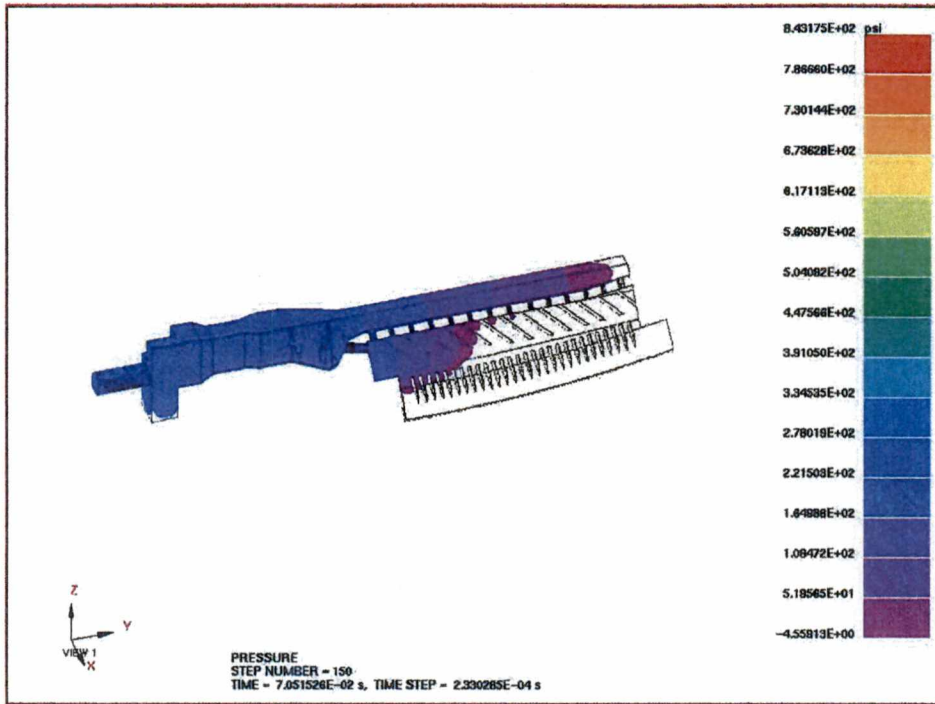
B.2 Pressure contour plot of the case V-5 at time of 30.5 ms



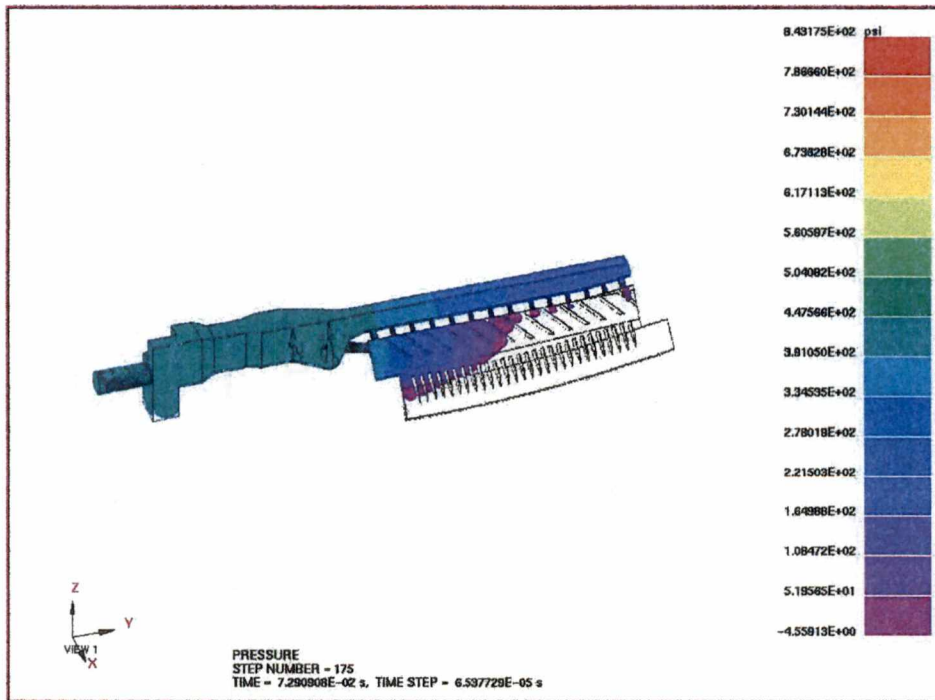
B.3 Pressure contour plot of the case V-5 at time of 59.4 ms



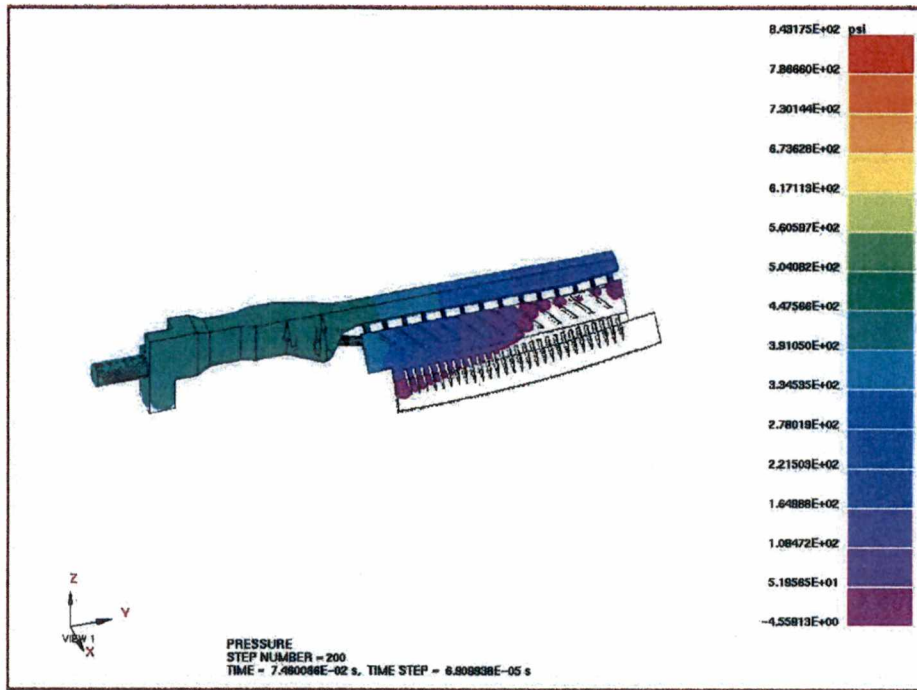
B.4 Pressure contour plot of the case V-5 at time of 65.0 ms



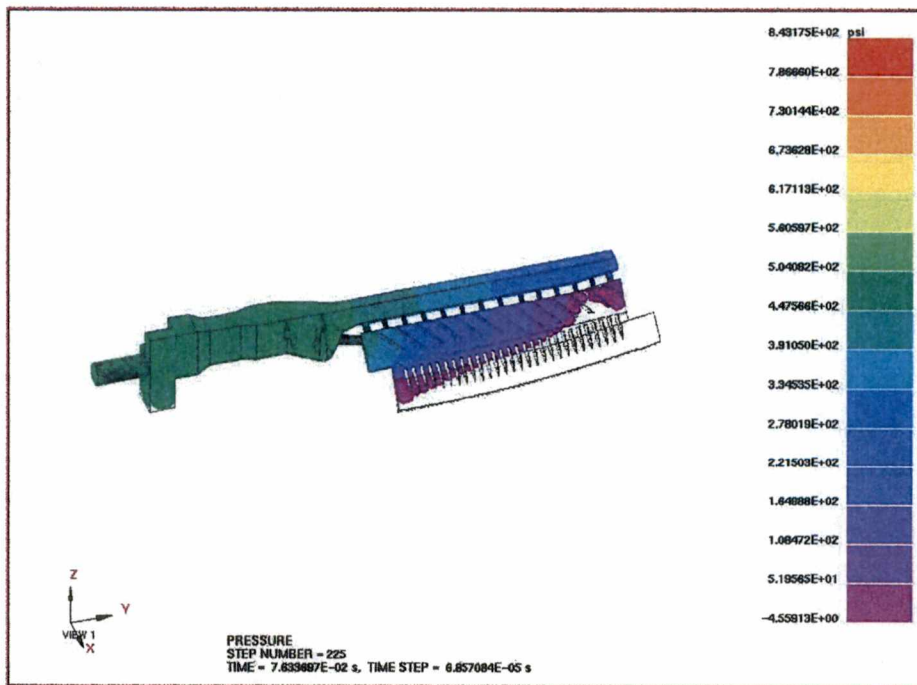
B.5 Pressure contour plot of the case V-5 at time of 70.5 ms



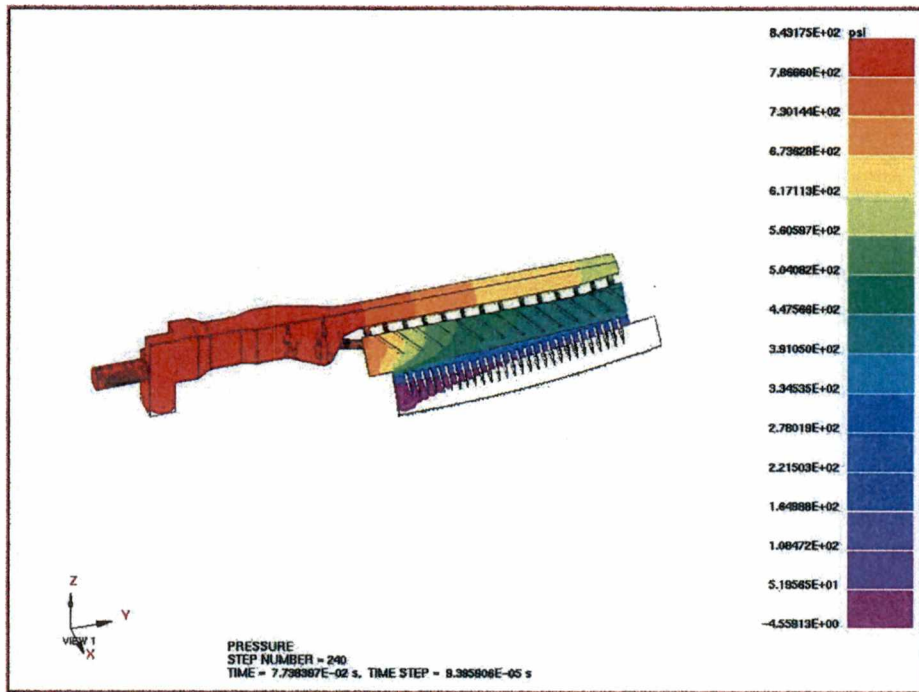
B.6 Pressure contour plot of the case V-5 at time of 72.9 ms



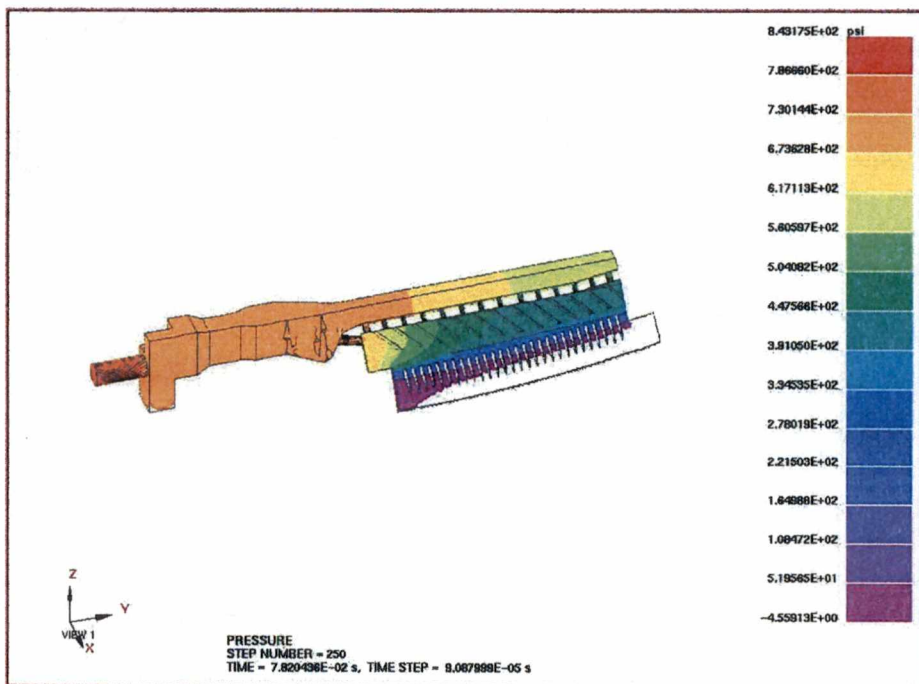
B.7 Pressure contour plot of the case V-5 at time of 74.6 ms



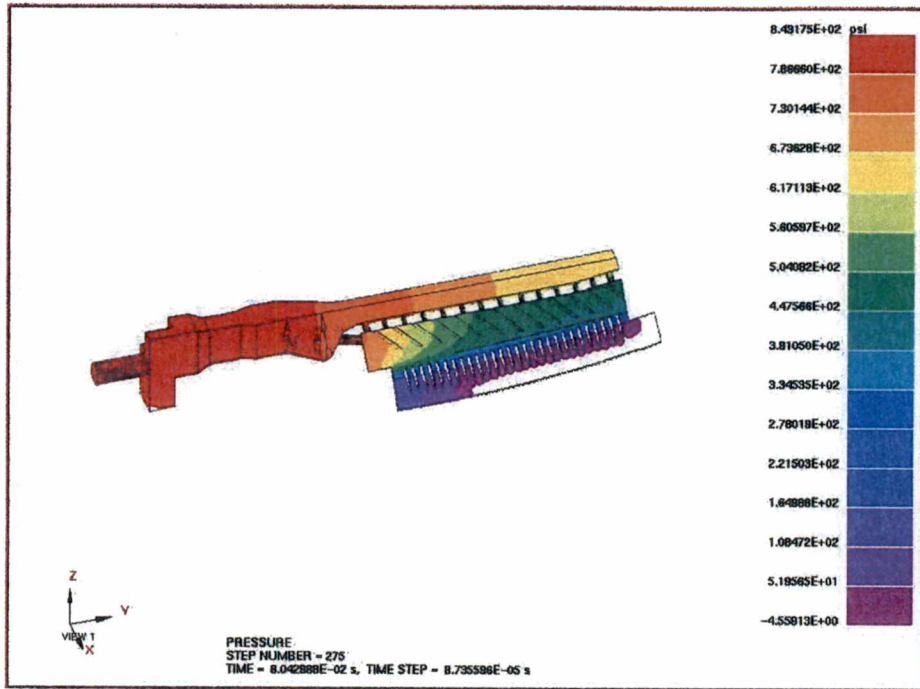
B.8 Pressure contour plot of the case V-5 at time of 76.3 ms



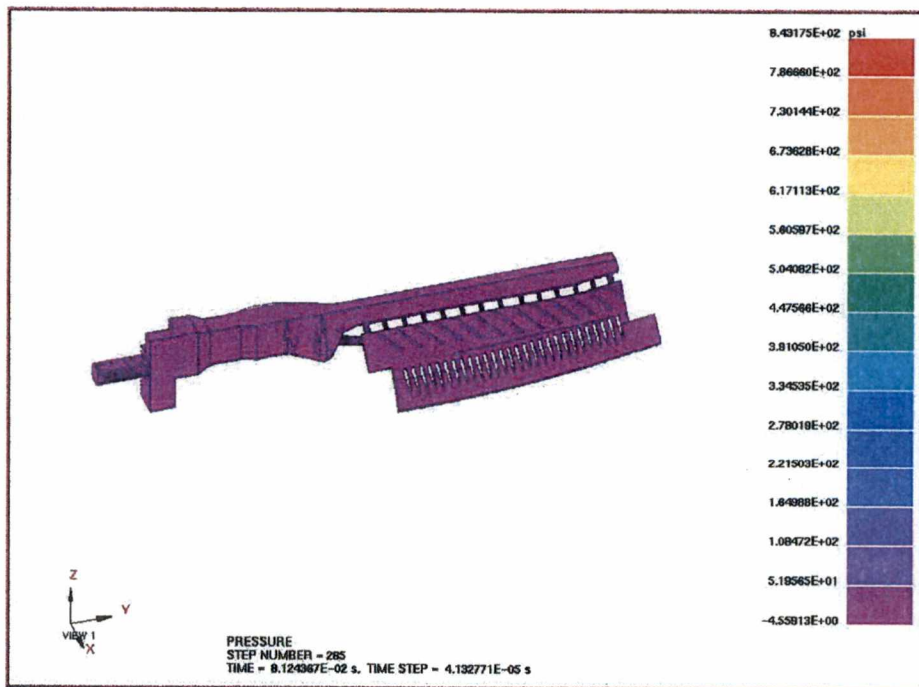
B.9 Pressure contour plot of the case V-5 at time of 77.4 ms



B.10 Pressure contour plot of the case V-5 at time of 78.2 ms

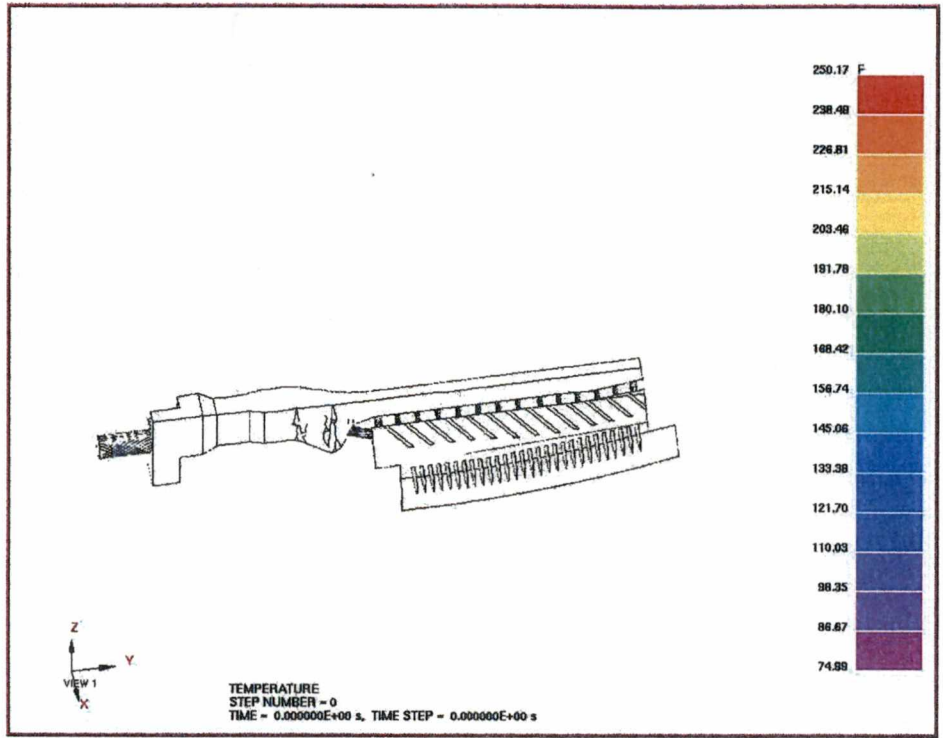


B.11 Pressure contour plot of the case V-5 at time of 80.4 ms

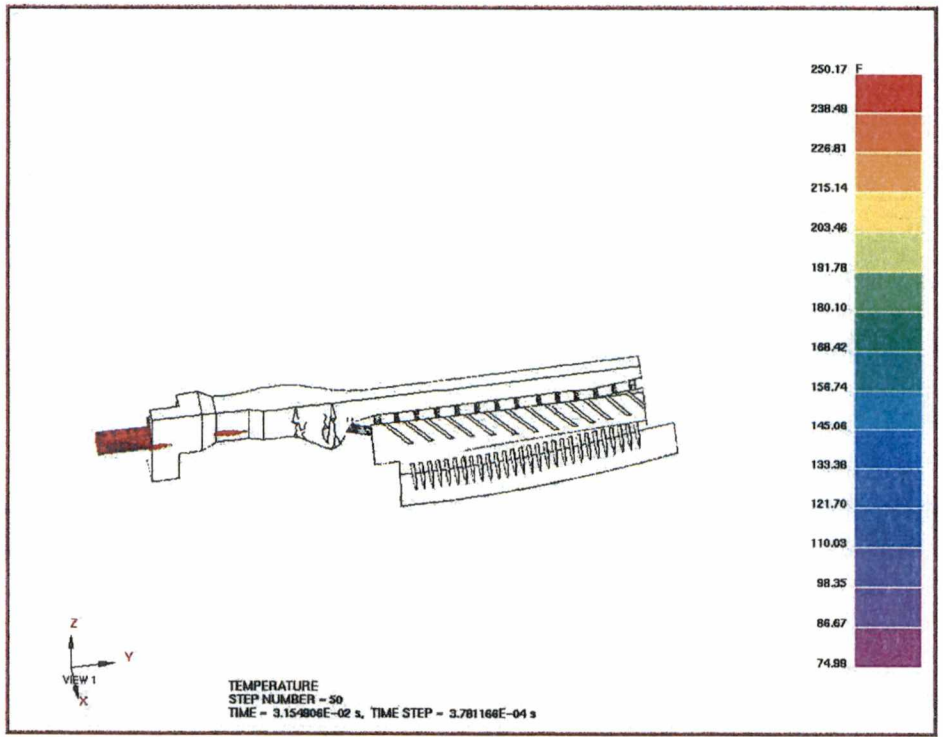


B.12 Pressure contour plot of the case V-5 at time of 81.2 ms

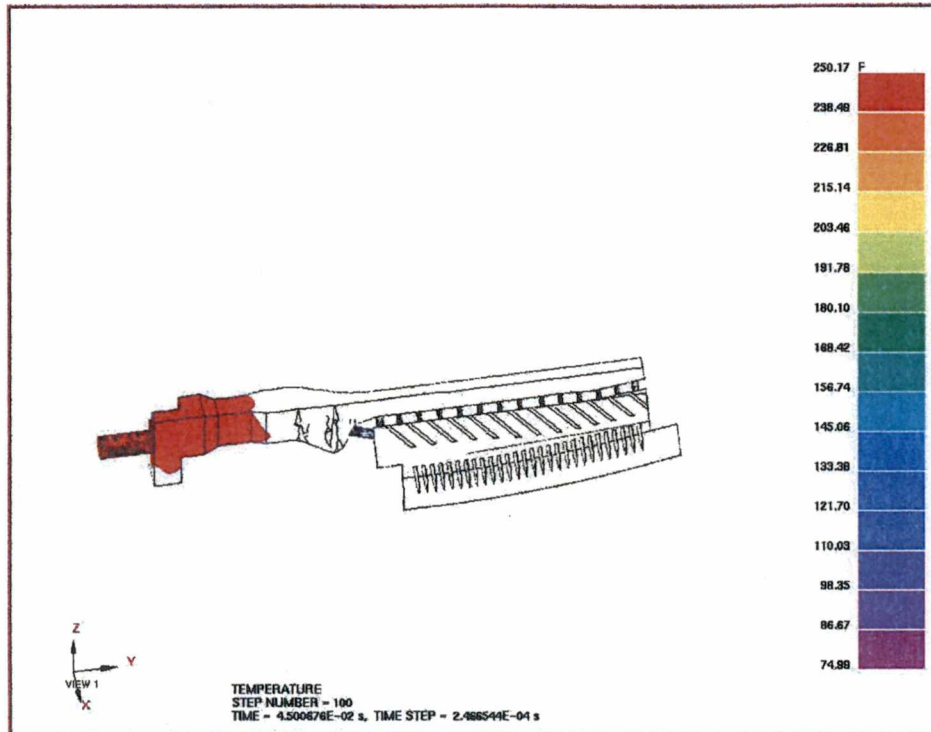
APPENDIX C



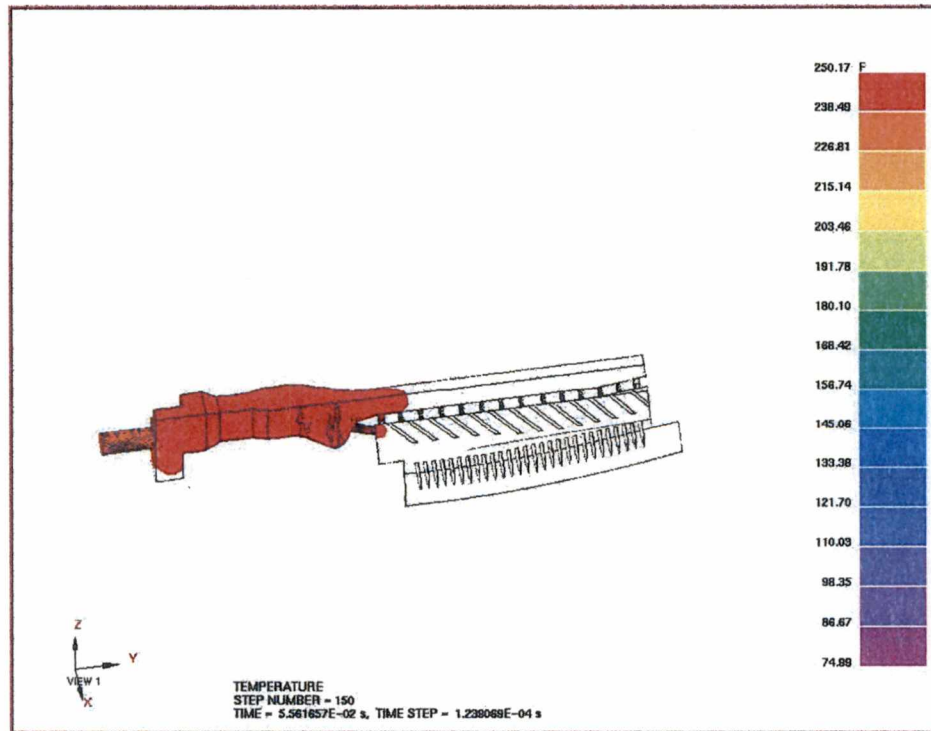
C.1 Temperature contour plot of the P-2 case at time of 0 sec



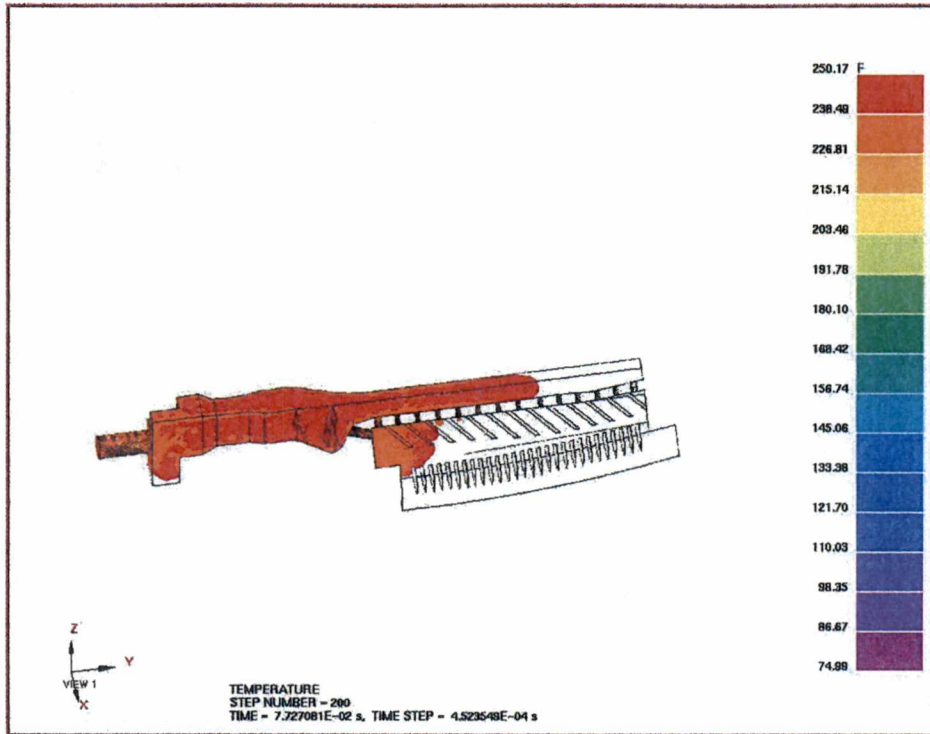
C.2 Temperature contour plot of the P-2 case at time of 0.0316 sec



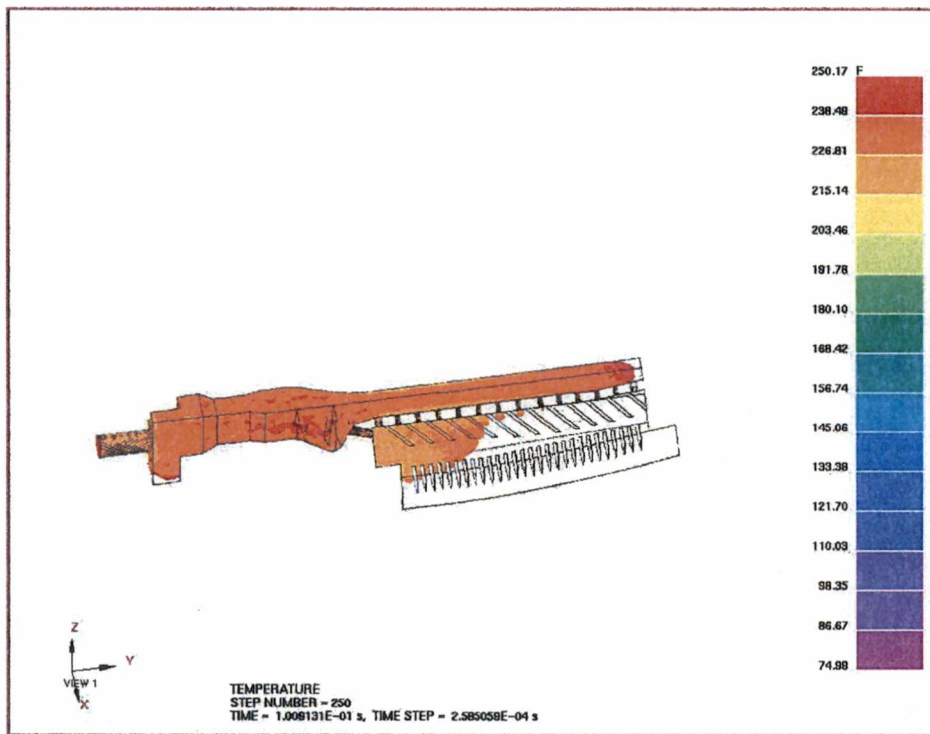
C.3 Temperature contour plot of the P-2 case at time of 0.0450 sec



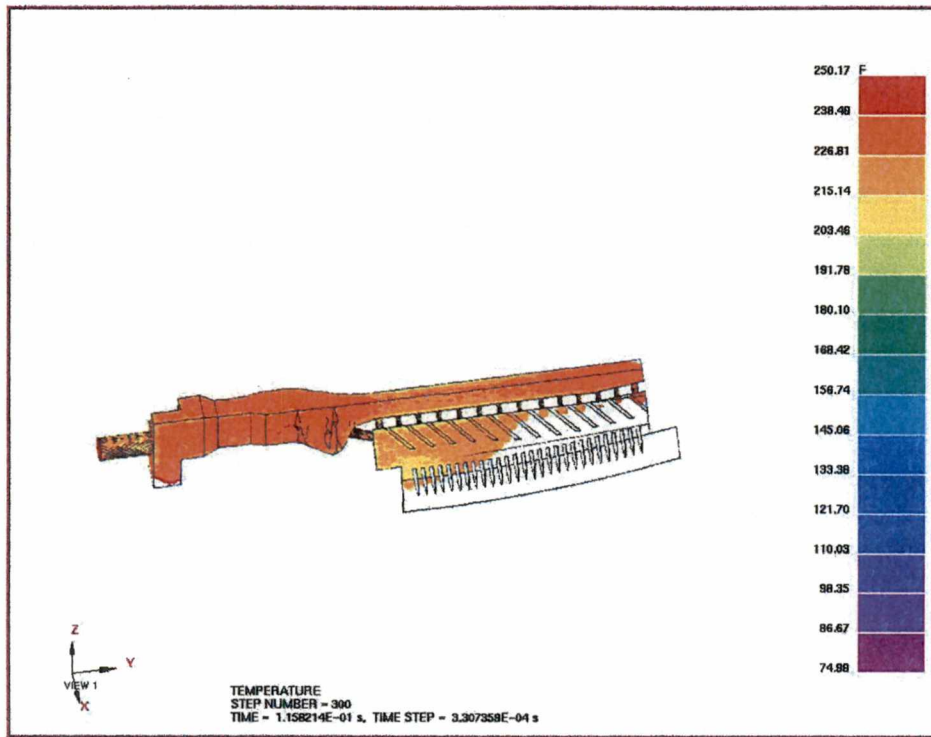
C.4 Temperature contour plot of the P-2 case at time of 0.0562 sec



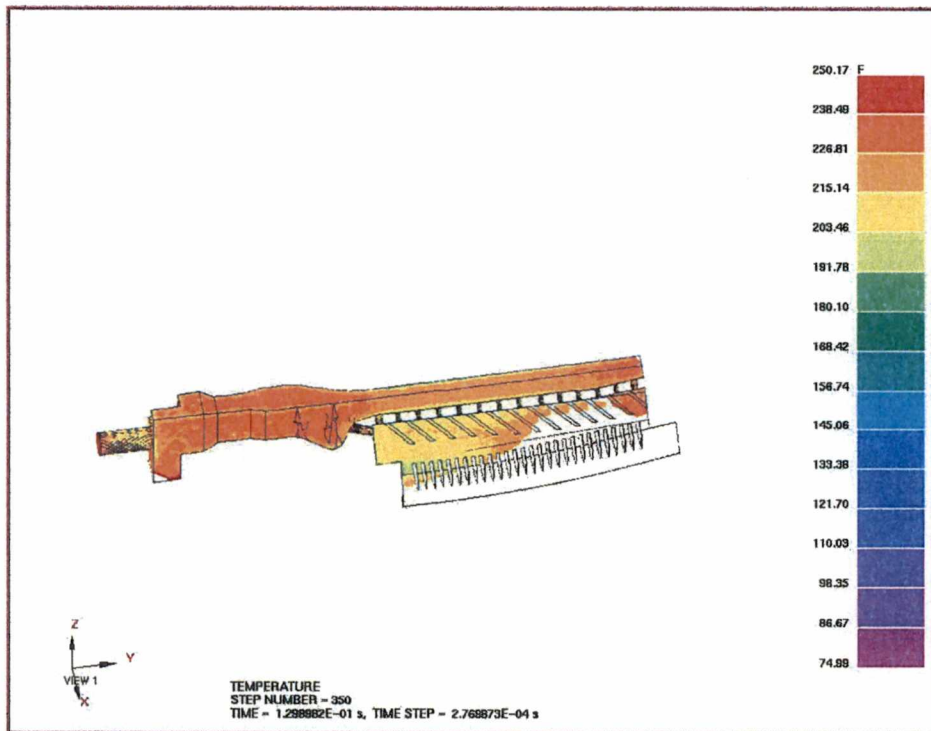
C.5 Temperature contour plot of the P-2 case at time of 0.0727 sec



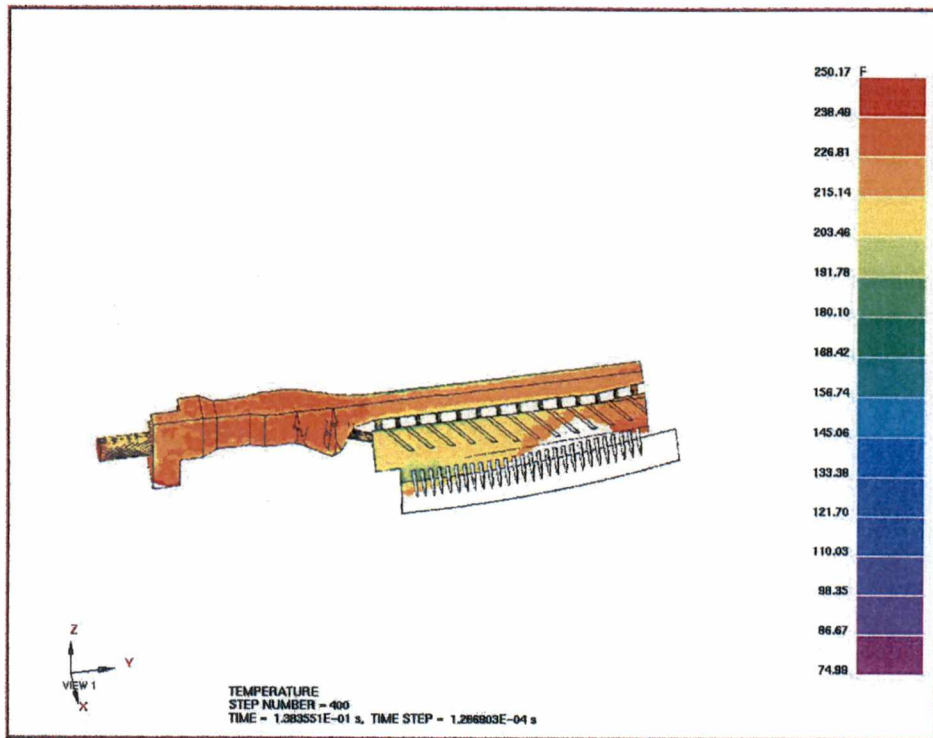
C.6 Temperature contour plot of the P-2 case at time of 0.1009 sec



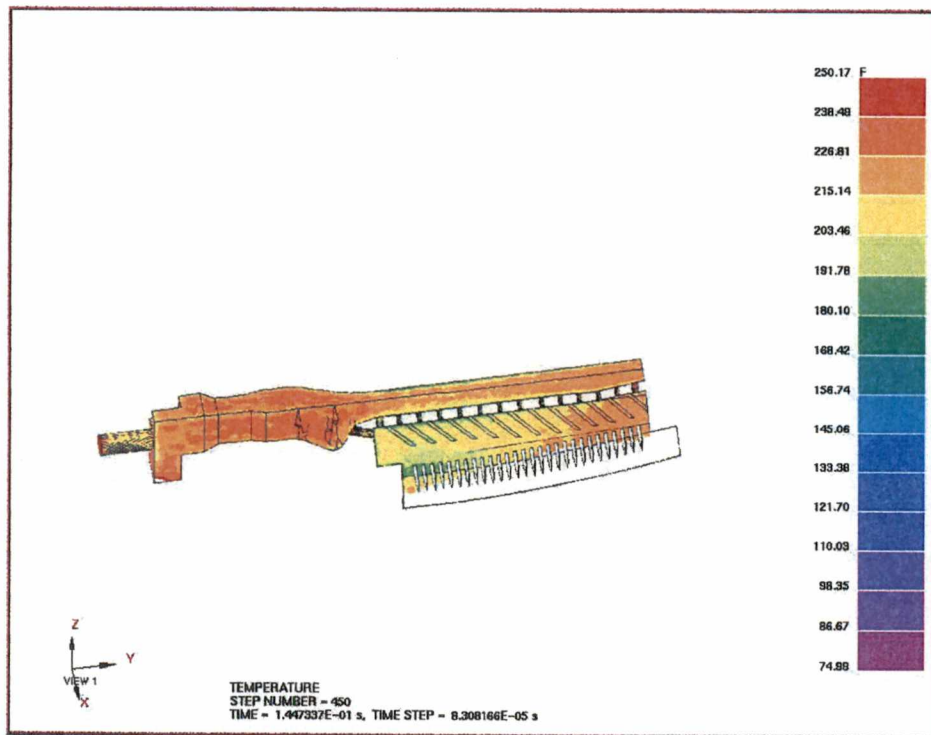
C.7 Temperature contour plot of the P-2 case at time of 0.1158 sec



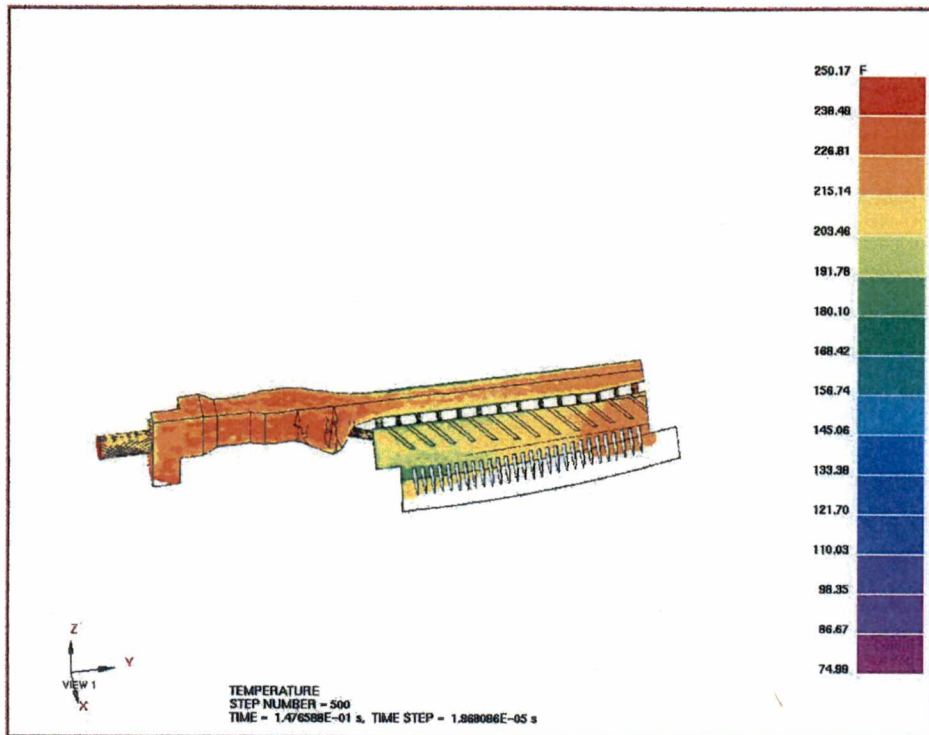
C.8 Temperature contour plot of the P-2 case at time of 0.1299 sec



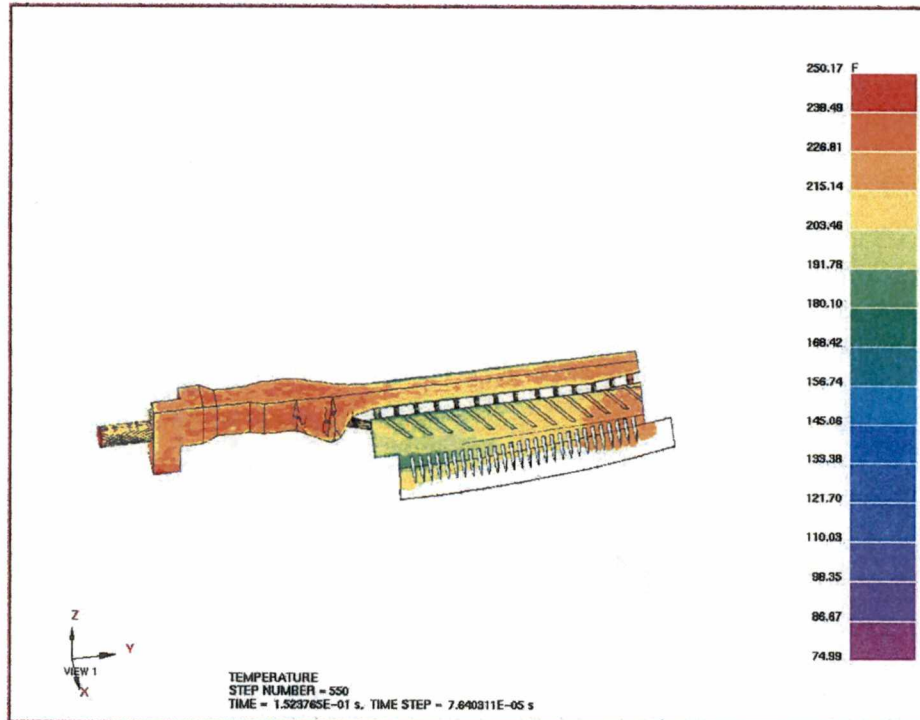
C.9 Temperature contour plot of the P-2 case at time of 0.1384 sec



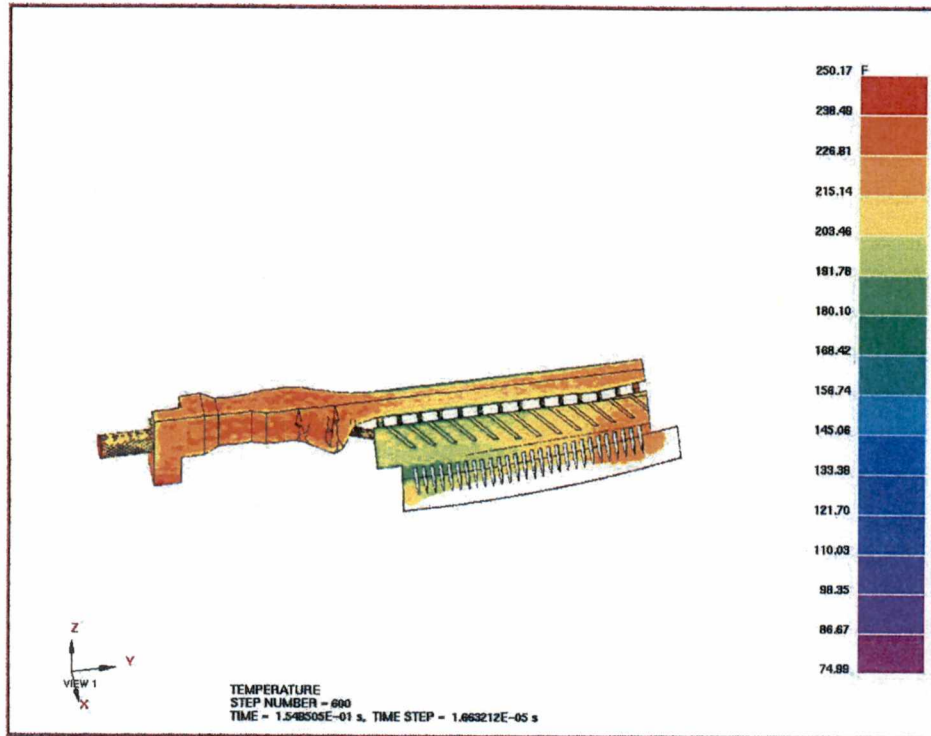
C.10 Temperature contour plot of the P-2 case at time of 0.1447 sec



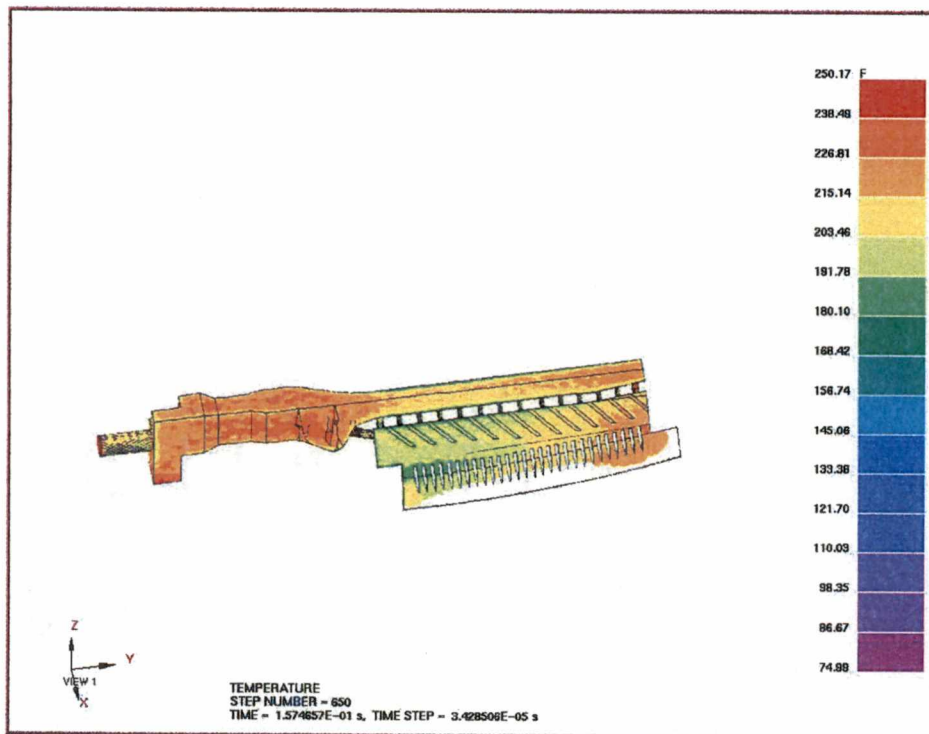
C.11 Temperature contour plot of the P-2 case at time of 0.1477 sec



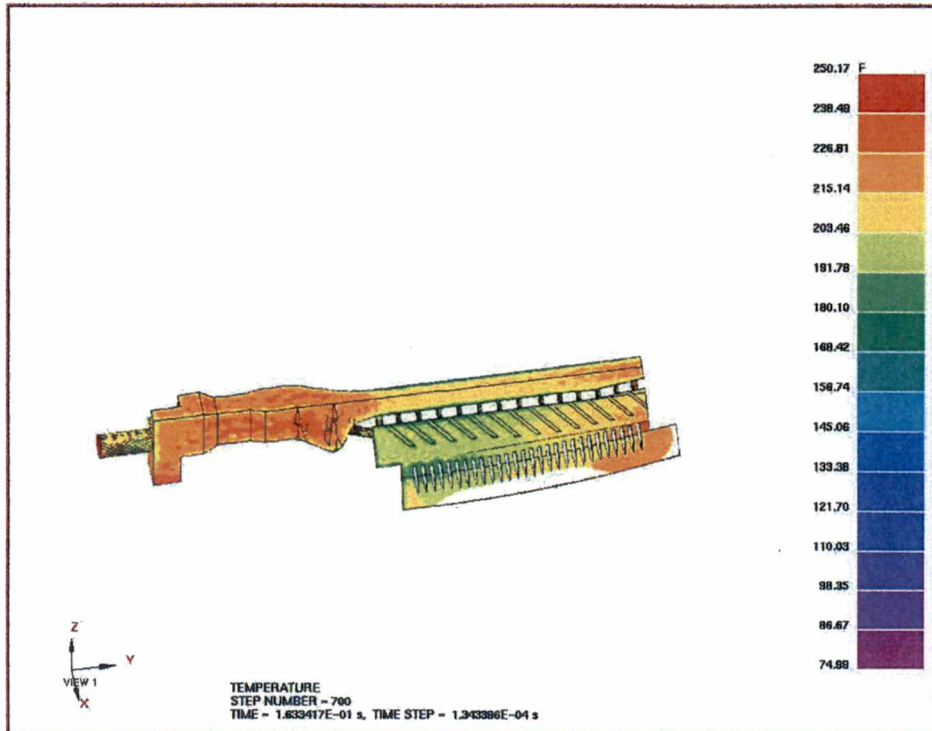
C.12 Temperature contour plot of the P-2 case at time of 0.1524 sec



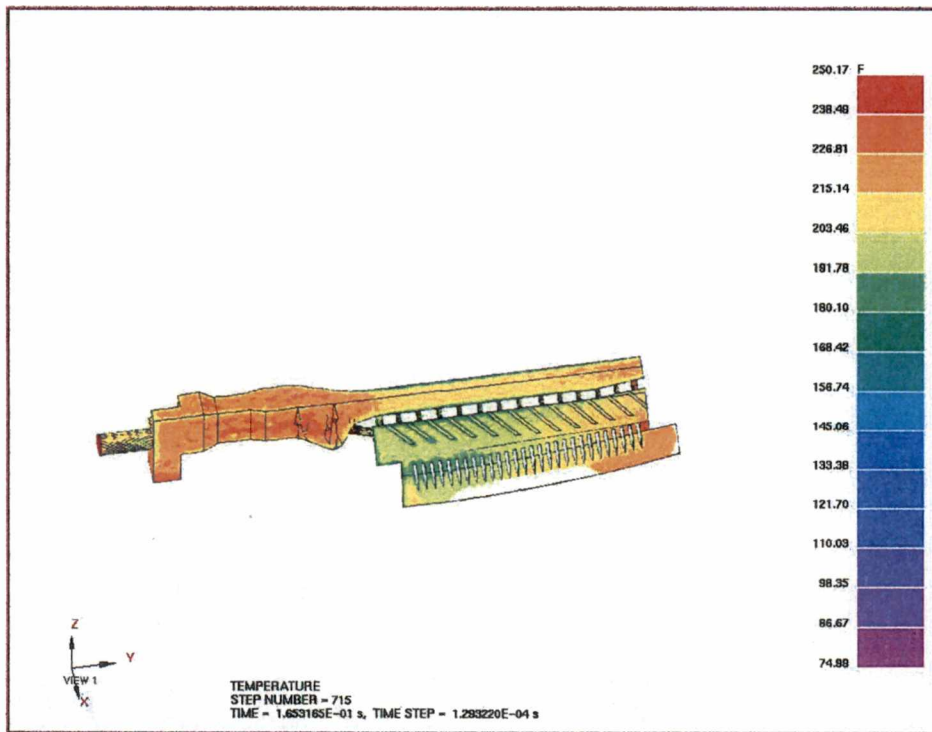
C.13 Temperature contour plot of the P-2 case at time of 0.1550 sec



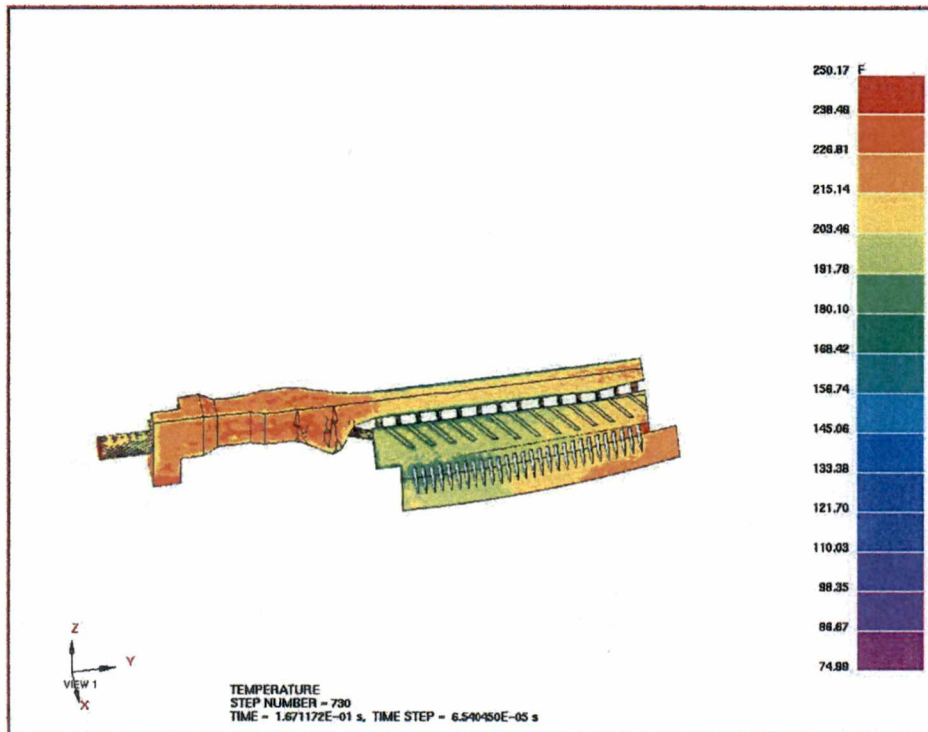
C.14 Temperature contour plot of the P-2 case at time of 0.1575 sec



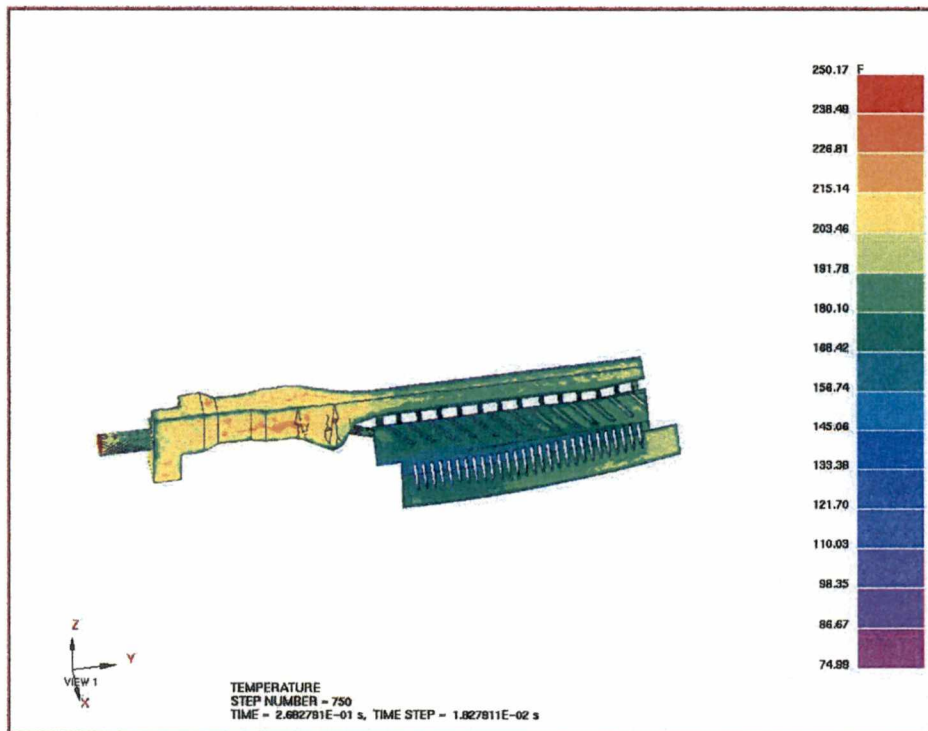
C.15 Temperature contour plot of the P-2 case at time of 0.1633 sec



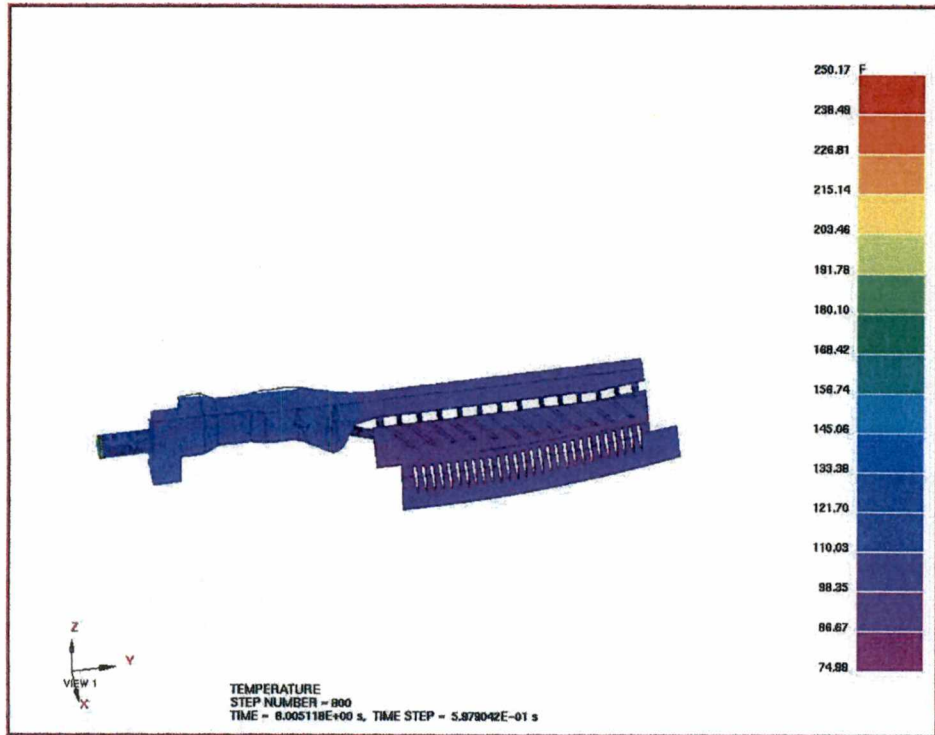
C.16 Temperature contour plot of the P-2 case at time of 0.1653 sec



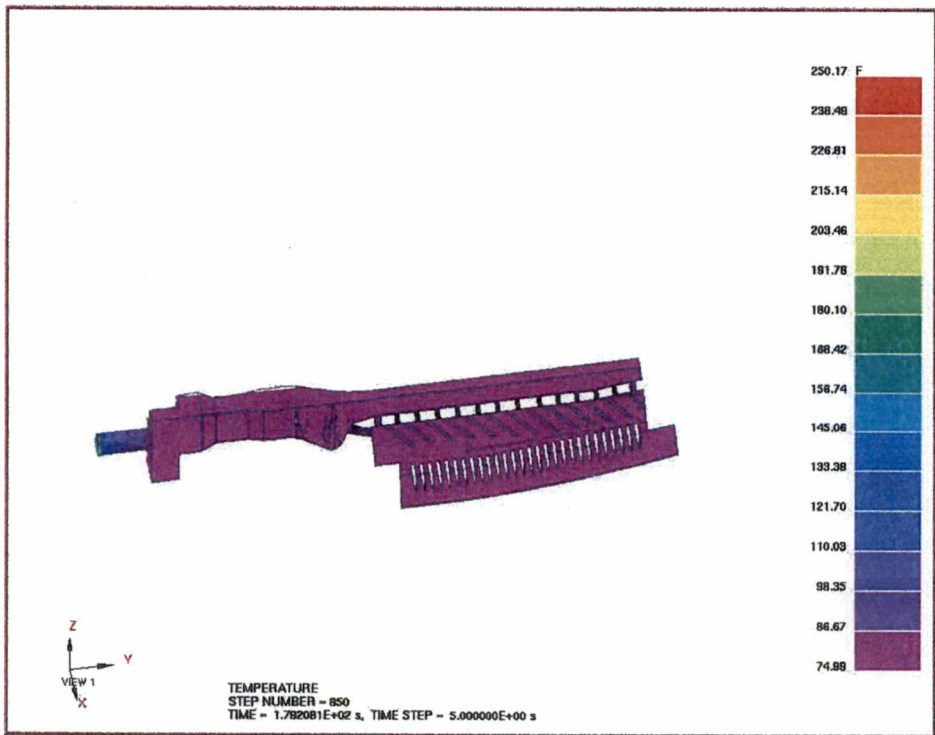
C.17 Temperature contour plot of the P-2 case at time of 0.1671 sec



C.18 Temperature contour plot of the P-2 case at time of 0.2683 sec

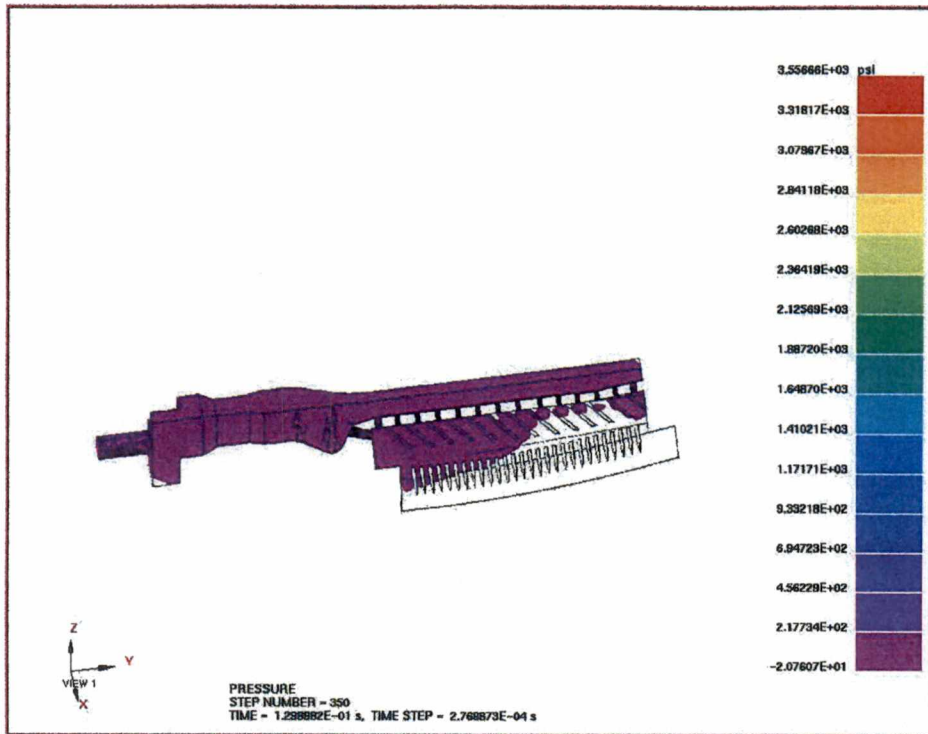


C.19 Temperature contour plot of the P-2 case at time of 8.005 sec

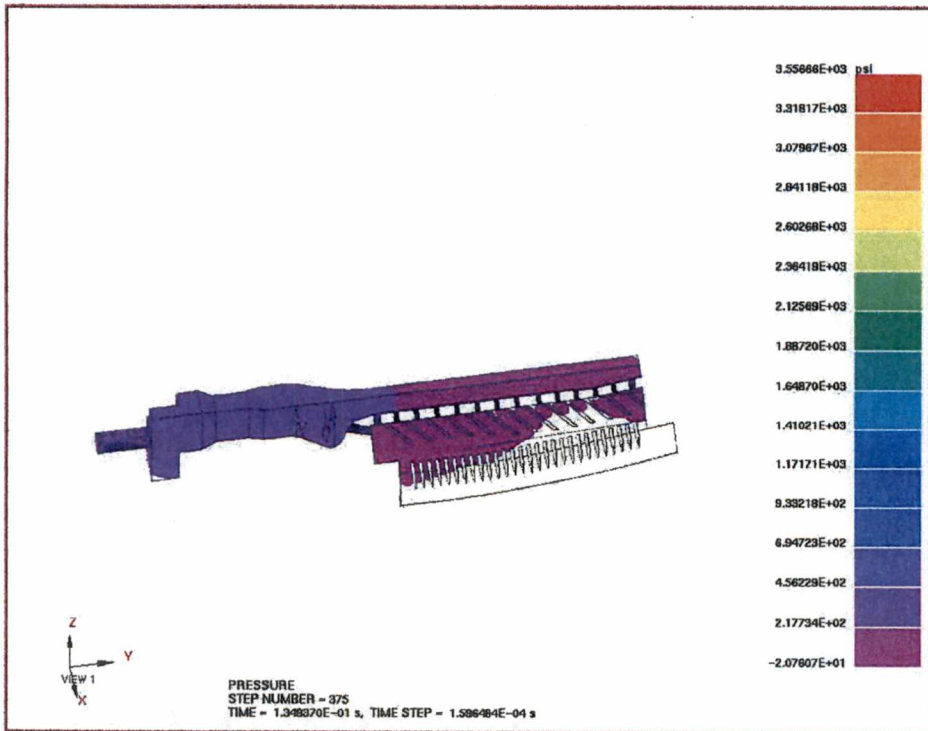


C.20 Temperature contour plot of the P-2 case at time of 179.2 sec

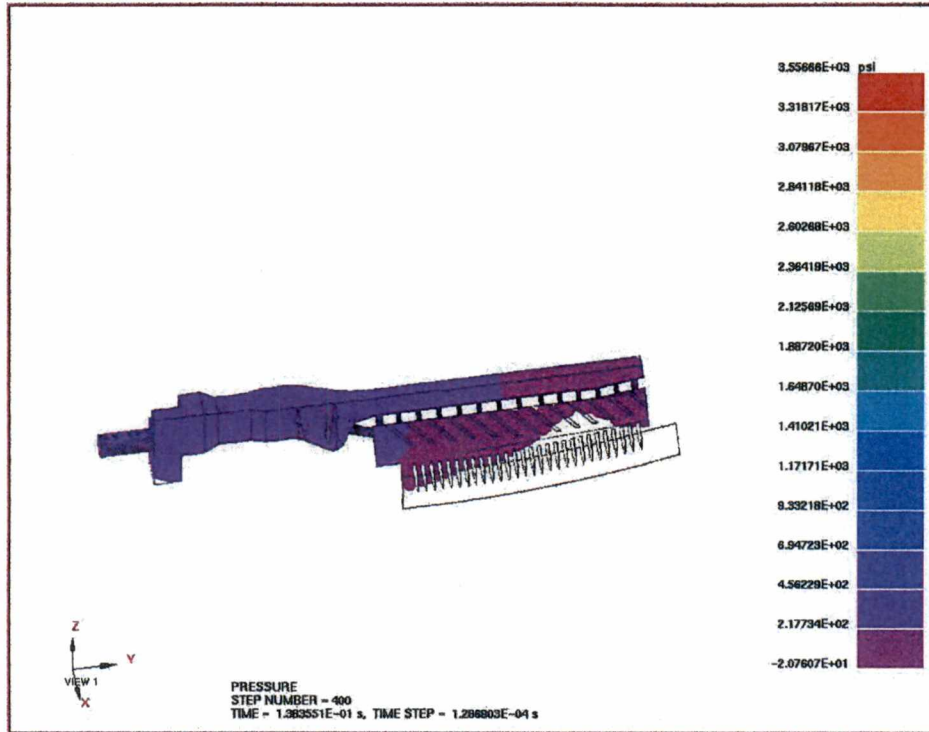
APPENDIX D



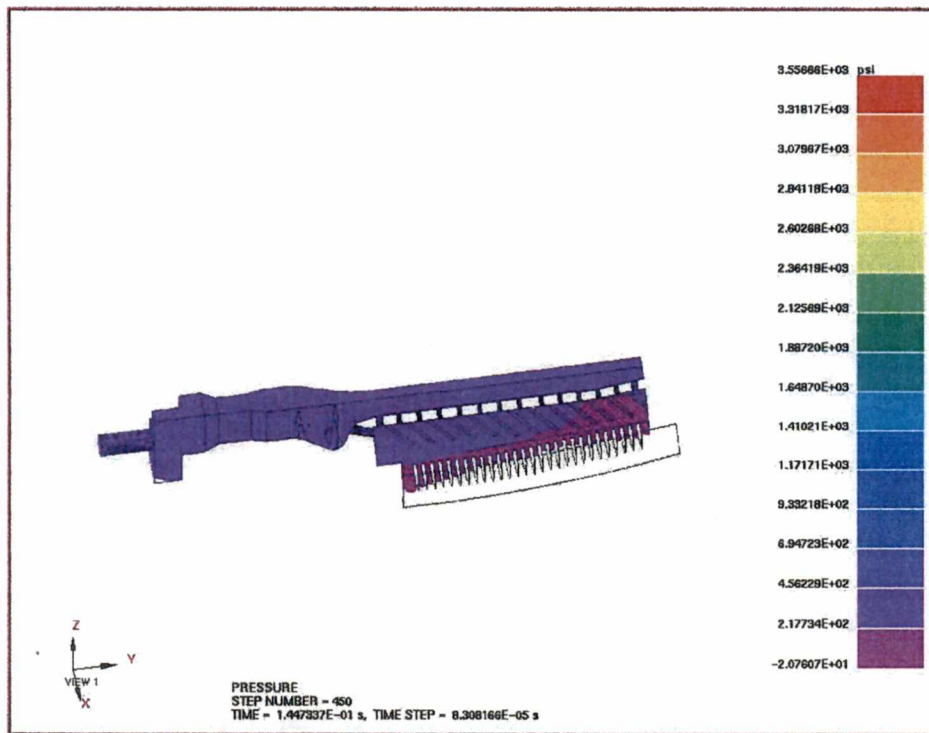
D.1 Pressure contour plot of the P-2 case at time of 129.9 ms



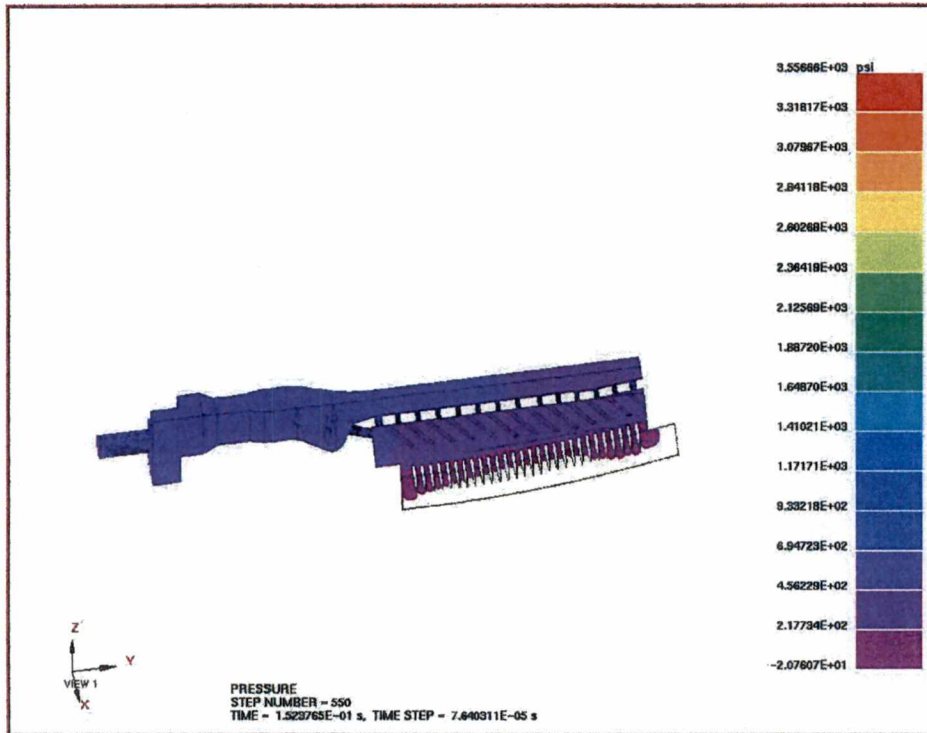
D.2 Pressure contour plot of the P-2 case at time of 134.9 ms



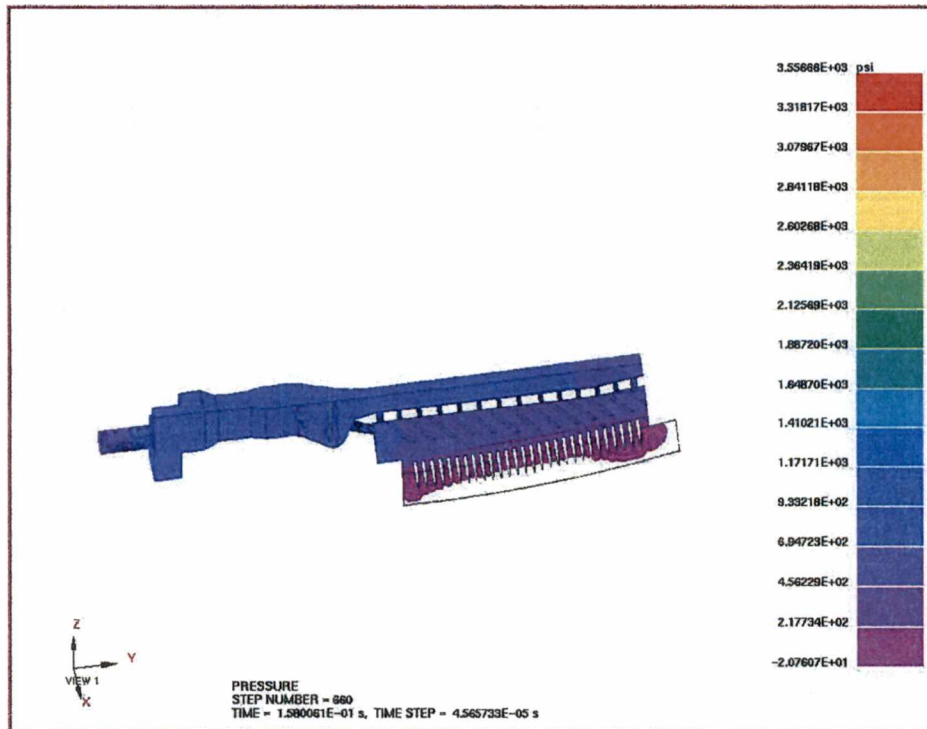
D.3 Pressure contour plot of the P-2 case at time of 138.3 ms



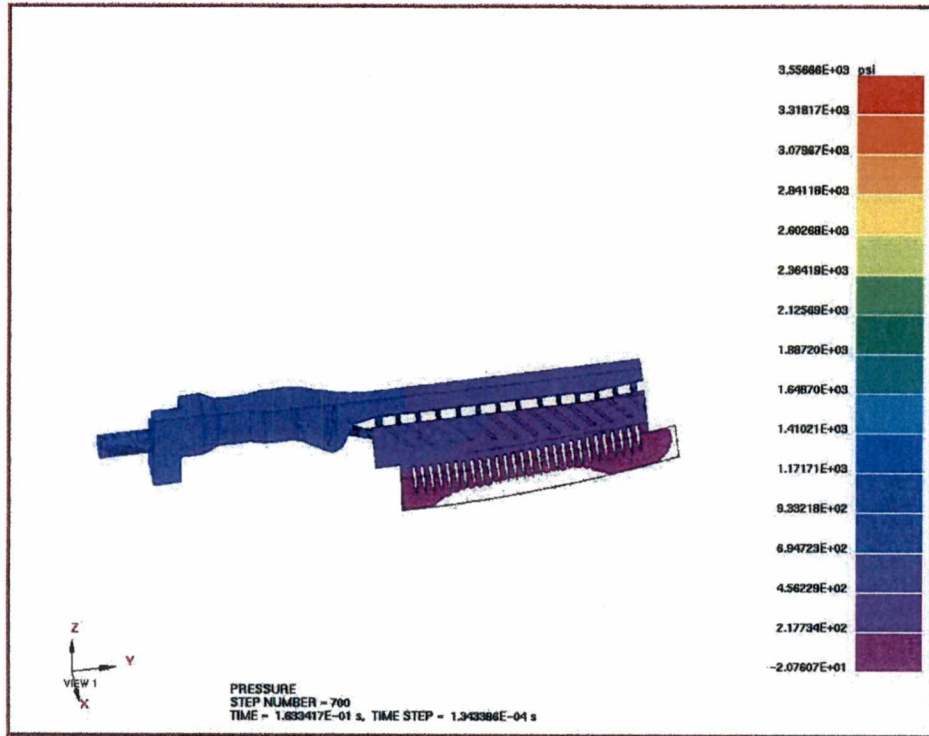
D.4 Pressure contour plot of the P-2 case at time of 144.7 ms



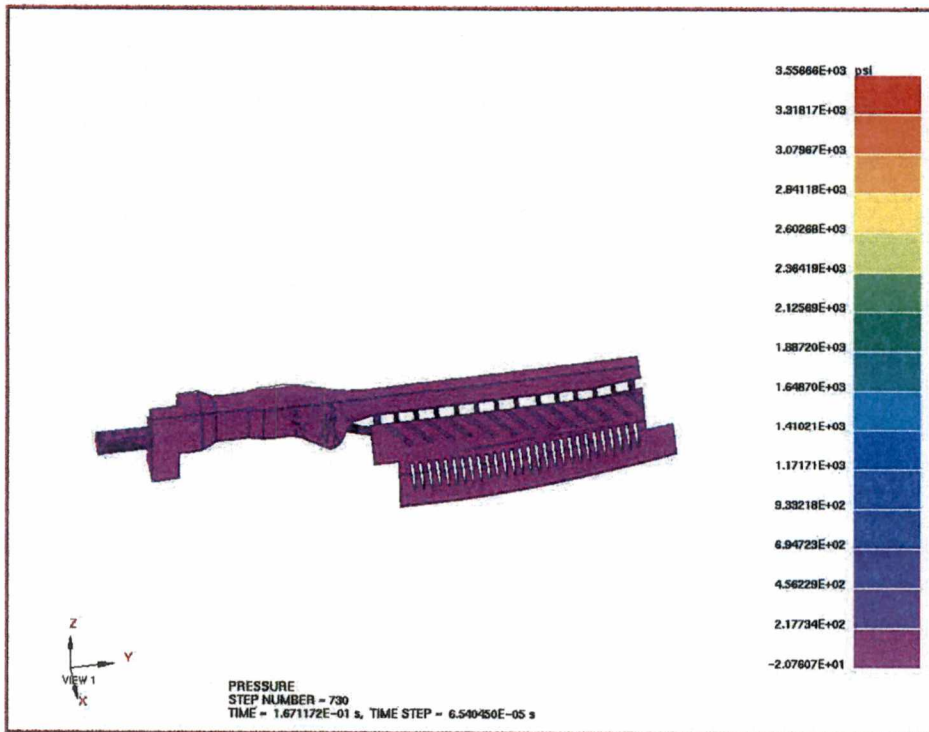
D.5 Pressure contour plot of the P-2 case at time of 152.4 ms



D.6 Pressure contour plot of the P-2 case at time of 158.0 ms



D.7 Pressure contour plot of the P-2 case at time of 163.3 ms



D.8 Pressure contour plot of the P-2 case at time of 167.1 ms

VITA

Thanh Cong Nguyen was born in Ninh Hoa, Vietnam on March 20, 1972 and lived there for most years of his youth. He attended the first through ninth grades at Tran Binh Trong Elementary and Middle School. He graduated from Nguyen Trai High School in May 1987. He was the president of the class from eighth to twelfth grade. He and his family members immigrated to the United States of America to reunite with his brothers in California in 1991. He took English as A Second Language classes at the Rancho Santiago College and Westminster High School. He moved to Knoxville, Tennessee in August 1993. He began his undergraduate study at Pellissippi State Technical Community College in August of 1994 and transferred to the University of Tennessee, Knoxville in August 1997. He graduated and received his Bachelor of Science degree in Mechanical Engineering in May 1999 at the University of Tennessee, Knoxville. Following that, he was offered to pursue a Master of Science degree in Mechanical Engineering and also successfully received teaching and research assistantships from the Department of Mechanical and Aerospace Engineering and Engineering Science. He will receive his Master of Science degree in Mechanical Engineering in May 2001.